CANADIAN THESES

THÈSES CANADIENNES

NOTICE

The quality of this microfiche is heavily dependent upon the quality of the original thesis submitted for microfilming. Every effort has been made to ensure the highest quality of reproduction possible.

If pages are missing, contact the university which granted the degree.

Some pages may have indistinct print especially if the original pages were typed with a poor typewriter ribbon or if the university sent us an inferior photocopy.

Previously copyrighted materials (journal articles, published tests, etc.) are not filmed.

Reproduction in full or in part of this film is governed by the Canadian Copyright Act, R.S.C. 1970, c. C-30.

AVIS

La qualité de cette microfiche dépend grandement de la qualité de la thèse soumise au microfilmage. Nous avons tout fait pour assurer une qualité supérieure de reproduction.

S'il manque des pages, veuillez communiquer avec l'université qui a conféré le grade.

La qualité d'impression de certaines pages peut laisser à désirer, surtout si les pages originales ont été dactylographiées à l'aide d'un ruban usé ou si l'université nous a fait parvenir une photocopie de qualité inférieure.

Les documents qui font déjà l'objet d'un droit d'auteur (articles de revue, examens publiés, etc.) ne sont pas microfilmés.

La reproduction, même partielle, de ce microfilm est soumise à la Loi canadienne sur le droit d'auteur, SRC 1970, c. C-30.

THIS DISSERTATION HAS BEEN MICROFILMED EXACTLY AS RECEIVED

LA THÈSE A ÉTÉ MICROFILMÉE TELLE QUE NOUS L'AVONS REÇUE

A STUDY OF THE AUTO-IGNITION OF SINGLE DROPLETS OF LIQUID FUEL

by

Carol A. Bergeron

B.A.Sc Chem. Eng.

A Thesis

Submitted to the School of Graduate Studies

in Partial Fulfillment of the Requirements for

the Degree of Master of Applied Science

in

Chemical Engineering

University of Ottawa

ISBN 0-315-36471-8

UNIVERSITÉ D'OTTAWA
UNIVERSITY OF OTTAWA

Acknowledgments

I would like to express my sincere gratitude to my research director, Dr. W. L. H. Hallett, Professor of Mechanical Engineering at the University of Ottawa, for his support and for the opportunity to work on this project.

I have also appreciated the help of the technical staff of the Department of Mechanical Engineering of the University of Ottawa. My thanks go out to Mr. G. Spack, Mr. G. Toth and Mr. O. Dalnoki.

Finally, I would like to acknowledge the financial support of the Department of National Defence.

Abstract

In order to understand the physical and chemical processes involved in the ignition of a liquid fuel spray, one must study the ignition properties of liquid fuel droplets. The experimental method used is the "suspended droplet" technique, in which a single fuel droplet suspended from a fine quartz fibre is subjected to a hot environment in order to initiate ignition. The study involves determining ignition delay for various pure hydrocarbons of differing boiling points, as a function of environmental temperature and droplet diameter. The experimental work supplemented the development of a mathematical ignition model, which assumes quasi-steadiness in the gas phase, spherical symmetry of the droplet, a uniform droplet temperature and constant properties. It was found that radiation affects droplet pre-heating and the physical properties of the fuels have a significant effect on ignition delay, whereas the chemical properties have a minor effect. It was observed, for two of the paraffins tested, that at high temperatures the ignition behaviour changes radically; this is due to a change in chemical kinetics which may result from a phenomenon called two-stage ignition observed previously for paraffins.

Nomenclature

a, b, c, d	coefficients of the discretization equation
C_P	constant pressure specific heat (J/kg K)
C_V	constant volume specific heat (cal/mol K)
EA	energy of activation (kcal/mol)
G	mass flux (kg/m^2 s)
h	heat of formation (J/kg)
ΔH	lower heating value (J/kg)
h_{fg}	heat of vaporization (J/kg)
j	diffusion velocity (kg/m^2 s)
k	thermal conductivity (W/m K)
K	pre-exponential factor
M	molecular weight (kg/kmol)
N	number of grid points
p	partial pressure (Pa)
P	pressure (Pa)
P_c	critical pressure (Pa)
Pe	Peclet number
Q	total heat flux (W/m^2)
Q_{RAD}	radiative heat flux (W/m^2)
r	radial position (m)
R	droplet radius (m)
$\mathcal{R}$	gas constant (J/mol K) or (cal/mol K)
t	time (s)
T	temperature (K)
T_c	critical temperature (K)
T_{BOIL}	boiling point (K)
u	radial velocity (m/s)
W	source term due to chemical reaction (kg/m^3 s)
Y	mass fraction

Greek letters:

- α · absorptivity
- Γ · diffusion coefficient (kg/m s)
- ς · dimensionless coordinate
- ρ · density (kg/m^3)
- σ · Stefan-Boltzmann constant (W/m^2 K^4)

Superscripts:

- 0 · from previous time step

Subscripts:

- A · air
- d · droplet
- e · eastern boundary
- E · eastern grid point
- F · fuel
- $Furn$ · furnace
- i · chemical species
- ℓ · liquid
- N · nitrogen
- O · oxygen
- P · grid point P
- R · droplet surface
- RAD · radiation
- v · vapour
- w · western boundary
- W · western grid point
- 0 · at time zero

Contents

Acknowledgments i

Abstract ii

Nomenclature iii

1 Introduction 1
1.1 Description of the Ignition Process 2

2 Literature Review 4
2.1 Introduction 4
2.2 Mathematical Model 4
2.3 Experimental 6
2.3.1 Suspended droplet studies 6
2.3.2 Free droplet studies 7
2.3.3 Porous sphere studies 8

3 Mathematical Model 10
3.1 Introduction 10
3.2 Description of Basic Equations 11
3.2.1 Diffusion Equation 11
3.2.2 Continuity Equation 11
3.2.3 Energy Equation 11
3.2.4 Boundary Conditions 12
3.3 Assumptions 14
3.3.1 The fuel 14
3.3.2 The effect of chemical reaction 14

3.3.3 Quasi-steadiness: Elimination of the transient term $(\partial/\partial t)$ from the species diffusion and continuity equations . . . 15
3.3.4 Constant gas-phase transport properties . . . 16
3.3.5 Spherical symmetry and still atmosphere . . . 17
3.3.6 Uniform droplet temperature . . . 17
3.4 Basic Equations Reduced By Assumptions . . . 19
3.4.1 Coordinate transformation . . . 19
3.4.2 Continuity equation . . . 19
3.4.3 Diffusion equation . . . 19
3.4.4 Energy equation . . . 20
3.5 Liquid Phase Equations . . . 22
3.6 Development of the Finite Volume Solution . . . 23
3.6.1 Finite volume solution . . . 23
3.6.2 Grid spacing . . . 25
3.6.3 TriDiagonal-Matrix Algorithm . . . 26
3.6.4 Chemical reaction modelling . . . 26
3.6.5 Heat flux calculation . . . 27
3.7 Properties . . . 28
3.7.1 Heat capacity . . . 28
3.7.2 Diffusion coefficient . . . 28
3.7.3 Thermal conductivity . . . 29
3.7.4 Density . . . 30
3.7.5 Absorptivity of droplet . . . 30
3.8 Solution of the System of Equations . . . 32
3.8.1 Flow chart . . . 32
3.9 Checking the Program . . . 34

4 Experimental Apparatus and Procedure 36
4.1 The Furnace . . . 36
4.2 Ignition Detection . . . 38
4.3 Droplet Suspension and Size Measurement . . . 41
4.4 Temperature Measurement . . . 41
4.5 Choice of Fuels . . . 43
4.6 Experimental Procedure . . . 44
4.7 Effect of Fibre . . . 45

5 Results and Discussion 46
5.1 Experimental Results 46
5.2 Modelled Results 50
5.3 Comparison of Fuels 52
5.3.1 The effect of chemical properties 52
5.3.2 The effect of physical properties 63
5.4 General Results 64
5.4.1 The effect of chemical reaction 64
5.4.2 The effect of initial droplet temperature 64
5.4.3 The effect of radiation 67
5.4.4 The effect of reaction constants 71

6 Conclusions and Recommendations 74
6.1 Conclusions 74
6.2 Recommendations 75

Bibliography 76

A Simplification of the Energy Equation 80

B Integration of the Energy Equation 82

C TriDiagonal-Matrix Algorithm 85

D Estimating the Temperature Gradient at the Droplet Surface 87

E Temperature Correction Due To Radiation 89

F Listing of Computer Program for Ignition Model 91

List of Figures

1.1 Temperature and fuel vapour concentration profiles near a vaporizing fuel droplet. 2

3.1 Diagram of cell 23
3.2 Exponentially spaced grid 26
3.3 Flow Chart for Ignition Model 33

4.1 Experimental apparatus 37
4.2 Cross-section of the experimental furnace 39
4.3 Sudden temperature rise characterizing ignition 40
4.4 Equivalent diameter of droplet 42

5.1 Two-stage ignition 49
5.2 Ignition delay as a function of droplet diameter for n-heptane 53
5.3 Ignition delay as a function of droplet diameter for n-hexadecane 54
5.4 Ignition delay as a function of droplet diameter for iso-octane 55
5.5 Ignition delay as a function of droplet diameter for benzene 56
5.6 Ignition delay as a function of droplet diameter for α-methylnaphthalene 57
5.7 Ignition delay as a function of temperature for n-heptane . 58
5.8 Ignition delay as a function of temperature for n-hexadecane 59
5.9 Ignition delay as a function of temperature for iso-octane . 60
5.10 Ignition delay as a function of temperature for benzene . . . 61
5.11 Ignition delay as a function of temperature for α-methylnaphthalene 62
5.12 Temperature profile development around droplet (without reaction) 65

5.13 Temperature profile development around droplet (with reaction) 66
5.14 Ignition delay as a function of initial droplet temperature . 68
5.15 Ignition delay as a function of droplet diameter with and without radiation for benzene 69
5.16 Ignition delay as a function of droplet diameter with and without radiation for α-methylnaphthalene 70
5.17 Ignition delay as a function of temperature for n-heptane using different reaction constants 72
5.18 Ignition delay as a function of temperature for n-hexadecane using different reaction constants 73

List of Tables

4.1 Liquid Fuel Properties 44

5.1 Chemical Reaction Constants of the Fuels 50

Chapter 1

Introduction

This thesis represents the initial work required in fullfilling a contract for the Department of National Defence. The work undertaken under the present contract is a study of the auto-ignition properties of single droplets of liquid fuels composed of two components of differing boiling points. The purpose of this is to develop an understanding of the dependence of ignition characteristics on the physical and chemical properties of a fuel blend, which in turn will assist in the application of future off-specification liquid fuels, particularly those from the Alberta Tar Sands, to Diesels and gas turbines. Although it is fuel sprays that are used in engines, a study of isolated single droplets is required as a first step toward understanding the complex physical and chemical processes fundamental to fuel spray combustion.

The present thesis represents the first step in this; it confines itself to studying five pure single component fuels. After satisfactory results have been obtained for these, blends of these fuels will be studied in order to fullfill the requirements of the contract.

The present study includes both experimental work and mathematical modelling. Experiments were carried out to measure ignition time of single suspended droplets of various pure fuels as a function of temperature and droplet size; at the same time, a mathematical model of the processes of evaporation, vapour diffusion and chemical reaction about a single droplet was developed to predict the ignition time. These two phases of the work complement each other: experiments were necessary to furnish reaction constants for the model, while the model is used to make more general statements about ignition than are possible from experiments alone. At-

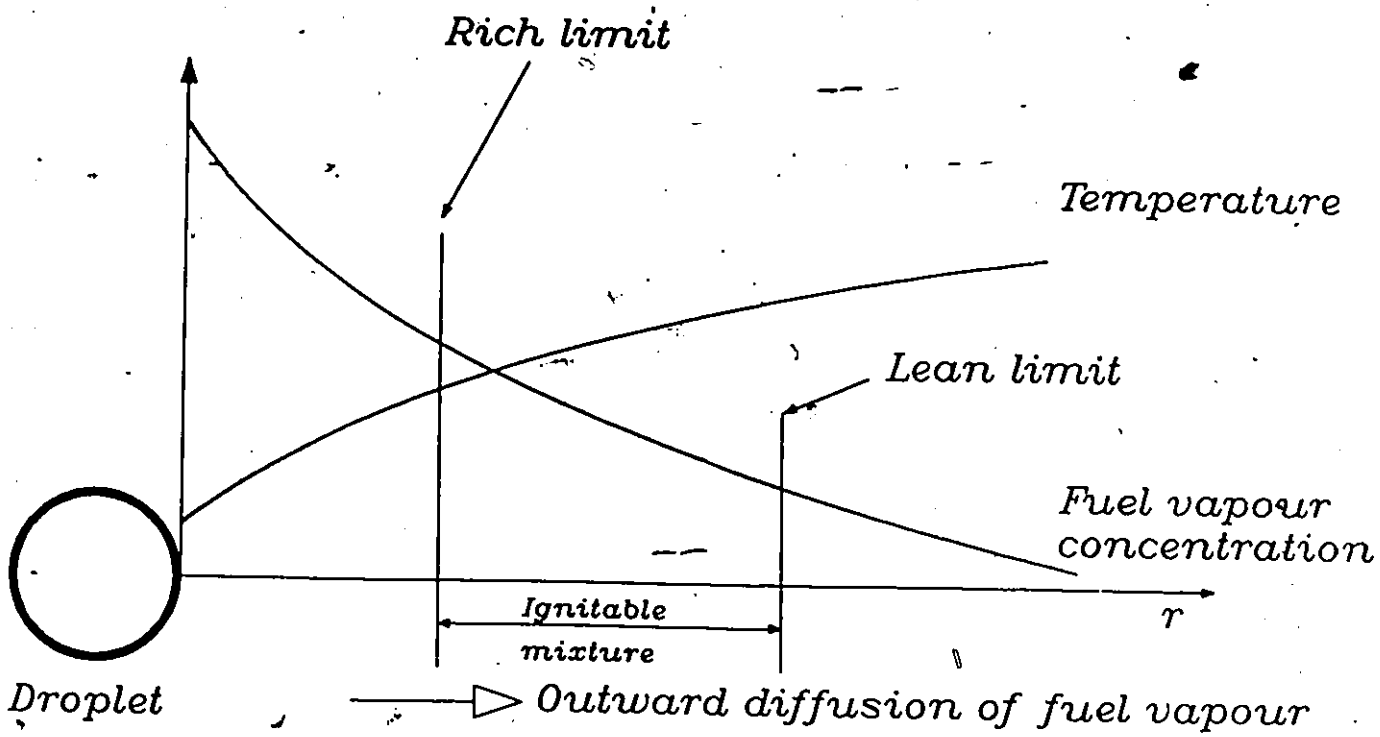

Figure 1.1: Temperature and fuel vapour concentration profiles near a vaporizing fuel droplet.

tention is confined to autoignition (spontaneous ignition) resulting from exposure of the droplet to a hot environment alone, as distinct from spark or flame ignition.

1.1 Description of the Ignition Process

In modelling the ignition process of a single droplet of liquid fuel, the physical problem is that of a spherical droplet which is suddenly exposed to a hot environment and begins to vaporize. The droplet is heated by heat conduction and convection from the hot surrounding air and by radiation from the hot walls of the furnace. The fuel components evaporate at the droplet surface, and the vapour diffuses radially outward, mixing progressively with the air (see Figure 1.1). Ignition depends on both physical and chemical factors. The processes of evaporation and diffusion must produce enough mixture to sustain reaction, and sufficient time must be allowed for reaction to be initiated in this mixture. Ignition will occur if

1. A zone of ignitable mixture is formed: there must exist a fuel vapour concentration gradient in space between the location of mixture at the lean flammability limit of the fuel and that at the rich limit.

2. The temperature of this mixture must be at or above the spontaneous ignition temperature of the mixture.

3. The chemical delay (time required to initiate rapid chemical reaction) must be less than the time necessary for a fuel molecule to diffuse from the rich limit to the lean limit. In other words, fuel molecules must spend the entire chemical delay in an ignitable mixture above the spontaneous ignition temperature.

Thus, the total ignition delay consists of a physical delay, which is the time elapsed from the instant the droplet is subjected to the hot air environment until it becomes sufficiently heated for the initiation of appreciable gas phase reactions, and a chemical delay, which accounts for the time required for these reactions to reach a runaway situation [5].

The above simplified physical description of the ignition process indicates that ignition is affected by

1. the temperature of the surrounding air;

2. the vapour pressure (volatility) of the fuel components;

3. the reaction rate behaviour of the fuel components;

4. the droplet diameter.

Items (1) and (3) relate to chemical ignition delay processes, while (2) and (4) affect the rate at which vapour is produced and diffuses. The vapour diffusion velocity is roughly inversely proportional to droplet radius; hence, vapour may leave a very small droplet at a high enough velocity to make ignition impossible [6,33]. Droplet ignition therefore involves the interaction of simultaneous physical and chemical processes.

Chapter 2

Literature Review

2.1 Introduction

Most of the research on droplet combustion has been devoted to studies of the combustion of isolated single droplets because this is believed to be fundamental to the understanding of spray combustion. When performing the literature search, the subjects of interest were, therefore single liquid droplet evaporation, ignition and combustion. Papers collected were either experimental, theoretical (mathematical model) or a combination of both. The search for papers dealing with theoretical models was aimed at finding a method that would simulate the experimental furnace conditions.

2.2 Mathematical Model

The present model was developed by referring to several thermal ignition models published by various researchers. In 1968, Faeth and Olson [6] developed an ignition model in which the differential equations and the associated boundary conditions were solved using a numerical integration technique. In their model they included droplet heating and the effect of radiation. They also applied the quasi-steady assumption in the gas phase (ie. neglecting transient terms in the diffusion and energy equations) and used variable gas phase properties. The ignition criterion used by Faeth and Olson is that of an accumulation of chemical intermediates: ignition occurred when the concentration of critical intermediate produced through

chemical reaction reached a specified value.

Polymeropoulos [29], in 1969, developed a model which did not predict ignition delay times but determined whether or not combustion was possible under given conditions. Like that of Faeth and Olson [6], the mathematical technique used was numerical integration. He applied the quasi-steady assumption in both the liquid and gas phases and assumed constant properties and a one-step chemical reaction.

Law [17,20] developed two ignition models; the first, in 1975 [17], used a finite difference technique for solving the differential equations. This model specified conditions necessary for ignition to occur, but did not predict ignition delay times. The model applied the assumption of quasi-steadiness in the liquid and gas phases, and assumed constant properties, a uniform droplet temperature and a one-step chemical reaction of first order with respect to the fuel and the oxygen.

The second ignition model developed by Law [20] was in 1978. In this model ignition delay times were determined by combining the first model [17] with a calculation of transient heating of the droplet. Law also assumed constant properties, a uniform droplet temperature, and a one-step chemical reaction of first order with respect to the fuel and the oxygen.

In 1977, Sangiovanni and Kesten [34] developed an ignition model in which analytical solutions for temperatures and species concentrations in the gas and liquid phases were combined with a numerical procedure for advancing the time. In this model they used the same ignition criterion developed by Faeth and Olson [6]. They applied the quasi-steady assumption in the gas phase, assumed transient heating of the droplet, but neglected the effect of radiation. With this model they showed that free and forced convection compared to pure diffusion had little effect on the ignition delay time.

Niioka, Ishiguro and Saitoh [25] developed a full transient model in 1980. A numerical finite difference method was used for solving the differential equations. They considered the droplet temperature to be nonuniform, but assumed constant properties and a one-step chemical reaction.

Other papers on droplet vaporization without chemical reaction [12,16] and steady combustion [18,22,31,32,35] were consulted to back up modelling assumptions; these are discussed in Chapter 3.3.

2.3 Experimental

Experimental studies of droplet combustion have employed the three following techniques:

1. a single droplet suspended on the end of a thin quartz fibre;
2. a free-falling single droplet or droplet stream;
3. a porous sphere with liquid fuel being fed to its interior at such a rate that the surface is just wetted to support combustion.

2.3.1 Suspended droplet studies

This technique represents the simplest type of droplet experiment. A fuel droplet is suspended on the end of a filament made of an inert material, and ignites as a result of a) a flame; b) a spark; or c) a hot air environment resulting from a heated chamber or a hot air stream. Observations of droplet ignition and combustion are usually made by high speed photography, which can also be used as a time base to measure ignition delay and combustion time.

Saitoh et al. [33], Kobayasi [14], and Nishiwaki [26] performed droplet combustion experiments using a similar apparatus. This consisted of a heated droplet ignition chamber or furnace which moved over a droplet supported on a silica filament. Saitoh et al. detected ignition according to a change in intensity of light and measured initial droplet diameter by direct photography. Kobayasi and Nishiwaki recorded droplet evaporation and combustion in the furnace by shadow photographs taken with a motion-picture camera.

El-Wakil and Abdou [5] performed self-ignition experiments by passing a heated air stream over a single fuel droplet suspended on a fine-wire thermocouple. The droplet size history and flame history were recorded photographically. Monaghan et al. [23] suspended droplets on fine silica fibres in a controlled atmosphere; these were ignited by a spark discharge and photographed using a modified drum camera.

Faeth and Olson [6] required droplet sphericity for their theoretical model, so that the entire apparatus, enclosed in an air-tight chamber, was

dropped 5 meters into a tub filled with chopped foam plastic. The experiment was conducted within the chamber during this free fall period. By doing so gravitational effects and natural convection were eliminated. A droplet was suspended on a glass filament and a movable furnace was allowed to drop over it at the start of the experiment. Okajima and Kumagai [27] also performed combustion experiments under zero-gravity conditions by suspending fuel droplets in a uniform air flow and allowing the apparatus to fall freely. The fuel droplet was suspended at the end of a silica filament and spark ignited. Droplet size history was recorded using a movie camera.

Advantages [21]:

1. Suspended droplet experiments can be easily set up and performed.
2. The droplet being stationary, detailed cine-microphotography can be taken of its burning sequence.

Disadvantages [21]:

1. Because of the thickness of the suspension fibre, it is difficult to suspend a droplet much smaller than 1 mm in diameter, which is much larger than typical droplet sizes within sprays.
2. The suspension fibre distorts the droplet shape from spherical.
3. Heat may be conducted through the fibre, heating the droplet and increasing the vaporization rate.
4. The technique is limited to fuels which are relatively non-volatile, otherwise some vaporization would occur during the period required to suspend the droplet.

2.3.2 Free droplet studies

Here studies are considered in which single droplets are injected directly into an environment conducive to ignition and combustion. The method of ignition may vary from single shot injectors to vibrating hypodermic needles producing a stream of uniform droplets.[3]

Hieftje and Malmstadt [9] devised a system that allowed droplet size and spacing to be varied independently. A stream of uniformly sized and spaced droplets was generated by a vibrating capillary tube, which also gave each droplet a positive charge. The droplet frequency and spacing could be controlled using a pulsing electrode to neutralize every n^{th} droplet in the stream. A set of highly charged magnetic plates then deflected all but this chosen droplet to a collector, while the chosen droplet proceeded to the flame for observation. The droplets were observed using normal and stroboscopic photography with background lighting. Sangiovanni and Kesten [34] adapted an experimental system similar to that of Hieftje and Malmstadt, injecting droplets upward into the hot gases from a flat flame burner.

Advantages [21]:

1. Small droplet sizes.
2. No interference from suspension fibre.
3. Capability of using volatile fuels.

Disadvantages [21]:

1. Experimental method is more complex and delicate.
2. Droplets in motion may leave the field of the camera before reactions are completed. [3]
3. Spacing must be sufficient, or else axial conduction of heat in closely spaced droplets can effect ignition; the droplets are then no longer auto-ignited by virtue of the temperature of the surroundings.
4. Droplets are subjected to forced convection by their motion relative to the gas.

2.3.3 Porous sphere studies

In porous sphere experiments fuel is supplied to the center of a porous sphere suspended in a combustion chamber [2]. These experiments can be

used to simulate steady state evaporation or combustion.
Advantages [21]:

1. Conforms most closely with the steady state assumption of the "d^2 Law" derived from the simple droplet evaporation theory.
2. Allows detailed probing of the flame structure.

Disadvantages [21]:

1. Relatively large droplet size (natural convection has a much stonger effect).
2. Elimination of transient phenomena present during regular droplet combustion. In particular, the droplet heating transient which is important for ignition is absent, so that this technique is not suitable for ignition studies.

Chapter 3

Mathematical Model

3.1 Introduction

A model was developed to simulate the droplet ignition process under experimental furnace conditions. The purpose of this model is to predict the ignition delay of a single droplet of liquid fuel which is instantaneously exposed to a high temperature atmosphere at constant atmospheric pressure. This requires a mathematical description of the processes of droplet evaporation, fuel vapour and oxygen diffusion, chemical reaction, and heat conduction in the gas phase surrounding the droplet. This model was developed using finite volume methods described by Patankar [28] for heat transfer and fluid flow problems.

One of the goals set in developing the model was keep it as realistic as possible, but use as little computational time as possible. The resulting model is mid-way in difficulty between the analytical model developed by Law [20] and the full numerical models developed by Faeth and Olson [6] and Saitoh [32].

3.2 Description of Basic Equations

The physical transport equations governing the present problem are those of diffusion, continuity and energy for the vapour phase surrounding the droplet. Their basic general forms are given below and these will be reduced to their final forms in Section 3.4.

3.2.1 Diffusion Equation

The diffusion equation describes the concentration of each species (fuel, oxygen, nitrogen and products) as a function of position and time and is formulated as follows for species i:

Rate of change of mass of i in control volume	+	Change of mass of i due to convection	=	Change of mass of i due to diffusion	+	Change of mass of i due to chemical reaction

$$\rho\frac{\partial Y_i}{\partial t} + \rho v\frac{\partial Y_i}{\partial r} = \frac{1}{r^2}\frac{\partial}{\partial r}\left(r^2\Gamma\frac{\partial Y_i}{\partial r}\right) + W_i \tag{3.1}$$

3.2.2 Continuity Equation

The continuity equation describes the flow velocity field and is formulated as follows for the mixture:

$$\frac{\partial \rho}{\partial t} + \frac{1}{r^2}\frac{\partial}{\partial r}\left(r^2\rho v\right) = 0 \tag{3.2}$$

3.2.3 Energy Equation

The energy equation describes the temperature field surrounding the droplet and is formulated as follows for the mixture:

Rate of change of internal energy in control volume	+ Change in internal energy due to convection	

= Change in internal energy due to conduction	+ Change in internal energy due to diffusion	+ Change in internal energy due to chemical reaction	

$$\rho C_P \frac{\partial T}{\partial t} + \rho v C_P \frac{\partial T}{\partial r} = \frac{1}{r^2}\frac{\partial}{\partial r}\left(r^2 k \frac{\partial T}{\partial r}\right) - \sum C_{P,i} j_i \frac{\partial T}{\partial r} - \sum h_i W_i \qquad (3.3)$$

The equations above assume spherical symmetry for the droplet; this assumption is justified in Section 3.3.5.

3.2.4 Boundary Conditions

The simple boundary conditions and initial conditions which apply to the system are as listed below:

- At the droplet surface (r = R)

  1. The gas temperature is set equal to the temperature of the droplet, $T_R = T_l$.
  2. The fuel mass fraction is calculated with

  $$Y_{FK} = \left[1 + \frac{M_A}{M_F}\left(\frac{p_\infty}{p_v} - 1\right)\right]^{-1} \qquad (3.4)$$

  where the vapour pressure of the fuel is calculated using the simple correlation given by the Cox-Antoine equation [7]

  $$p_v = exp\left[A - B/(T_l + C)\right] \qquad (3.5)$$

  and the constants A, B and C can be found in Reid et al. [30, pages 629–665].

  3. No oxygen penetrates the droplet surface, meaning that all the oxygen which arrives by diffusion leaves by convection.

  $$\Gamma \frac{\partial Y_O}{\partial r}\Big|_{r=R} = G Y_{O0} \qquad (3.6)$$

- At infinity ($r = \infty$),

  1. The temperature is constant and equal to the furnace temperature, $T_\infty = T_{Furn}$.
  2. The fuel vapour concentration is equal to zero, $Y_{F\infty} = 0$.
  3. The oxygen concentration is equal to that in ambient air, $Y_{O\infty} = 0.232$.

3.3 Assumptions

Since a complete model consisting of a full transient finite difference solution of all the governing equations, including the effects of property variations, and chemical reaction, would be too cumbersome and require too much computer time, the following assumptions have been made to produce a simplified model and reduce computational effort.

3.3.1 The fuel

The fuel is a single chemical species that behaves as an ideal gas in the boundary layer.

3.3.2 The effect of chemical reaction

During the initial stages of the ignition process the rates of reactant consumption are small and the temperature rise is low. Events in the gas phase can be described roughly by the classical thermal ignition theory for a homogeneous gas mixture [13]: During most of the ignition delay period, reactant consumption is slight and only a small temperature rise is observed. When the temperature reaches a sufficiently high level, the gas-phase reaction rate accelerates in an exponential fashion. Eventually a chemical runaway takes place with a sudden sharp temperature rise; this is the actual ignition event. Only during the final runaway does reactant consumption become large, therefore reactant consumption prior to ignition can be neglected to good accuracy. The diffusion equation for the products can then be dropped entirely, and the source terms W_i in the remaining diffusion equations eliminated. The reaction term must be retained in the energy equation, because it is the temperature rise resulting from reaction which signals ignition, but the fuel and oxygen concentrations used to calculate the reaction rate will neglect depletion due to reaction. This approach has been used in several ignition models by various researchers [6,20,29,35,5].

3.3.3 Quasi-steadiness: Elimination of the transient term $(\partial/\partial t)$ from the species diffusion and continuity equations

Ignition delay is a direct result of transient physical and chemical processes. These transients are of two kinds: the heating of the liquid phase, and the response of the gas phase in adjusting itself to the varying liquid surface boundary conditions.

The droplet, which is initially at room temperature, begins to heat up as it is exposed to the hot environment. The time required for the droplet to reach its final equilibrium ('wet-bulb') temperature is typically of the same order of magnitude as the ignition delay [21]. As the droplet temperature increases, the vapour pressure at the surface rises substantially, and the rate of vaporization increases. As the vapour pressure changes and chemical reaction occurs in the vapour, the gas phase undergoes transients to adjust itself. These transients are described by the $(\partial/\partial t)$ terms in the equations. Because of the significant difference in density between liquid and gas, the liquid possesses great thermal inertia, so that properties at the droplet surface (regression rate, species concentrations, temperature) change at rates much slower than those of the gas-phase transport processes. In a standard environment the gas-phase heat and mass diffusivities are of the order of $10^0 cm^2 s^{-1}$ [21], whereas the droplet surface regression rate is of the order of $10^{-3} cm^2 s^{-1}$ for conventional hydrocarbon fuels. Their ratio, 1000/1, is of the same order as the ratio of the liquid to gas densities [21]. This ratio also characterizes the rates of temperature rise in the gas and liquid phases in response to a given heat flux. The gas phase transient being much more rapid, its effects are of a low order, and the liquid droplet heating becomes the controlling transient process.

These arguments allow the transient terms to be eliminated, yielding 'quasi-steady' solutions for the concentration and velocity fields. These represent the state attained under constant boundary conditions (ie. droplet diameter and temperature) after the initial gas phase transient has died down. The transient term in the energy equation must, however, be retained, otherwise the physical process of local temperature rise during ignition will be suppressed.

The quasi-steady assumption is not valid in some cases [21]:

1. In regions far away from the droplet, the flow velocity is extremely

slow, such that the characteristic diffusion time is of the same order as the surface regression time. However, these regions are far from the location of significant chemical reaction.

2. When the pressure approaches or exceeds the critical pressure of the liquid fuel, the density ratio (ρ_l/ρ_g) approaches unity and the liquid/gas interface is no longer distinguishable.

The quasi-steady assumption is the basis of the 'classical' droplet vaporization theory [21], and has been used in many ignition and combustion theories [20,19,17,29,35]. Matalon and Law [22] and Hubbard et al. [12] have given some attention to the validity of the quasi-steady assumption by performing calculations of droplet vaporization with and without the gas-phase transient terms. They concluded that the effect of the transient terms is negligibly small and that the assumption is a useful and realistic one in modeling droplet vaporization at atmospheric pressure.

3.3.4 Constant gas-phase transport properties

Computational time has been further reduced by assuming the specific heats, thermal conductivities and diffusion coefficients to be constant. These transport properties are generally a function of temperature and mixture composition in the gas phase and hence of time and location, and there is no doubt that significant variations in properties do occur over the temperature and concentration gradients present. However, Hubbard et al. [12] have compared calculations of droplet vaporization with constant and variable properties, to conclude that the vaporization rate could be calculated with good accuracy using constant properties if these are evaluated at an average temperature and composition. Hubbard et al. favoured using Sparrow's 1/3 rule in estimating a reference temperature and composition,

$$T = \frac{2}{3}T_R + \frac{1}{3}T_\infty \tag{3.7}$$

$$Y_i = \frac{2}{3}Y_{iR} + \frac{1}{3}Y_{i\infty} \tag{3.8}$$

where subscripts R and ∞ represent the droplet surface and ambient conditions respectively. Hubbard et al. did not include chemical reaction in

their model, but assumption 3.3.2 above allows their results to be applied directly to the present problem.

The density, however, is not considered constant and is calculated from the ideal gas law using a local mixture molecular weight.

3.3.5 Spherical symmetry and still atmosphere

In reality there is some degree of natural convection. The effect of natural convection on a vaporizing droplet is that the vapour, which is more dense than air, diffuses downward as well as radially, therefore changing the concentration of vapour surrounding the droplet.

However, Faeth and Olson [6], who performed droplet ignition experiments at '0' and '1' gravity, have shown that the differences are not large at atmospheric pressure, so that gravity (ie. natural convection) has little effect on ignition time. Sangiovanni and Kesten [34] who made calculations with and without convection (both natural and forced) also found little effect on ignition time, although ignition location varied strongly.

Forced and natural convection being neglected, the droplet is assumed to be an isolated one immersed in an infinite stagnant oxidizing environment, and is assumed to be spherically symmetric, so that only radial transport is possible. The analysis is thus reduced to one dimension.

3.3.6 Uniform droplet temperature

For simplicity, the liquid phase transport processes are ignored and the droplet temperature is assumed uniform in space. In reality, transient heat conduction causes the surface temperature to be greater than the internal temperature [18]. Counteracting this are internal liquid circulation induced by convection currents in the gas phase, and absorption of radiation by the liquid.

A spatially uniform temperature is unlikely without the existence of some degree of internal circulation. It may be noted that the requirement for the existence of external convective gas motion, to produce and sustain the internal circulation, contradicts the assumption of spherical symmetry. However, Law [18] has shown that the mass vaporization rates obtained by assuming spherical symmetry and rapid internal circulation agree qualitatively with experimental observations, implying that these assumptions

are realistic. Furthermore, Law has shown that the droplet vaporization process is practically identical for the model with rapid internal mixing and without it. A fact supporting the present assumption is that while setting up the experiments for the present study, circulation of dirt particles was observed inside the droplets.

Calculations of radiant heat absorption by hydrocarbon droplets performed by Hottel et al. [11] show that internal absorption can lead to nearly uniform droplet temperatures, regardless of other liquid phase processes. In the present experiments, heat is supplied by radiation from the furnace walls and by conduction from the hot ambient gases. The radiation is focussed towards the center of the droplet by refraction at the droplet surface while the conduction of heat from the ambient gases heats up the outside of the droplet. For extreme cases, when radiant heat transfer predominates, the inside of the droplet can actually be slightly hotter than the surface.

Further support for the uniform droplet temperature assumption is given by the fact that, owing to spherical geometry, most of the liquid mass lies near the droplet surface. Hence, the interior, low temperature regions only represent a small part of the droplet heat capacity.

Faeth and Olson [6] examined the role of temperature distribution within the liquid droplet in their ignition model. When comparing the assumption of uniform temperatures with radial calculations for varying temperatures, results showed that the error was small for droplet sizes representative of normal sprays.

3.4 Basic Equations Reduced By Assumptions

In this section the governing equations for the gas phase are simplified to their final form by applying the assumptions discussed above.

3.4.1 Coordinate transformation

Since a numerical solution is required for solving the system, it is necessary to keep the surface of the droplet on the first grid point. This is done by performing the following coordinate transformation.

$$\zeta = \frac{r}{R} \tag{3.9}$$

If this transformation was not introduced, the droplet surface would recede with respect to the first grid point as the droplet vaporized, and the system could not easily be solved.

3.4.2 Continuity equation

Applying the assumption of quasi-steadiness, Equation 3.2 is reduced to:

$$\frac{1}{r^2}\frac{\partial}{\partial r}\left(r^2 \rho v\right) = 0 \tag{3.10}$$

or $r^2 \rho v = R^2 G$ = mass flux from the droplet surface, and G is described by Equation 3.12.

3.4.3 Diffusion equation

Applying the assumptions of quasi-steadiness and negligible reactant consumption, Equation 3.1 is reduced to the following form

$$\rho v \frac{\partial Y_i}{\partial r} = \frac{1}{r^2}\frac{\partial}{\partial r}\left[r^2 \Gamma \frac{\partial Y_i}{\partial r}\right] \tag{3.11}$$

where i now represents only fuel, oxygen and nitrogen. It is noted that the transient term along with the source term due to reaction have been dropped.

The solution of this equation is a standard one and may be found in Kanury [13]. It involves using the solution of the continuity equation above and integrating to obtain

$$G = \frac{\Gamma}{R} \ell n \left(1 - Y_{FR}\right)^{-1} \tag{3.12}$$

and

$$Y_F = 1 - \left(1 - Y_{FR}\right)^{R/r} \tag{3.13}$$

Equation 3.13 represents the fuel vapour concentration profile.

For oxygen:
Since no oxygen penetrates the surface of the droplet, and the products are neglected up to the point of ignition,

$$Y_F + Y_{O_2} + Y_{N_2} = 1 \tag{3.14}$$

at all points and the ratio of oxygen to nitrogen remains constant. Therefore,

$$Y_O = Y_{O\infty}\left(1 - Y_F\right) \tag{3.15}$$

where $Y_{O\infty} = 0.232$, the concentration of oxygen in air. Equation 3.15 represents the oxygen concentration profile. Equations 3.13 and 3.15 have been developed using the classical droplet vaporization theory.

When applying the coordinate transformation to Equations 3.13 and 3.15 the final reduced form of the concentration profiles is obtained.

$$Y_F(\varsigma) = 1 - \left(1 - Y_{FR}\right)^{1/\varsigma} \tag{3.16}$$

$$Y_O(\varsigma) = Y_{O\infty}\left(1 - Y_F(\varsigma)\right) \tag{3.17}$$

$$Y_N(\varsigma) = \frac{Y_{N\infty}}{Y_{O\infty}} Y_O(\varsigma) \tag{3.18}$$

3.4.4 Energy equation

The assumption of quasi-steadiness does not apply to the energy equation because without the transient term the process of local temperature rise during ignition will not occur. The source term also requires knowledge of the temperature profile developed at the previous time step. Although

reactant consumption is assumed negligible up to the time of ignition, the source term W_F is retained in the energy equation because it is multiplied with the heat of reaction of the fuel ΔH_F, which is large and brings the term to the same order of magnitude as the others in the equation. The energy equation valid for a single component droplet is as follows:

$$\rho C_P \frac{\partial T}{\partial t} + \rho v C_{PF} \frac{\partial T}{\partial r} = \frac{1}{r^2} \frac{\partial}{\partial r} \left(r^2 k \frac{\partial T}{\partial r} \right) - W_F \Delta H_F \qquad (3.19)$$

The convection term contains C_{PF} rather than C_P, as it is the fuel vapour which diffuses, while the other species remain nearly stationary (see Appendix A for mathematical development). Applying the coordinate transformation, the following form is obtained:

$$\rho C_P \frac{\partial T}{\partial t} + \left[\frac{\rho v C_{PF}}{R} - \rho C_P \zeta \frac{\dot{R}}{R} \right] \frac{\partial T}{\partial \zeta} = \frac{1}{\zeta^2 R^2} \frac{\partial}{\partial \zeta} \left[\zeta^2 k \frac{\partial T}{\partial \zeta} \right] - W_F \Delta H_F \quad (3.20)$$

where $\dot{R} = \frac{dR}{dt}$. The $\zeta \frac{\dot{R}}{R}$ term represents a flux of energy relative to the new coordinate system, caused by the fact that this new coordinate system is no longer fixed in space. Substituting G into the ρv ($G = \zeta^2 \rho v$) and $\dot{R}/R$ (see next section) terms and multiplying by ζ^2/C_P yields the final form of this equation:

$$\zeta^2 \rho \frac{\partial T}{\partial t} + \frac{G}{R} \left(\frac{C_{PF}}{C_P} + \frac{\rho}{\rho_l} \zeta^3 \right) \frac{\partial T}{\partial \zeta} = \frac{1}{R^2} \frac{k}{C_P} \left(\zeta^2 \frac{\partial T}{\partial \zeta} \right) - \frac{W_F \zeta^2}{C_P} \Delta H_F \quad (3.21)$$

3.5 Liquid Phase Equations

In addition to the gas phase transport equations the following equations are required for determining droplet heating and the rate of droplet surface recession.

1. A mass balance at the droplet surface describes the mass flux of vapour from the droplet surface or the recession rate of the droplet surface.

$$\frac{dR}{dt} = \frac{G}{\rho - \rho_\ell} \tag{3.22}$$

Since the density of liquid is much greater than the vapour density, the equation may be reduced to

$$\frac{dR}{dt} \approx \frac{-G}{\rho_\ell} \tag{3.23}$$

2. An energy balance at the droplet surface describes the transient heating of the liquid droplet.

Energy absorbed in droplet + Energy for evaporation = Heat flux to droplet

$$\frac{4}{3}\pi R^3 \rho_\ell C_{P\ell} \frac{dT_\ell}{dt} + 4\pi R^2 G h_{fg} = 4\pi R^2 Q \tag{3.24}$$

Rearranging leads to

$$\frac{dT_\ell}{dt} = \frac{3}{R\rho_\ell C_{P\ell}} (Q - G h_{fg}) \tag{3.25}$$

where the heat flux Q to the droplet surface is calculated from the temperature gradient at the surface (conduction) and the thermal radiation transfer to the droplet.

$$Q = k \left.\frac{\partial T}{\partial r}\right|_R + Q_{RAD} \tag{3.26}$$

The radiative transfer is calculated using the Stefan-Boltzmann equation.

$$Q_{RAD} = \sigma \alpha_d \left(T_{RAD}^4 - T_R^4\right) \tag{3.27}$$

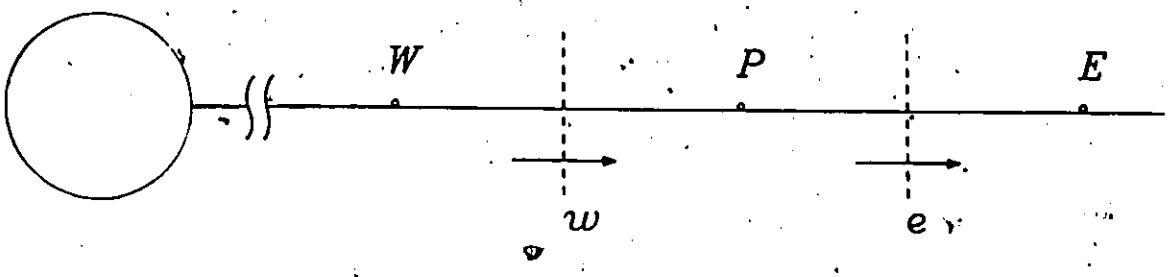

Figure 3.1: Diagram of cell

3.6 Development of the Finite Volume Solution

3.6.1 Finite volume solution

The only equation requiring a numerical solution is now the energy equation. A finite volume technique based on the methods of Patankar [28] was chosen, in which the governing differential equation is integrated over a radial control volume (see Figure 3.1) to obtain a discretization equation of the following form:

$$aT_P = bT_E + cT_W + d \tag{3.28}$$

Here P is the point being solved for and W and E are its west and east neighbours.

The coefficients a, b, c and d are obtained by integrating each term in equation 3.20 over the control volume shown in Figure 3.1 and over the time interval t to $t + \Delta t$. The complete solution is shown in Appendix B. The coefficients must always be positive in order that the system remain stable [28]; to ensure this a hybrid differencing scheme is used for the convection and diffusion terms, giving

$$b = [AMAX(C_e, D_e) - C_e]\,\Delta t \tag{3.29}$$

$$c = [AMAX(C_w, D_w) + C_w]\,\Delta t \tag{3.30}$$

where C and D represent convection and diffusion respectively, and are given by

$$C_e = \frac{G}{2R}\left[\frac{\rho_e}{\rho_\ell}\zeta_e^3 + \frac{C_{PF}}{C_P}\right] \tag{3.31}$$

$$C_w = \frac{G}{2R}\left[\frac{\rho_w}{\rho_\ell}\zeta_w^3 + \frac{C_{PF}}{C_P}\right] \tag{3.32}$$

$$D_e = \frac{k}{R^2 C_P}\left[\frac{\zeta_e^2}{\zeta_E - \zeta_P}\right] \tag{3.33}$$

$$D_w = \frac{k}{R^2 C_P}\left[\frac{\zeta_w^2}{\zeta_P - \zeta_W}\right] \tag{3.34}$$

At low flow rates the present formulation of the convection term uses central differencing. It assumes that the value of T convected into the cell is T_w, midway between T_W and T_P, so that

$$T_e - T_w = \frac{T_E + T_P}{2} - \frac{T_W + T_P}{2} = \frac{T_E - T_W}{2} \tag{3.35}$$

However, this causes the coefficient b to become negative when

$$\frac{C_e}{D_e} > 1. \tag{3.36}$$

The quantity C_e/D_e can be recognized as a Peclet number

$$\frac{C_e}{D_e} \propto \frac{GRC_{PF}}{k} = P_e \tag{3.37}$$

For "large" Peclet number, central differencing becomes unrealistic, and the numerical scheme becomes unstable, because a negative b implies that an increase in T_E will cause T_P to decrease [28]. A more realistic scheme is then upwind differencing, which assumes that the value of T upstream from the control volume boundary is convected into the cell, so that $T_e - T_w = T_P - T_W$, and

$$\begin{aligned} \mathrm{b} &= 0 \\ \mathrm{c} &= 2C_w\Delta t \end{aligned}$$

This means that the flow is sufficiently fast that T_E has no more effect on T_P. This is the case when convection of heat at the cell boundary is much greater than diffusion, so that diffusion becomes negligible. The present scheme, as can be seen from Equations 3.29 and 3.30, switches to upwind differencing whenever $(C_e/D_e) > 1$. This was found to happen occasionally in the initial development of the temperature profile from the step change between the temperature at the droplet surface and the temperature of the furnace. Hybrid differencing is a standard numerical technique in the solution of flow problems [28].

The remaining coefficients in Equation 3.28 are

$$\mathrm{a} = \frac{\rho}{3}\left(\varsigma_e^3 - \varsigma_w^3\right) + \mathrm{b} + \mathrm{c} \tag{3.38}$$

and

$$\mathrm{d} = \frac{\rho}{3}\left(\varsigma_e^3 - \varsigma_w^3\right) T_P^0 - \left(\varsigma_e^3 - \varsigma_w^3\right) \frac{W_F \Delta H_F}{3C_P} \Delta t \tag{3.39}$$

where T_P^0 represents the temperature from the previous time step. Patankar [28] outlines the different schemes that can be used for modelling the time step; two of these are the explicit and implicit schemes. The explicit scheme means that T_P is not related to other unknowns such as T_E or T_W, but is explicitly obtainable in terms of the known temperatures T_P^0, T_E^0, T_W^0, while in the implicit scheme, T_P is linked to the unknowns T_E and T_W, and the solution of a set of simultaneous equations is necessary. The convenience of the explicit scheme is offset by a serious limitation: for the system to remain stable (the coefficient of T_P^0 to remain positive), the time step Δt would have to be smaller than 5×10^{-5} second. This is an unreasonable restriction; 10^5 time steps would be required to obtain ignition. Therefore the temperature equation must be solved implicitly, where there is no limitation on time step.

The moving coordinate term $(\rho\varsigma^3/\rho_l)$ has been included in the convection term because it represents a flow through the control volume boundary due to motion of the ς coordinate system in space. Failure to do this resulted in unstable solutions at large ς.

3.6.2 Grid spacing

Because of the nature of the temperature profile it is necessary to have more points near the droplet surface and fewer points far from the surface.

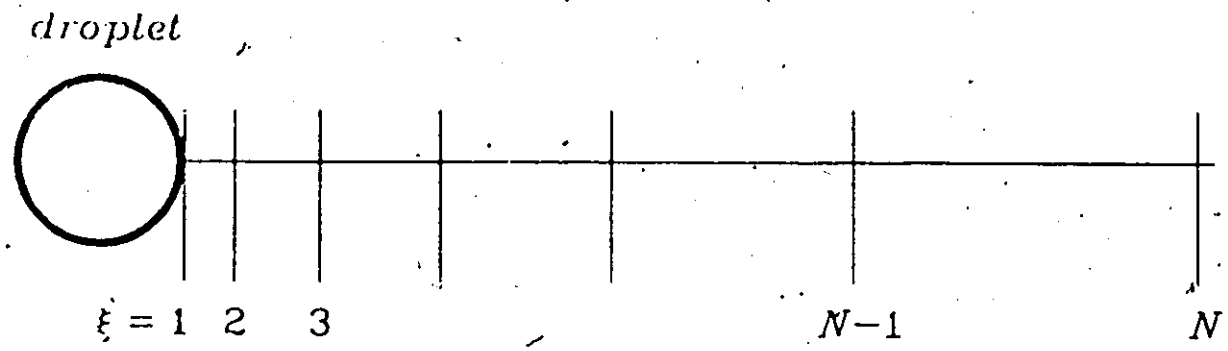

Figure 3.2: Exponentially spaced grid

This is obtained by using an exponentially spaced grid as shown in Figure 3.2.

$$\varsigma(i) = exp\left[\frac{\ell n\, \varsigma(N)}{N-1}(i-1)\right] \tag{3.40}$$

where N is the number of grid points.

3.6.3 TriDiagonal-Matrix Algorithm

When applying the discretization equation (Equation 3.28) to the system, a series of equations is obtained which take the form of a sparse matrix. The solution of this matrix is obtained using a standard Gaussian-elimination method; due to the simple form of the matrix the elimination process takes the form of a convenient algorithm developed by Patankar [28], the TriDiagonal-Matrix Algorithm, TDMA (see Appendix C). This algorithm solves for the temperature profile surrounding the droplet when the temperature at the droplet surface and at infinity are known.

3.6.4 Chemical reaction modelling

The reaction rate is modelled using a single step Arrhenius equation, therefore the rate of reaction term for fuel in the energy equation (Equation 3.20)

is as follows:

$$W_F = -M_F K \rho^{a+b} \frac{Y_F^a Y_O^b}{M_F^a M_O^b} exp\left(-\frac{EA}{RT^0}\right) \tag{3.41}$$

The temperature is set equal to the value T^0 at the beginning of the time step (time t) rather than at $t + \Delta t$. This is essential for stability of the numerical solution [28].

Previous ignition models [32,18,35] have all assumed the reaction was of second order (first order in fuel and oxygen, $a = b = 1$); the single exception has been the model of Faeth and Olson [6]. Recent work in the study of the kinetics of combustion reactions has shown that this is a poor assumption. The reaction orders used in the present model are therefore based on a study by Westbrook and Dryer [36] in which various reaction kinetic schemes are compared in a detailed model of laminar flame propagation. By comparing predicted and measured flame speeds, the kinetic constants a, b, K and EA were deduced for a one-step reaction. Their recommendation for reaction orders for paraffins have been adopted here; the reaction orders for the aromatic hydrocarbons used had to be adjusted for use in the present model. Westbrook and Dryer [36] also recommend values for the pre-exponential factor and the activation energy, but these did not fit the present experimental data; they were fitted for each fuel. This will be further discussed in Section 5.2.

3.6.5 Heat flux calculation

The temperature gradient at the droplet surface is required for calculating the heat flux Q (Equation 3.26), therefore the method of estimating this gradient influences Q directly. A linear variation of temperature between grid points was found to be inadequate; a much better prediction of Q was had by fitting an exponential function to the temperature profile near the surface of the droplet (see Appendix D). The resulting equation is

$$\left.\frac{dT}{dr}\right|_R = \frac{\ell n(1-\theta_2)}{R(1-\zeta_2)} (T_\infty - T_R) \tag{3.42}$$

where $\theta_2 = \frac{T_2 - T_R}{T_\infty - T_R}$.

3.7 Properties

As mentioned previously all properties but the local mixture density are assumed constant and are calculated at a reference temperature and concentration.

3.7.1 Heat capacity

The heat capacity at constant pressure for fuel, O_2 and N_2 is calculated using the ideal gas polynomial equations given in Reid,Prausnitz and Sherwood [30, page 226].

3.7.2 Diffusion coefficient

The method used to estimate the diffusion coefficient is the Chapman-Enskog theory with the Lennard-Jones 12-6 Potential [30, page 549]

$$D_{AB} = 1.858 \times 10^{-3} T^{3/2} \frac{[(M_A + M_B)/M_A M_B]}{P \sigma_{AB}^2 \Omega_D} (1 \times 10^{-4}) \tag{3.43}$$

where the subscripts A and B refer to air and fuel respectively. Ω_D is a function only of $\kappa T/\epsilon_{AB}$ and was found using the relation of Neufeld et al. [30, page 549]:

$$\Omega_D = \frac{A}{T^{*B}} + \frac{C}{expDT^*} + \frac{E}{expFT^*} + \frac{G}{expHT^*} \tag{3.44}$$

where $T^* = \kappa T/\epsilon_{AB}$. The simple equations shown below are used for obtaining the binary values σ_{AB}, ϵ_{AB}:

$$\epsilon_{AB} = (\epsilon_A \epsilon_B)^{1/2} \tag{3.45}$$

$$\sigma_{AB} = \frac{\sigma_A + \sigma_B}{2} \tag{3.46}$$

The characteristic Lennard-Jones energy ϵ and length σ are estimated using:

$$\frac{\epsilon}{\kappa} = T_c\,(0.7915 + 0.1693\omega) \tag{3.47}$$

$$\sigma = \left(\frac{T_c}{P_c}\right)^{1/3} (2.3551 - 0.087\omega) \tag{3.48}$$

where κ is Boltzmann's constant. The constants A to H in Equation 3.44 are given in Reid et al. [30, page 550] along with the acentric factor ω [30, pages 629–665] in Equations 3.47 and 3.48.

3.7.3 Thermal conductivity

The thermal conductivity of the pure components (air and fuel) is estimated using the Eucken equation [30, page 473]

$$k = [C_V + 4.47]\,\frac{\eta}{M} \tag{3.49}$$

where η is the dynamic viscosity in poise. The heat capacity at constant volume is calculated from the fact that

$$C_V = C_P - \mathcal{R} = C_P - 1.99 \tag{3.50}$$

where C_V and C_P are in cal/mol K. The viscosity required is estimated using the Chapman-Enskog theory with the Lennard-Jones 12-6 Potential

$$\eta = 26.69\frac{\sqrt{MT}}{\sigma^2\Omega_v} \tag{3.51}$$

where Ω_v is calculated using an equation proposed by Neufeld et al. [30, page 396]

$$\Omega_v = \frac{A}{T^{*B}} + \frac{C}{expDT^*} + \frac{E}{expFT^*} \tag{3.52}$$

The constants A to F are listed in Reid et al. [30, page 396] while ϵ and σ are calculated using Equations 3.47 and 3.48 respectively.

The thermal conductivity of the air-fuel vapour mixtures is estimated with the Mason-Saxena equation [30, page 508]

$$k_m = \sum_{i=1}^{n} \frac{y_i k_i}{\sum_{j=1}^{n} y_i A_{ij}} \tag{3.53}$$

where k_m and k_i are the thermal conductivity of the mixture and pure component i respectively, also

$$A_{ij} = K\frac{\left[1 + (k_{tr_i}/k_{tr_j})^{1/2}(M_i/M_j)^{1/4}\right]^2}{[8(1 + M_i/M_j)]^{1/2}} \tag{3.54}$$

The numerical constant K is taken as unity and the monatomic value of thermal conductivity k_{tr} is calculated using

$$\frac{k_{tr_i}}{k_{tr_j}} = \frac{\eta_i}{\eta_j}\frac{M_j}{M_i} \tag{3.55}$$

3.7.4 Density

The density of the local gas mixture is not assumed constant; it is estimated using the ideal gas law.

$$\rho = \frac{MP}{\mathcal{R}T} \tag{3.56}$$

where M is the local mixture molecular weight:

$$M = \frac{1}{\sum(Y_i/M_i)} \tag{3.57}$$

and the temperature is the temperature at the point P from the previous time step.

3.7.5 Absorptivity of droplet

Hottel et al. [11], who performed combustion experiments on droplets of heavy liquid fuels, measured the infrared absorption spectra of each of the fuels and from this calculated the absorptivities of droplets for 1000 $^{\circ}C$ black body radiation. He allowed for the refraction of radiation by the liquid and for the multiple reflections of the radiation at the droplet surface and obtained curves of total absorptivity of liquid spheres as a function of droplet radius for pure hydrocarbons. The curve obtained for absorption with both refraction and external reflection was fitted to give approximations to the absorptivity of the droplets used in the present model; the fitted equation is

$$\alpha_d = 0.89\left(1 - e^{-5.4R}\right) \tag{3.58}$$

where R is in mm and α_d is absorptivity of the droplet required in the Stefan-Boltzmann equation. Hottel et al. [11] found little difference in absorption characteristics of the pure fuels tested, and presented only one curve for all.

The absorptivity of the large droplets used in the present work is typically about 0.8, so that radiation makes a significant contribution to droplet heating. Only one other droplet ignition model [6] has included radiant heating.

3.8 Solution of the System of Equations

3.8.1 Flow chart

The equations developed in the previous section constitute a set which must be solved at each time step. The sequence of calculation used is shown in Figure 3.3. Since an implicit scheme was chosen for the solution of the temperature equation, an iteration must be performed at each time step.

As a safety measure, a method is required to prevent the temperature and the mass flux from becoming too large. The following limits the evaporation rate:

$$Gh_{fg} \leq Q$$

$$T < T_{BOIL}$$

When iterating for the droplet temperature at the end of a time step, a relaxation factor is necessary for the system to remain stable; without it, the temperature may oscillate, delaying convergence. A value of 0.30 was found to give quick and reliable convergence.

As an ignition criterion in the present model, ignition is said to occur if the temperature anywhere in the gas phase exceeds 2500 K, which is approximately the adiabatic flame temperature.

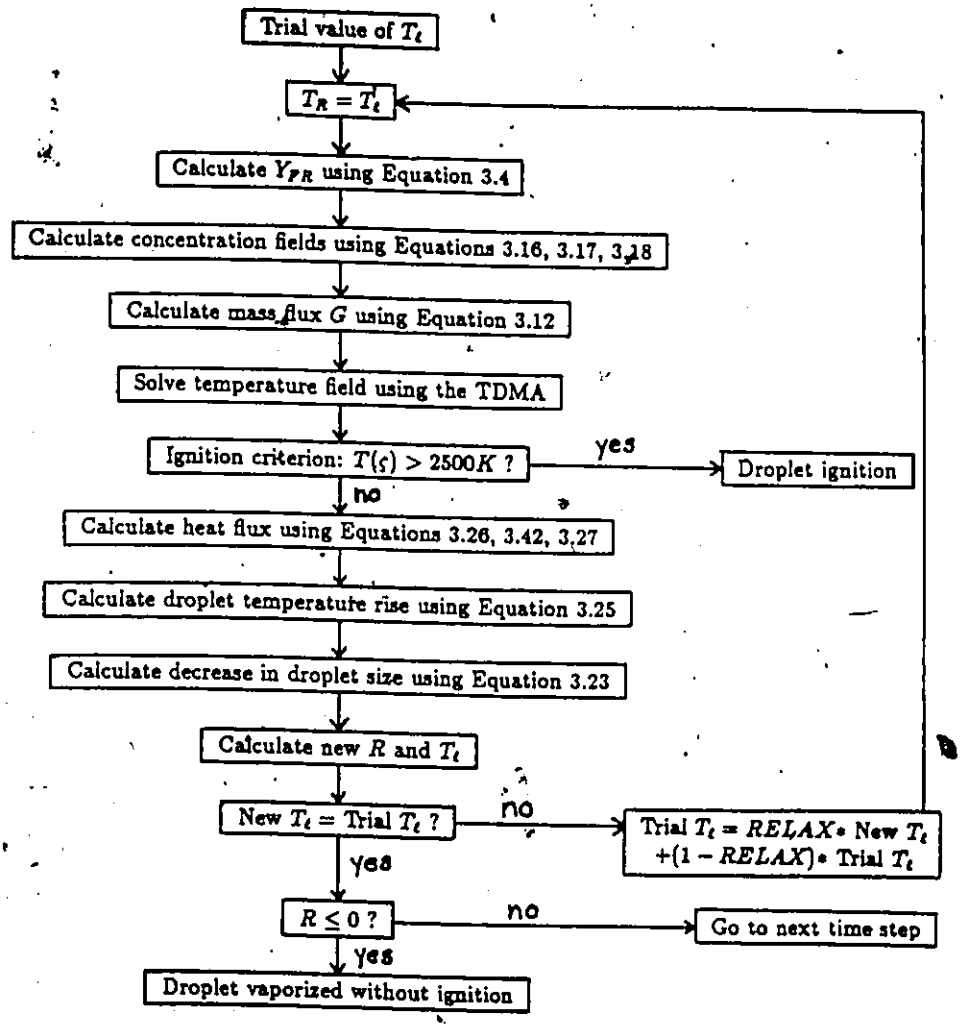

Figure 3.3: Flow Chart for Ignition Model

3.9 Checking the Program

Once the model was programmed it had to be checked for accuracy. For the following tests the temperature transient term was removed from the energy equation, the reaction term was set equal equal to zero and a constant radius was used to suppress the moving coordinate term.

The first test was to compare the temperature profiles obtained with theoretical temperature profiles for constant property quasi-steady vaporization which are generated from the classical solution [13].

$$\Theta = \frac{T - T_R}{T_\infty - T_R} = \frac{B^{(1-\frac{1}{r})} - 1}{B - 1} \tag{3.59}$$

where

$$B = \left[\frac{1}{1 - Y_R}\right]^{Le_F}$$

and

$$Le_F = \frac{\Gamma C_{PF}}{k}$$

is the Lewis number of the fuel. Results showed that the two sets of profiles obtained were very similar; the maximum differences were in the order of 3%.

The second test was to compare the conductive heat flux to the surface obtained from the program with that from a quasi-steady solution:

$$\frac{Q}{C_{PF}(T_\infty - T_R)} = \frac{G}{exp\left(\frac{GC_{PF}R}{k}\right) - 1} \tag{3.60}$$

where

$$G = \frac{\Gamma}{R} ln(1 + B)$$

and

$$B = \frac{Y_{FR}}{1 - Y_{FR}}$$

This test is required to verify whether or not the boundary condition at the droplet surface is adequate. The heat flux from the program is calculated from the temperature gradient at the droplet surface. Results showed that the two heat fluxes obtained differed by only 1.5%.

A third test was performed to determine the best grid size. The program was run with coarser grids (down to 15 points) and finer grids (up to 60 points) and the temperature profiles were compared. Results showed only 2.6% difference between temperature profiles for 20 and 35 grid points. The final decision was therefore to use 20 grid points so as to reduce computer time and minimize error.

The fourth test was to examine the temperature profile at large radius. Without the transient term the profile should be nearly flat toward the outer boundary. Results showed this to be true when the outer boundary is situated at 500 droplet radii; this also allows sufficient room for the concentration profiles to develop as though the system boundary were infinity.

Once these tests were completed, the droplet radius was allowed to vary; this started the moving coordinate term. The temperature profiles obtained did not vary significantly from those with constant radius. Little difference was expected from letting the droplet radius vary, because the droplet surface recedes slowly. At this point the transient term was added to the solution; again temperature profiles obtained did not vary significantly from those without transient heating. The fact that transient heating of the droplet (liquid phase) has little effect on temperature profiles gives confirmation of the correctness of the quasi-steady assumption. The reaction term was then added at this point.

The fifth and final test was to determine the best time step suited for the purposes of the model. Tests were performed for time steps varying from 0.005 to 0.1 second and results showed little difference 3%) in going from a time step of 0.02 to anything lower. Therefore a time step of 0.02 second was chosen for the present model.

Chapter 4

Experimental Apparatus and Procedure

The experimental technique selected was that of the single droplet suspended on the end of a thin quartz fibre. The method used is similar to that used by Kobayasi [14] and Nishiwaki [26] in which a furnace is rolled over the suspended droplet fast enough to achieve a step change in temperature. This technique was selected because of the simplicity with which experiments could be set up and performed. The alternative technique, that of freely falling droplets, was rejected because of the effects of forced convection and the difficulty of observing the droplets.

A sketch of the experimental apparatus is shown in Figure 4.1. It consists of (a) a furnace for providing high ambient temperatures; (b) a propulsion system for moving the furnace over the droplet; (c) an ignition detection system for recording ignition as it occurs and measuring ignition delay; (d) a photographic system for measuring droplet diameters; (e) a droplet suspension system, and (f) a system for measuring the temperature of the air inside the furnace.

4.1 The Furnace

The furnace used in this study is constructed of fire brick 5 cm thick and encloses four heating elements, two in the top and two in the bottom. These elements measure 17.8 cm by 7.0 cm and are rated for 57.5 volts and 240 watts each. Because of the high temperature requirements and the

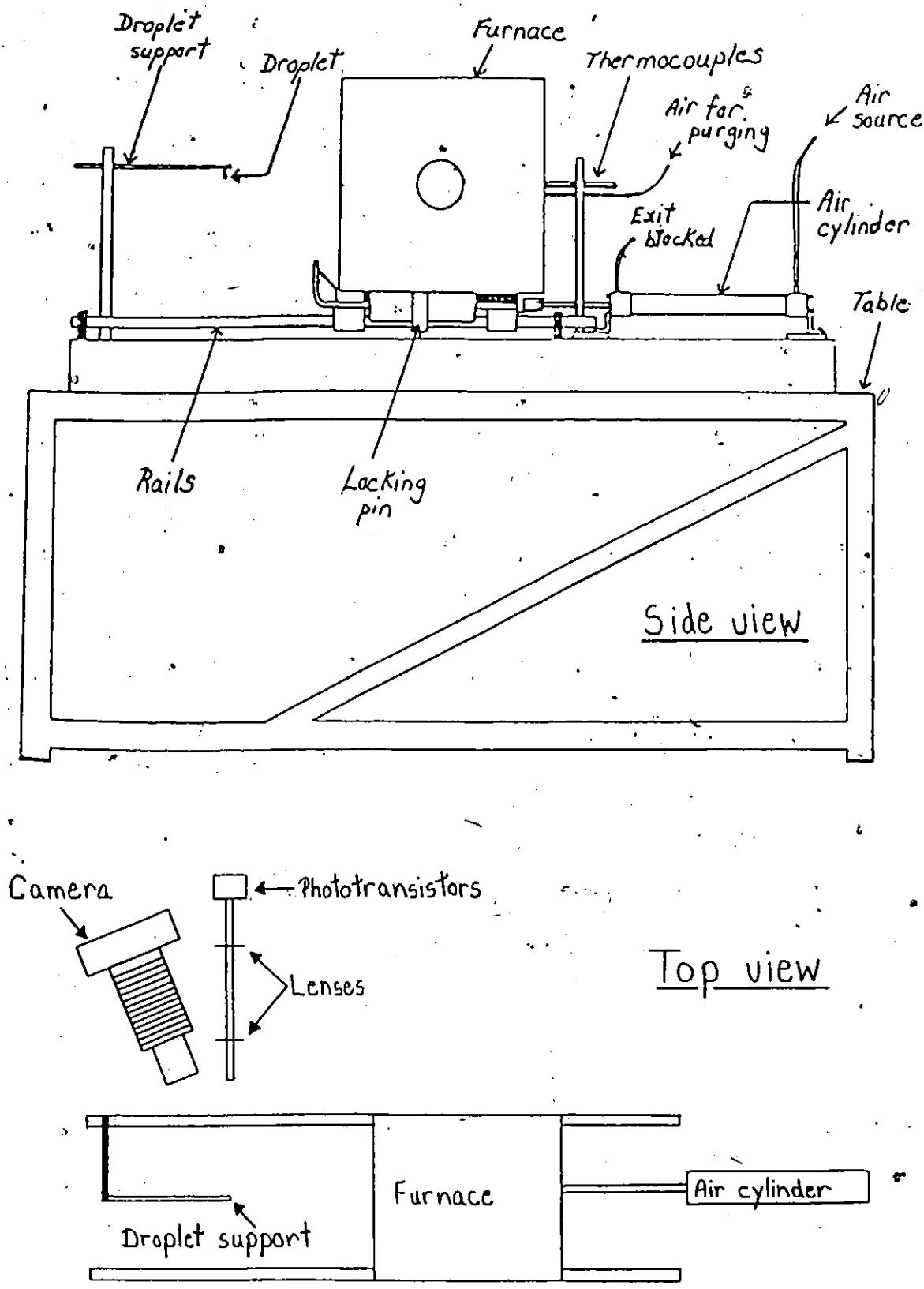

Figure 4.1: Experimental apparatus

limited output of the elements, the furnace is insulated on four sides with 3.8 cm of fiberglass insulation and on one side with 1 cm thick asbestos board. The bottom of the furnace is not insulated because of the way it is mounted. In opposite sides of the furnace there are two quartz windows, each measuring 3.2 cm in diameter, required for detecting ignition and observing the ignition process. Vertical slits measuring 4.0 cm by 1.0 cm are located in the front and back walls of the furnace. One serves as an entrance for the droplet support, the other as an entrance for the temperature probes and a purging tube. The dimensions of the inside of the furnace are 17.8 cm long by 14.0 cm square and are shown on the cross-section of the furnace in Figure 4.2. To ensure that there is an adequate amount of air inside the furnace for ignition to occur, the furnace is purged with an air stream for 45 seconds before each experimental run.

The furnace, which is mounted on rails, must be moved forward quickly to cover the droplet and start ignition; the furnace motion must be sufficiently fast that the droplet experiences a step change in temperature on entering the furnace. This is done using an air cylinder. A pressurized air bottle is used as the source of air, and the exit of the cylinder is blocked to create a cushion and stop the furnace. At the end of the air cylinder stroke the furnace is locked into place by a spring-loaded pin which drops into a hole in the guide rail. The speed of the furnace can be varied to some extent by regulating the pressure of the driving air. Care must be taken to minimize the vibration produced when the furnace comes to a stop; this is done by adjusting the driving pressure and the location of the locking pin hole so that the furnace comes to a stop just as the pin falls into place. As a further safeguard against vibration the entire apparatus is secured to a table of 2.5 cm steel plate.

4.2 Ignition Detection

Ignition detectors measure the onset of visible light, which is emitted by soot particles at high temperatures. Measured ignition delay therefore includes time for reactions to generate soot and raise the temperature to approximately the flame temperature. However, because ignition is characterized by a very sudden temperature rise (see Figure 4.3), this is not an appreciable source of error.

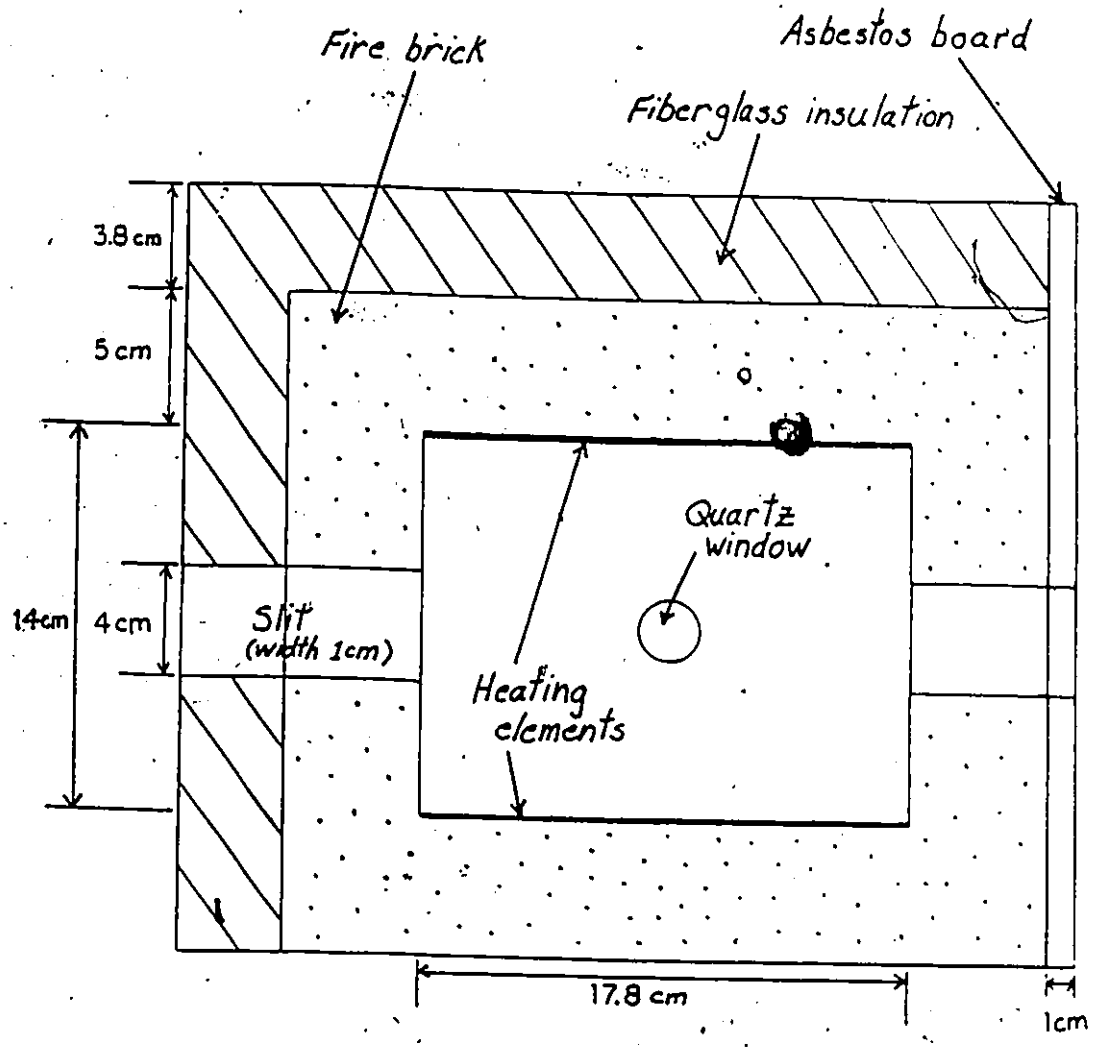

Figure 4.2: Cross-section of the experimental furnace

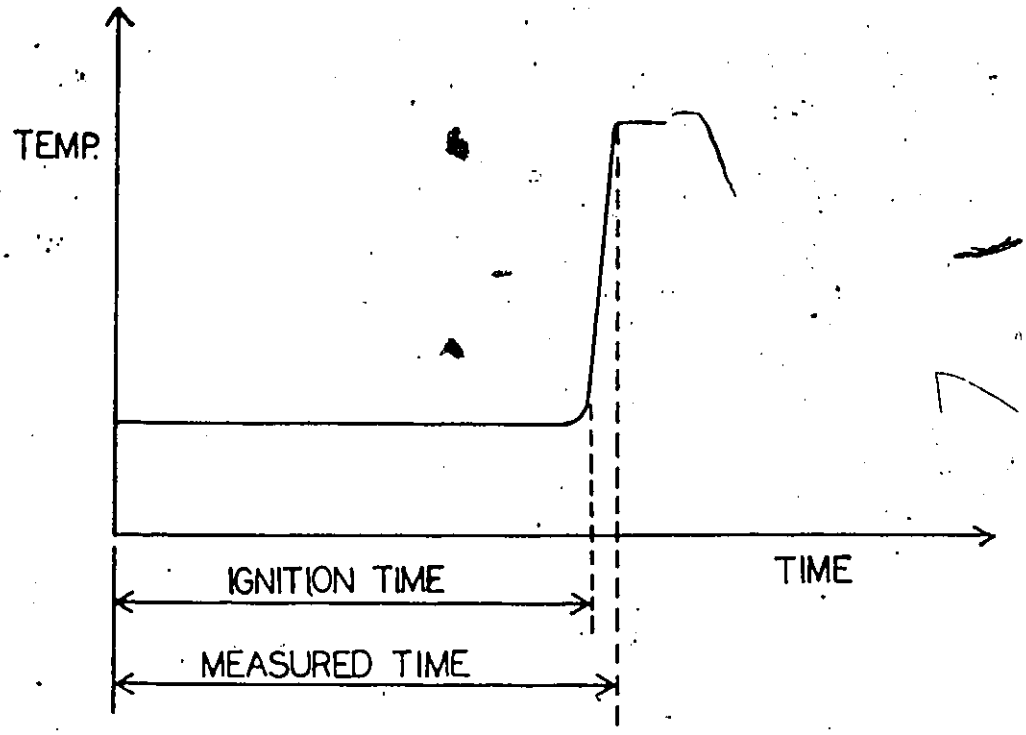

Figure 4.3: Sudden temperature rise characterizing ignition

The emission of visible light from the gas around the droplet, marking the onset of ignition, is detected by a series of three phototransistors. Three phototransistors are required, because as the droplet ignites the flame first appears below the droplet (fuel vapour descends due to gravity) and then moves upward due to natural convection. Because of this the flame moves in and out of the field of view of a single phototransistor. The phototransistors selected have a very short response time (1.5 μs) [4], therefore minimizing possible error in the measured ignition delay time. The phototransistors are connected to a digital storage oscilloscope, which is triggered with the use of a microswitch positioned so that the oscilloscope is triggered when the droplet has traveled half way through the opening in the front wall of the furnace. The oscilloscope then records the signal from the phototransistors as the latter detect the light emitted upon ignition of the fuel. The light is focussed onto the phototransistors with the use of two lenses, the first making the light parallel and the second converging it onto the phototransistors.

4.3 Droplet Suspension and Size Measurement

Droplets are supported on a quartz fibre with a bead at the end of it. The bead allows the droplets to be larger and to hang free of the end of the fibre. The fibre and the bead are respectively 0.18 to 0.22 mm and 0.58 to 0.61 mm in diameter. The quartz fibres are made from a piece of quartz rod, melted at one end to form a bead. The beads to be used are then measured using a micrometer to ensure that they all have the same diameter. The fibre is securely fixed to the support by being placed between two small stainless steel plates which are tightened together with a stainless steel screw. The support is fixed to the framework. For consistency of droplet sizes, droplets to be suspended on the quartz fibre are generated using a calibrated microlitre syringe. Droplet volumes used varied from 0.7 to 3.0 μl.

The droplet diameter is measured by photographing the droplet at a magnification of about 2.5. The photographic equipment used consists of a 35 mm camera, a 135 mm telephoto lens and a bellows. Droplets are photographed with back lighting to give the droplet contour only. A scale supported in the same plane as the droplet is also photographed before the beginning of a series of experiments. The image of the droplet on the negative is projected using a fixed film projector and measured by referring to the projection of the scale.

The droplet undergoes an oval deformation due to gravity, and its diameter is defined as that of an equivalent sphere as shown in Figure 4.4. This can be done by measuring along two axes and equating the volumes [14]; each axis is measured with an accuracy of +/- 0.05 mm.

$$D = (\ell_1 * \ell_2^2)^{1/3}$$

4.4 Temperature Measurement

The temperature measured using a simple thermocouple suspended in a furnace does not necessarily represent the actual ambient air temperature, as the measured temperature is also affected by radiant transfer with the

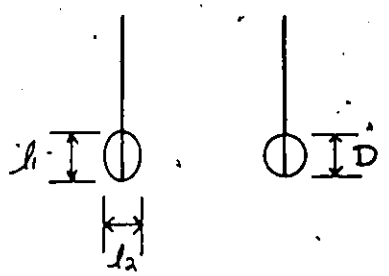

Figure 4.4: Equivalent diameter of droplet

hot furnace walls. To correct for this, a radiation correction factor is calculated for each measured temperature, which is obtained by performing a heat balance on the thermocouple (see Appendix E). The final result of this development contains three unknown variables; therefore, by measuring temperatures using three temperature probes with different bead diameters, a system of three equations is obtained which can be solved to give the true gas temperature. The temperature probes used are chromel-alumel with beads measuring 0.37, 1.25 and 1.88 mm in diameter. They are inserted together into the furnace through the slit in the back wall and are positioned to measure temperatures in the middle of the furnace. For ease of measurement the three temperature probes are connected to a selector switch. The correction to the measured temperatures was small: the readings of the three beads were always within 2 $^{\circ}C$ of one another, and the calculated true gas temperature was within 2 $^{\circ}C$ of the temperature measured by the smallest bead. In the present case, the measured temperatures were lower than the true gas temperature, indicating that the average radiating temperature of the furnace was lower than the gas temperature; this is due to the fact that only two of the six furnace walls are heated.

The temperature readout could be read to the nearest degree; with the correction for radiation, the error in the gas temperature is estimated at +/- 1°C.

4.5 Choice of Fuels

Fuels for the present experiments were chosen so as to represent a wide range of both boiling temperature and chemical reactivity. To separate the effects of chemical kinetics from those of physical processes, pure fuels with similar chemical properties but differing boiling points, and of differing chemical reactivity but similar boiling point were selected. Although boiling point data are widely available, very little information on the relative chemical reactivities of common hydrocarbon fuels is available.

The most readily available data for comparing chemical reactivities of fuels are values of minimum spontaneous ignition temperatures obtained from Table 32 in NACA Report 1300 [24]. These data were obtained from ignition experiments carried out at relatively low temperatures on liquid fuels in a procedure similar to the ASTM standard test for ignition temperature [1]. The conditions of the test are such that the fuel completely vaporizes before significant reaction begins, so that the minimum ignition temperature should be a function only of the chemical behaviour of the fuel. These data were then used as a basis for fuel selection. It was determined that straight chain hydrocarbons with five or more carbons all have similar spontaneous ignition temperatures and therefore similar chemical reactivity. Normal paraffins have the lowest ignition temperatures and therefore the highest reactivities, while unsaturated hydrocarbons, isomers, and aromatics have higher ignition temperatures.

The final choice of fuels was based on the considerations above. The fuels chosen are listed in Table 4.1 together with their properties. The reasons for choosing these fuels are:

1. α-methylnaphthalene and n-hexadecane together formerly defined the cetane scale for Diesel fuels.

2. Iso-octane and n-heptane define the octane number for gasolines.

3. Results from ignition experiments using these fuels are readily available for comparison [6,33,26].

Table 4.1: Liquid Fuel Properties

Fuel	Boiling Point ($^{\circ}C$)	Spontaneous Ignition Temperature ($^{\circ}C$)
n-heptane	98.4	247.2
n-hexadecane	287.5	230.0
iso-octane	99.3	418.0
benzene	80.1	591.7
α-methylnaphthalene	244.4	547.2

4.6 Experimental Procedure

Before performing the suspended droplet experiments it is required to (a) focus the camera on the suspended quartz bead; (b) photograph the scale in the same plane as that of the bead; (c) ensure that the phototransistors are in alignment with the quartz bead; and (d) adjust the pressure of the air required for the air cylinder, to reduce the amount of vibration. Having purged the furnace for 45 seconds, the temperature inside is allowed to rise to that required and the furnace is then ready to perform an experiment. The temperatures from the three probes are recorded, a droplet (0.9 - 1.7 mm) of pure fuel is placed on the end of the fibre and is photographed at the same instant the furnace is released. Prior to the experiment, a metal plate is hung before the furnace opening to shield the fibre and droplet from thermal radiation; this is removed an instant before releasing the furnace. Since back lighting is necessary for photographing the droplet, after having released the furnace the operator must stand in the path of the light in order for it not to be detected by the phototransistors. As the droplet enters the furnace, the oscilloscope is triggered by the microswitch and is ready to receive a signal from the phototransistors. As ignition occurs, it is observed through one of the quartz windows in the side of the furnace, and the phototransistors detect the visible light emitted; the oscilloscope receives the signal and the time required for ignition is read directly off the oscilloscope.

The time required for the droplet to traverse the furnace from the middle of the entrance slit where the oscilloscope is triggered to the window is

approximately 0.16 seconds and is consistent for all experiments. For most of this time the droplet is exposed to furnace temperature, and the very short time required for the droplet to pass through the varying temperatures of the inlet slit is therefore not considered to be a significant source of error.

Since the droplet is suspended at the end of a fibre it burns in a gravitational field, and buoyancy introduces some effects of flow around the droplet when compared to a spherically symmetrical droplet. However, other investigators show that the effects of convection on ignition delay times are small: Faeth and Olson [6], who performed tests at "0" and "1" gravity, show that the effects of buoyancy are not large at atmospheric pressure, while calculations of ignition times by Sangiovanni [35] show only a slight effect of the mode of gas-phase heat and mass transfer (diffusion, natural, or forced convection). From these results also, the brief period of forced convection of heat to the droplet as it enters the furnace has a negligible effect on ignition time.

4.7 Effect of Fibre

Experiments performed by Kumagai [15] showed a dependence of the evaporation constant on fibre materials and diameters. Even though the thermal conductivity of quartz is low, its effects on the evaporation constant cannot be disregarded. The true value of the evaporation constant should be somewhat smaller than that determined when the droplet is suspended on the end of a fibre, as heat is conducted through the stem of the fibre to the middle of the droplet and causes its temperature to increase more rapidly and evaporate more quickly. Results obtained by Kumagai [15] for burning droplets show that for fibres of the same size as used in the present experiments, the evaporation rate is approximately 10% higher than it should be. Since the temperatures around evaporating droplets prior to ignition are much lower than those for burning droplets, the error in the present experiments should be much smaller. It is not possible to eliminate this effect entirely, but the fibres were made as thin as possible, and consistency achieved by keeping fibre dimensions within narrow tolerances.

Chapter 5

Results and Discussion

5.1 Experimental Results

Droplet ignition tests were conducted to determine the effect of droplet size and ambient air temperature on ignition time for different liquid hydrocarbon fuels. These tests were performed at atmospheric pressure and results were obtained for n-heptane, n-hexadecane, iso-octane, benzene and α-methylnaphthalene. Figures 5.2 through 5.6 show ignition delay as a function of droplet diameter for various temperatures, and Figures 5.7 through 5.11 show ignition delay as a function of 1/T on a semi-log plot. In these figures the experimental results at different temperatures are represented by the different symbols, whereas the curves drawn represent predictions from the mathematical model (see Section 5.2).

As expected the experimental results indicate a pronounced dependence of ignition delay time on the ambient temperature; ignition delay times are shown to increase substantially with decreasing ambient temperature. However, for the range of droplet diameters experimented with, 1.0 through 1.8 mm, the dependence of ignition delay on droplet diameter is very weak. The results show that a minimum critical droplet size is required for ignition to occur; at the ignitable limit the droplet vaporizes completely without ignition occurring, and a somewhat larger droplet is required to produce ignition. In Figures 5.2 and 5.4 through 5.6 the minimum diameter ignition limit is symbolized by $\oplus$. In the case of $n - C_{16}H_{34}$ the limiting diameter was too small to be determined experimentally, because when the droplets became too small they would fall off the fibre.

As shown in Figures 5.2 through 5.6, there exists a minimum temperature at which ignition no longer occurs. This limiting temperature was difficult to measure experimentally because of the difficulty involved in producing consistently sized droplets and controlling the furnace temperature. The last point on the $1/T$ plots (see Figures 5.7 through 5.11) is the lowest temperature at which reliable ignition could be obtained; for the range of droplet sizes used, lower temperatures would result in the droplets vaporizing completely. The physical explanation for this limiting temperature is that the fuel vapour residence time in the zone of ignitable concentration is less than the induction time required for chemical reaction. If the droplet disappears before chemical reaction is induced, the fuel vapour diffuses away from the ignitable zone and ignition cannot occur [6]. For the fuels n-heptane, iso-octane, benzene, and α-methylnaphthalene, Figures 5.2, 5.4, 5.5 and 5.6 respectively show that ignition delay increased slightly as the droplet diameter decreased; the reason for this is that the range of droplet sizes used approached the ignition limit. Similar behaviour has been demonstrated for n-heptane by Saitoh et al. [33]. As shown for n-hexadecane (see Figure 5.3), ignition delay times increased slightly with increasing droplet diameter; this is so when the droplet diameter is much greater than the limiting value.

It appears that ignition time decreases slowly with droplet diameter until the limit is approached, when it rises again. For droplet diameters near the ignitable limit, droplet heating becomes insignificant and chemical reactivity becomes the limiting factor. As the diameter increases the reaction proceeds more rapidly because the ignitable mixture is obtained more quickly and ignition delay decreases. Ignition delay eventually lengthens with an increase in droplet diameter because droplet heating becomes predominant for larger droplets, reducing the influence of chemical properties.

Figures 5.7 through 5.11 show that ignition delay decreases with increasing temperatures; this behaviour is due to the fact that droplets heat up more rapidly and chemical reaction proceeds faster at higher temperatures.

Similar trends in ignition delay times with ambient temperature and droplet size were reported by El-Wakil and Abdou [5], Faeth and Olson [6] and Saitoh et al. [33] for pure hydrocarbon droplets suspended on a filament. Although the trends obtained are similar, the ignition times recorded are consistently almost double the times recorded by Faeth and Olson, and Saitoh et al. It is believed that this difference is due in part to radiant heat.

The experimental apparatus developed by Faeth and Olson [6] and Saitoh et al. [33] did not allow for the droplet to be protected from the radiant heat prior to entering the furnace, whereas in the present apparatus a metal sheet covers the opening in the furnace by which the droplet enters, up to the point in time when the furnace is propelled forward to cover the droplet. A further source of difference lies in the fact that the other authors used smaller furnaces than the present work (Faeth and Olson [6] used a cup that had a minimum inside diameter of $45mm$, and Saitoh et al. [33] used a chamber that was $88mm$ in internal diameter and $200mm$ long), giving rise to possible effects of the surrounding walls. It was observed that as the size of the furnace used by different authors increased, the ignition delays obtained by these approached those obtained in the present experiments.

As the ambient temperature decreased the amount of scatter in the experimental results increased; this is due to the fact that as ignition time increases, natural convection in the vapour surrounding the droplet affects the formation of mixture for a longer period of time, and its effect may vary slightly from one experiment to another.

As shown in Figures 5.2 and 5.4, n-heptane and iso-octane both experience a sudden sharp drop in ignition delay at 790 $°C$ and 810 $°C$ respectively: within a temperature change of 5 $°C$, the ignition delay time dropped by a factor of 2.5. It is suspected that this may mark a radical change in reaction kinetics. As stated by Halstead et al. [8], who studied the chemical reactions that lead to autoignition for hydrocarbon fuels under engine-like conditions using a rapid compression machine and a mathematical model, it has been observed that paraffins undergo a 2-stage ignition process at low temperatures, whereas aromatics do not. When a fuel undergoes 2-stage ignition, the first stage is represented by a cool flame which is simply the accumulation of radicals, whereas the second stage is represented by the emission of visible light and is the event which is recorded for determining total ignition delay. At high temperatures (800 $°C$) the two stages become one (see Figure 5.1) and the total ignition delay decreases radically. It is expected that n-hexadecane would behave in the same fashion if experiments could be performed at higher temperatures; it is also noted that the aromatics, benzene and α-methylnaphthalene, did not show this behaviour.

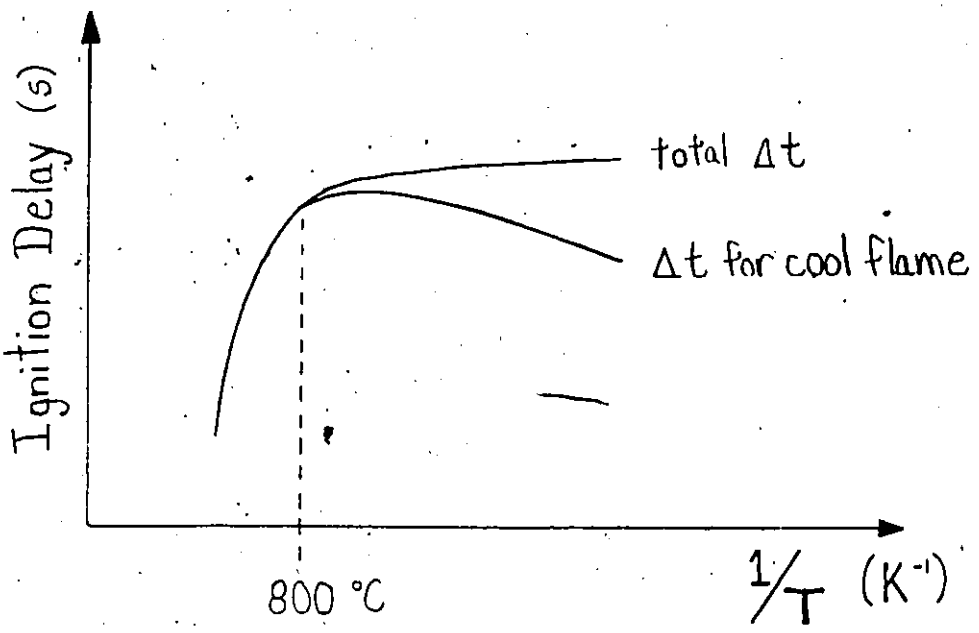

Figure 5.1: Two-stage ignition [8]

Table 5.1: Chemical Reaction Constants of the Fuels

Fuel	K ($\times 10^4$)	EA (kcal/mol)	a	b
n-heptane	0.77	16.20	0.25	1.50
n-hexadecane	0.72	17.71	0.25	1.50
iso-octane	0.90	16.93	0.25	1.50
benzene	0.38	14.33	0.30	1.45
α-methylnaphthalene	1.73	19.28	0.30	1.45
n-heptane	1.72	16.20	0.25	1.50
iso-octane	2.13	16.93	0.25	1.50

5.2 Modelled Results

For each fuel, the values of the pre-exponential factor and the activation energy had to be fitted to the experimental results. By experimenting with the model it was determined that the activation energy changes the slope of the straight line obtained on a plot of $\ell og(t_{ig})$ as a function of 1/T, whereas the pre-exponential factor changes the intercept with the vertical axis. The complete model with reaction was run for a series of furnace temperatures, varying the pre-exponential factor and activation energy separately for each fuel, and the model predictions were then compared to the experimental results. The pre-exponential factors and activation energies fitted are listed in Table 5.1 for all fuels.

The reaction orders (a, b) suggested by Westbrook and Dryer [36] were used for testing the present model, but while these gave satisfactory results for the paraffins, for the aromatic fuels a negative value of a was prescribed, causing the position at which ignition occurred to be at the outer edge of the model grid. The mathematical model was tested with different values of reaction orders for the aromatics in order to obtain ignition within about 20 droplet radii from the surface. In selecting a value of a for the aromatics, the sum $a + b$ was kept equal to that prescribed by Westbrook and Dryer [36]. The reaction orders used are the same for the three paraffin fuels and for the two aromatics; these are listed in Table 5.1 along with the pre-exponential factors and activation energies. The reaction orders for benzene and α-methylnaphthalene required more extensive fitting than the others, and the final values do not give ignition within 20 droplet radii in

all cases.

As shown in Figures 5.2 through 5.11, the mathematical model developed predicts the experimental ignition delays very well within the ignition limits. As expected for the paraffins n-heptane and iso-octane, the results obtained at the highest ambient air temperature cannot be predicted using the same pre-exponential factor and activation energy because of the effect of 2-stage ignition; these can be fitted with a different set of constants (see the last two entries in Table 5.1), which represent different reaction kinetics.

The model fails to predict the experimental ignition limits (minimum diameter as well as lowest temperature required for ignition), because in reality natural convection has some effect on ignition delay, and as the ignitable limit is approached the effect becomes more pronounced. As the diameter of the droplet decreases, the vaporization rate increases and the residence time within the ignitable region decreases. Because of this the vapour diffuses away from the droplet and downward due to natural convection at a faster rate, and the concentration surrounding the droplet is probably less than that predicted by the present model. Therefore for diameters larger than the ignition limit diameter predicted by the model, fuel vapour diffuses too rapidly to form an ignitable mixture. It is also possible that the simple one-step reaction model used here is an inadequate description of the real reaction kinetics near the limit.

As shown in Figures 5.2 through 5.6, the model becomes less accurate as the ignition delay times become longer (as the ambient air temperature decreases). The reason for this is that the ignition times being longer, natural convection affects the vapour surrounding the droplet for a longer period of time. Therefore if the droplet ignites at all it will have a longer ignition delay than that predicted by the model. The effect of natural convection therefore can become important for long ignition delays.

5.3 Comparison of Fuels

As stated previously, the fuels were chosen in a way that would allow the determination of the effect of both chemical and physical properties on ignition delay. In order to determine the effect of chemical properties, fuels with similar physical properties (ie. boiling point) but different chemical properties (ie. spontaneous ignition temperature) were compared. The effect of physical properties was determined by comparing fuels with different physical properties and similar chemical properties.

5.3.1 The effect of chemical properties

In order to determine the effect of chemical properties, the experimental results are compared for two combinations of fuels:

1. n-heptane versus iso-octane versus benzene:
   These three fuels have similar boiling points (98.4°C, 99.3°C, and 80.1°C respectively) but different spontaneous ignition temperatures (247.2°C, 418.0°C and 591.7°C respectively. By comparing Figures 5.7, 5.9 and 5.10, one can see that n-heptane ignites faster than iso-octane, which ignites faster than benzene. The differences in ignition times are not large (example: at 1023 K n-heptane = 0.88 s, iso-octane = 0.93 s, benzene = 0.98 s) but these differences increase as the ignitable limit is approached. The reason for these differences is that n-heptane is more reactive than iso-octane, which is more reactive than benzene.

2. n-hexadecane versus α-methylnaphthalene:
   The two fuels n-hexadecane and α-methylnaphthalene also have similar physical properties but different chemical properties (see Table 4.1). Results show that n-hexadecane ignites slightly faster than α-methylnaphthalene does and the difference in ignition delay decreases as the temperature increases; at higher temperatures ignition occurs too rapidly for the chemical differences to have an important effect.

Chemical properties therefore have little effect on ignition delay, but this effect increases and becomes significant near the ignitable limit.

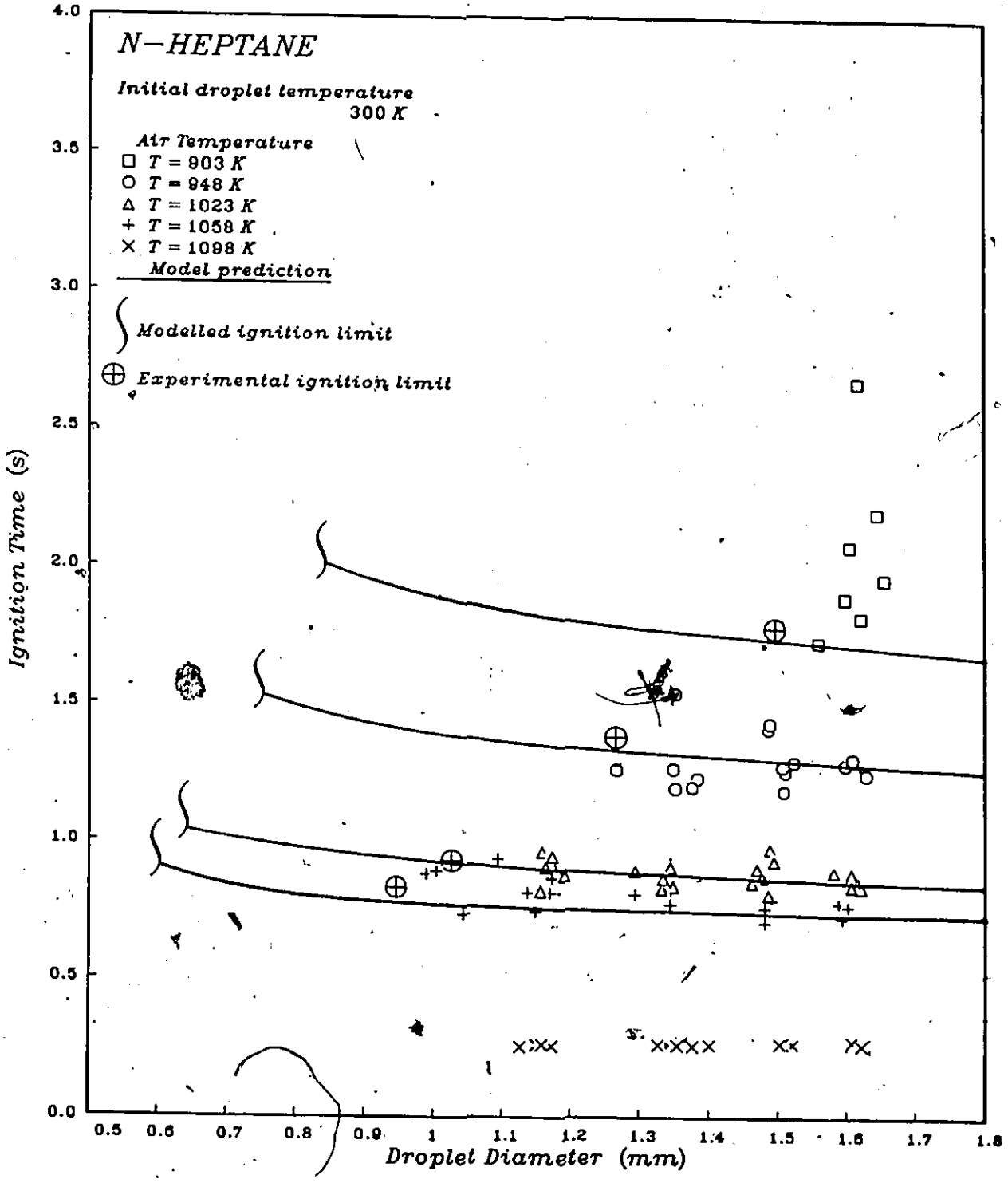

Figure 5.2: Ignition delay as a function of droplet diameter for n-heptane

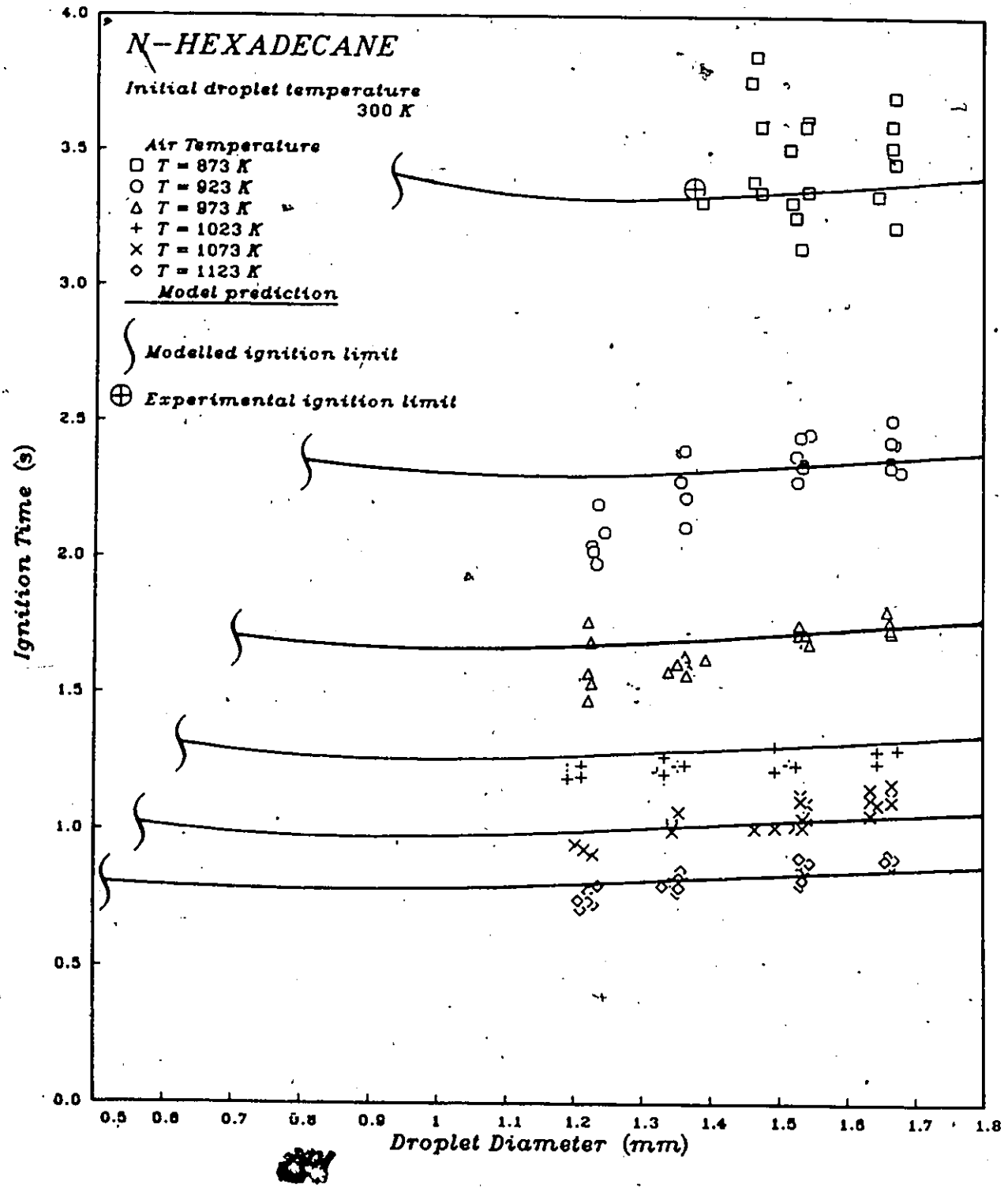

Figure 5.3: Ignition delay as a function of droplet diameter for n-hexadecane

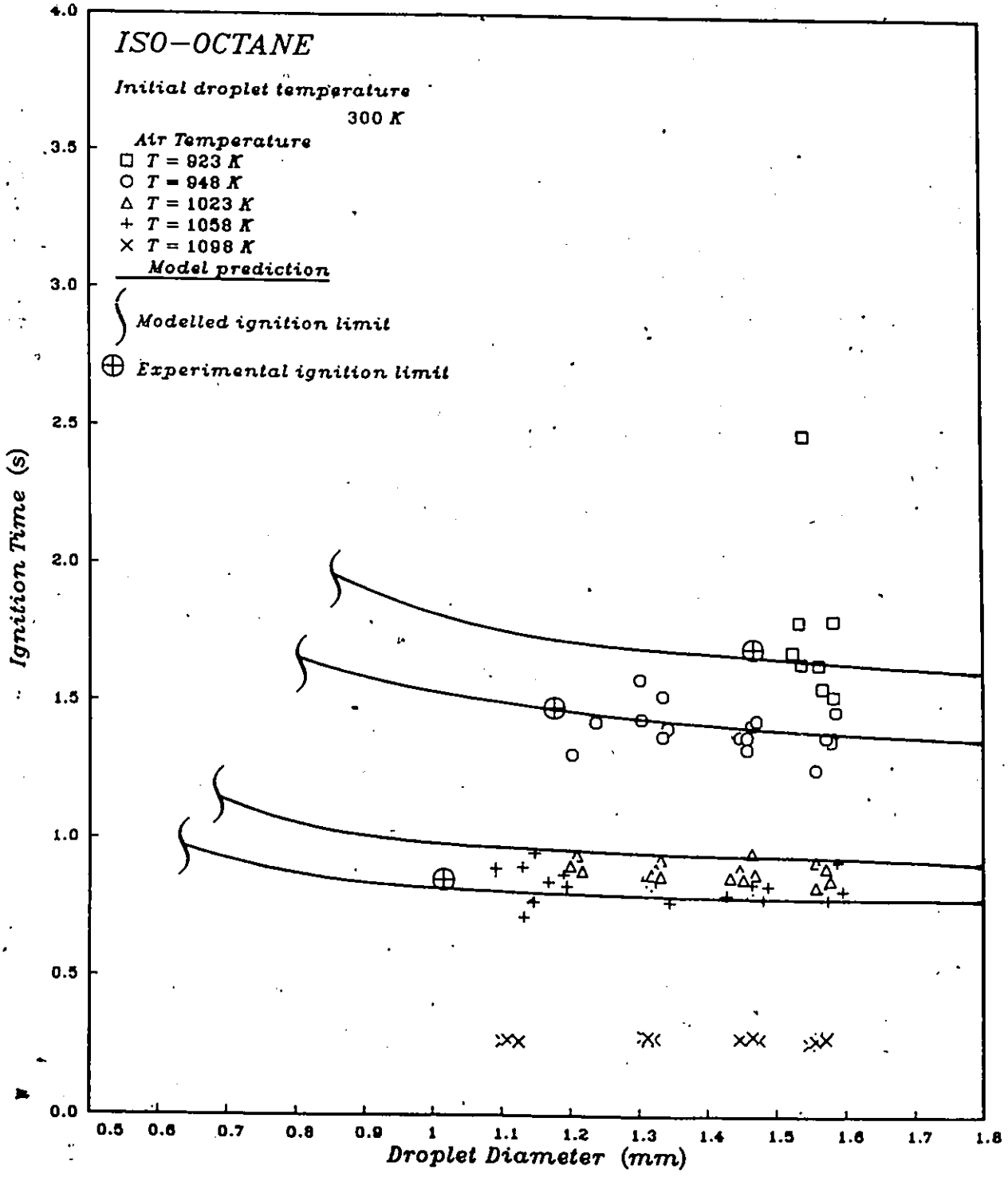

Figure 5.4: Ignition delay as a function of droplet diameter for iso-octane

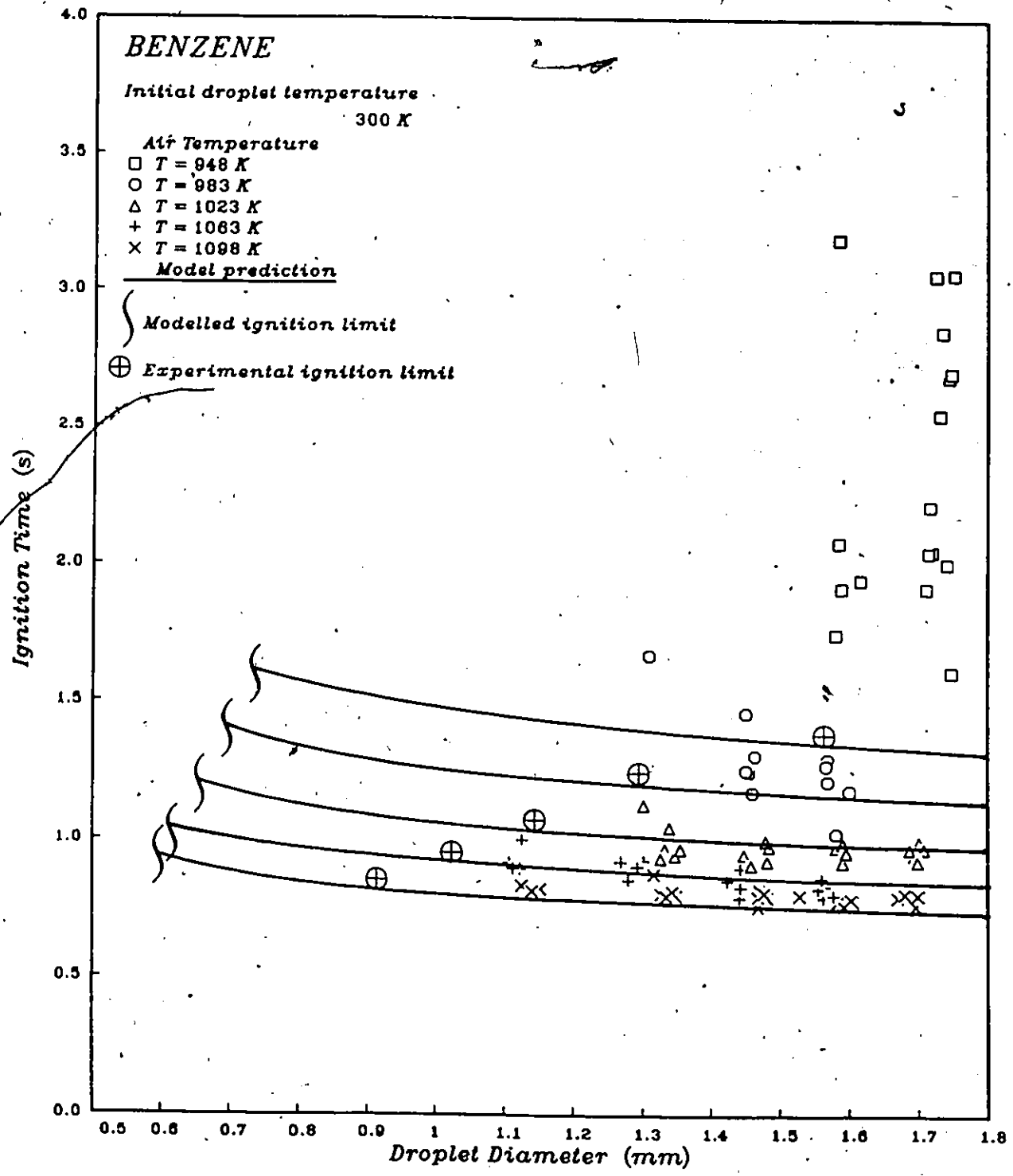

Figure 5.5: Ignition delay as a function of droplet diameter for benzene

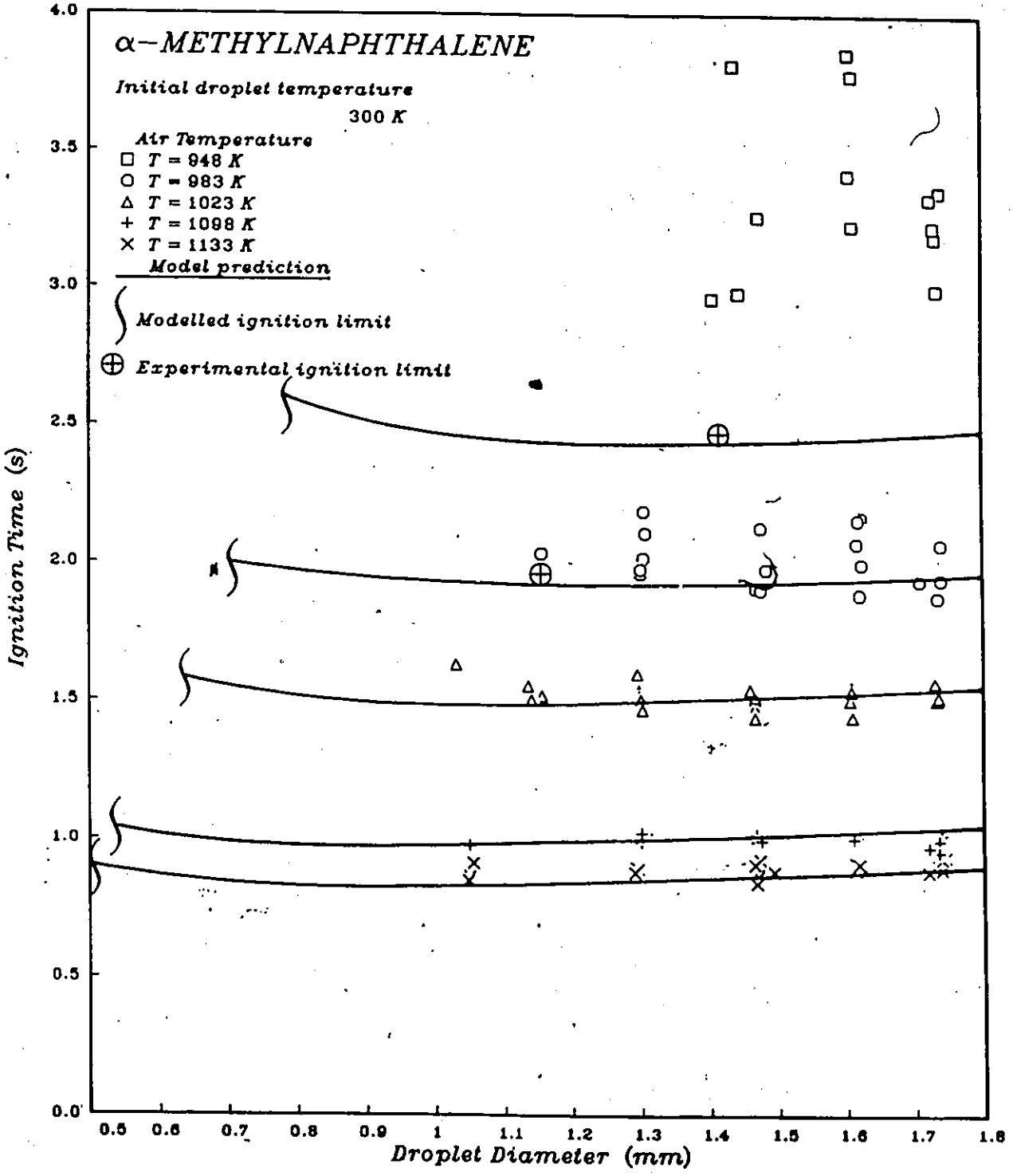

Figure 5.6: Ignition delay as a function of droplet diameter for α-methylnaphthalene

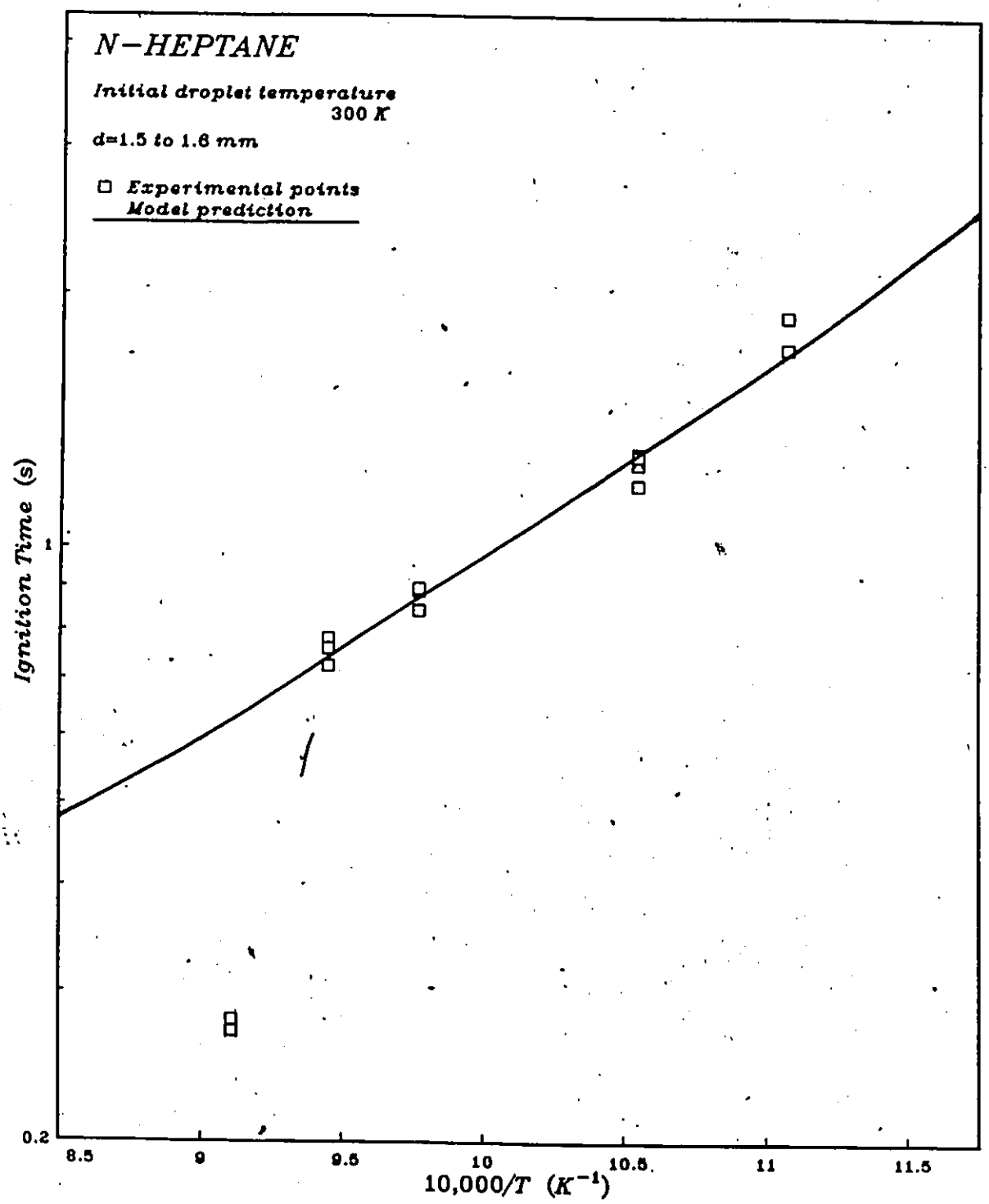

Figure 5.7: Ignition delay as a function of temperature for n-heptane

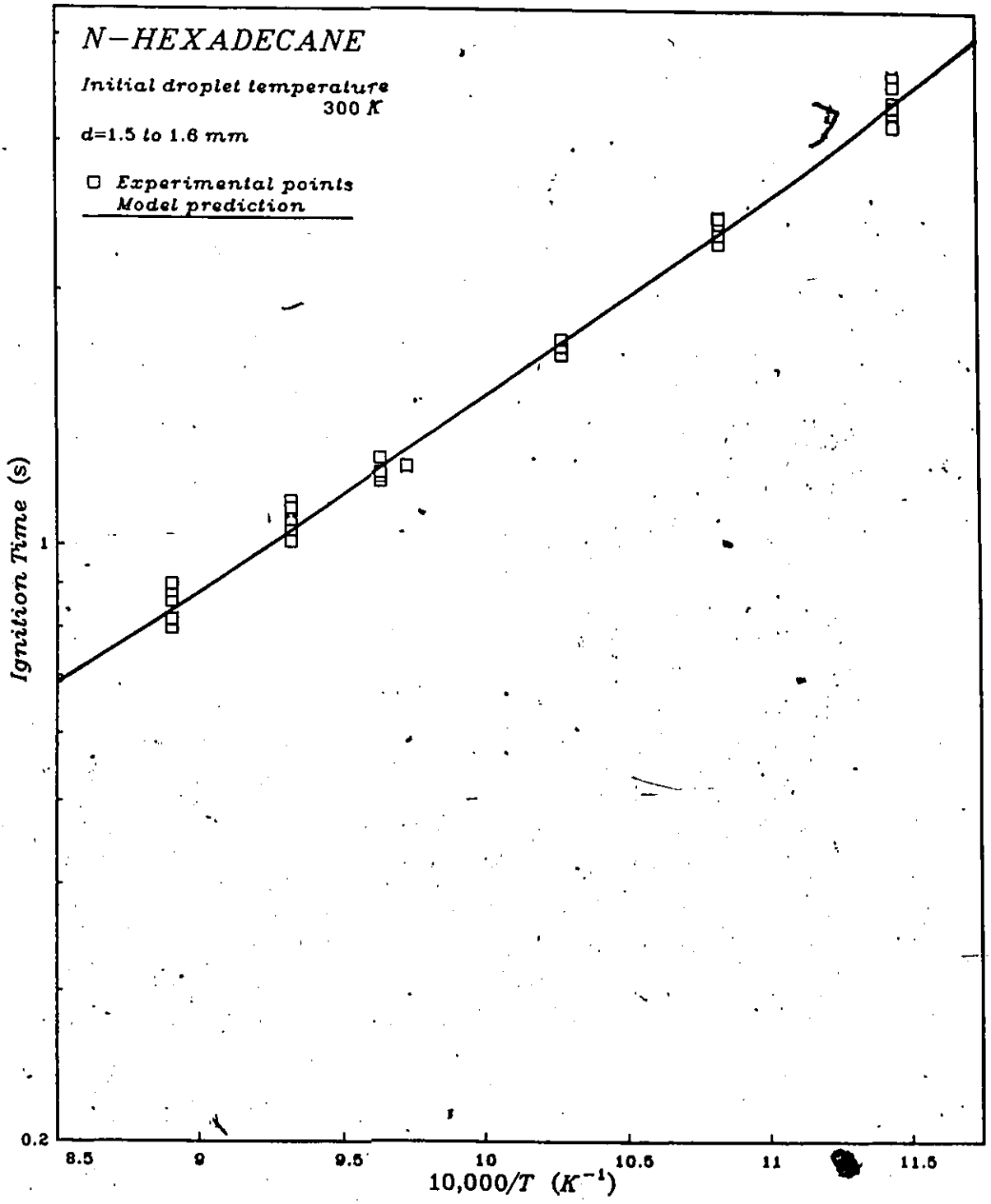

Figure 5.8: Ignition delay as a function of temperature for n-hexadecane

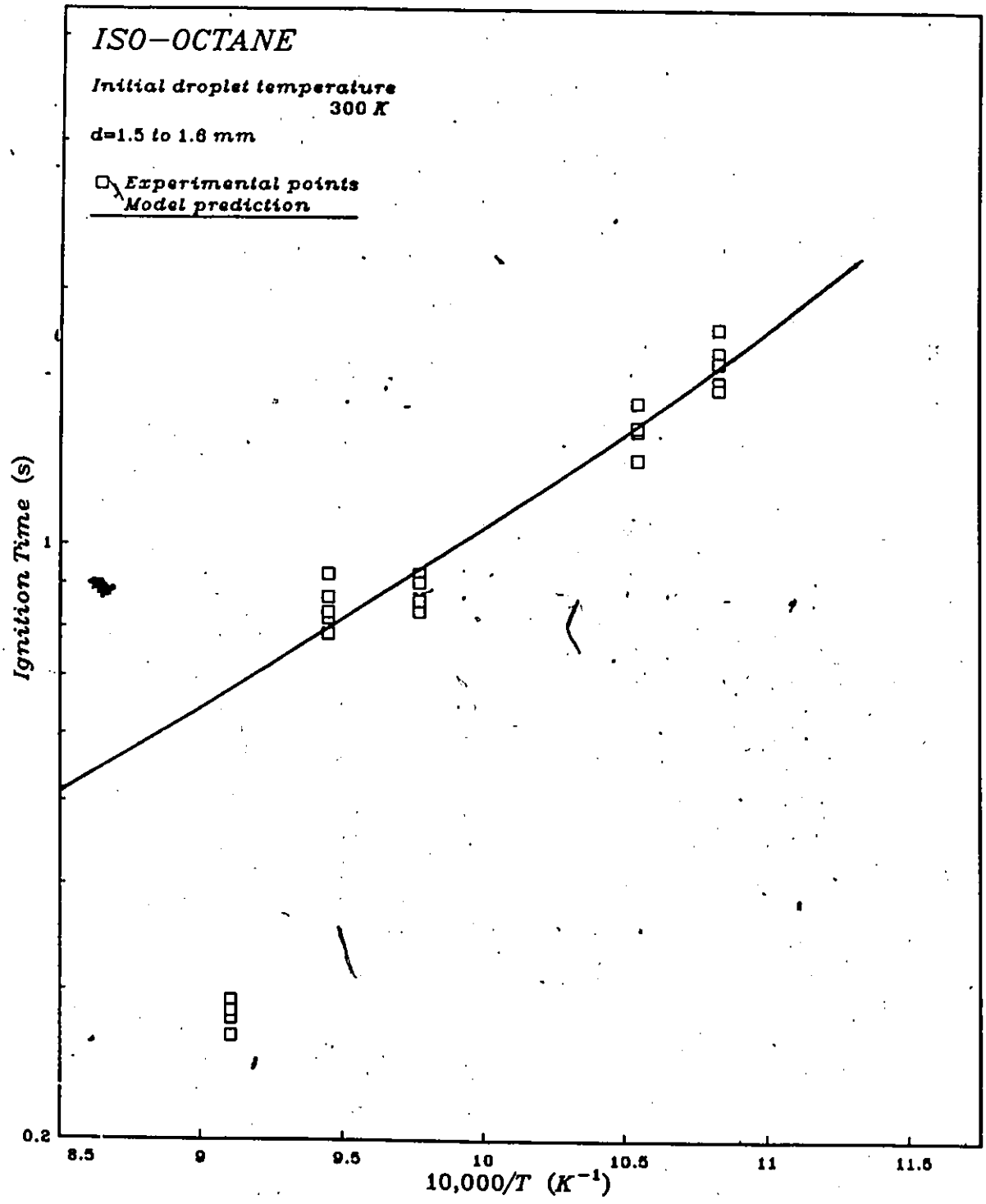

Figure 5.9: Ignition delay as a function of temperature for iso-octane

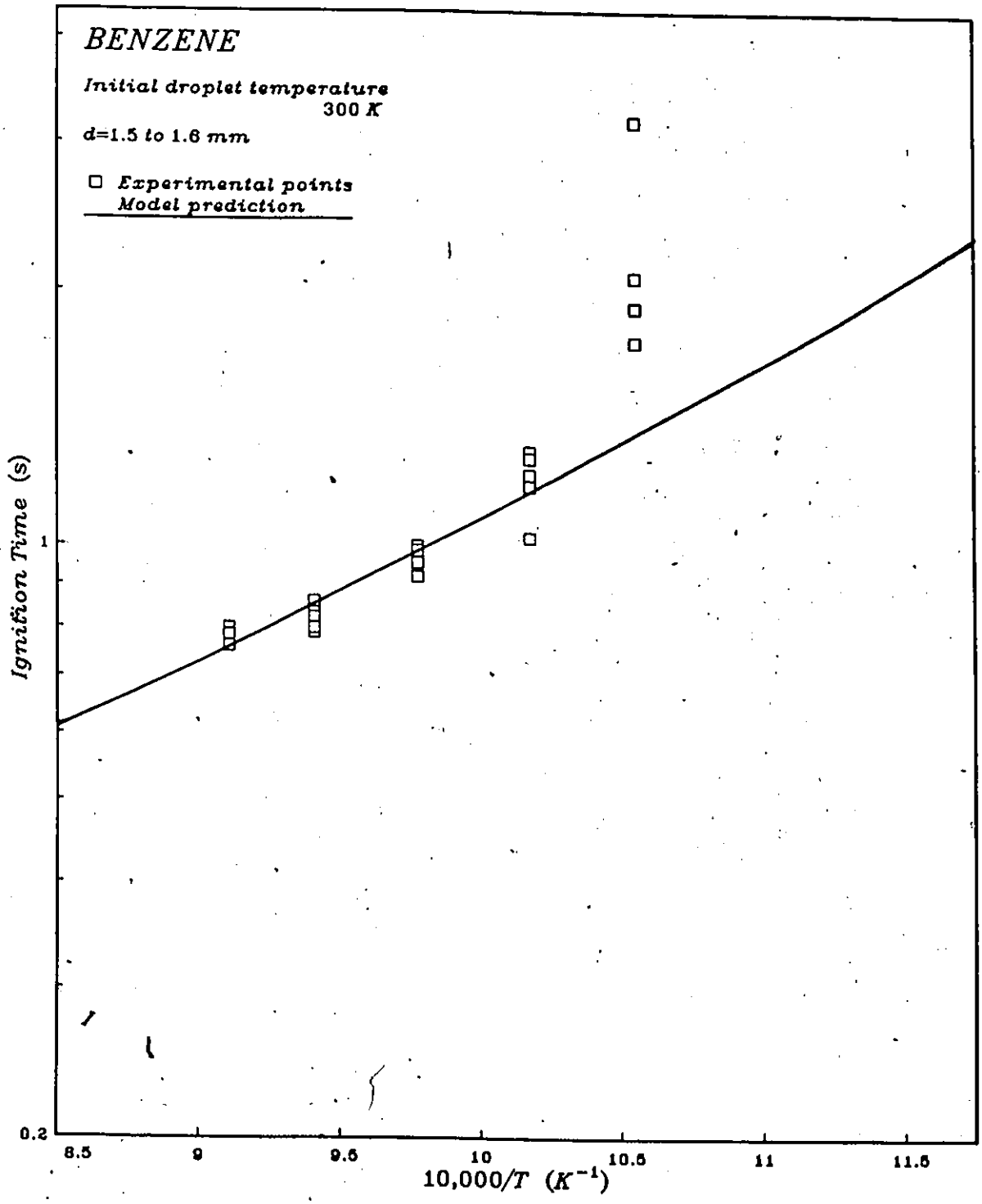

Figure 5.10: Ignition delay as a function of temperature for benzene

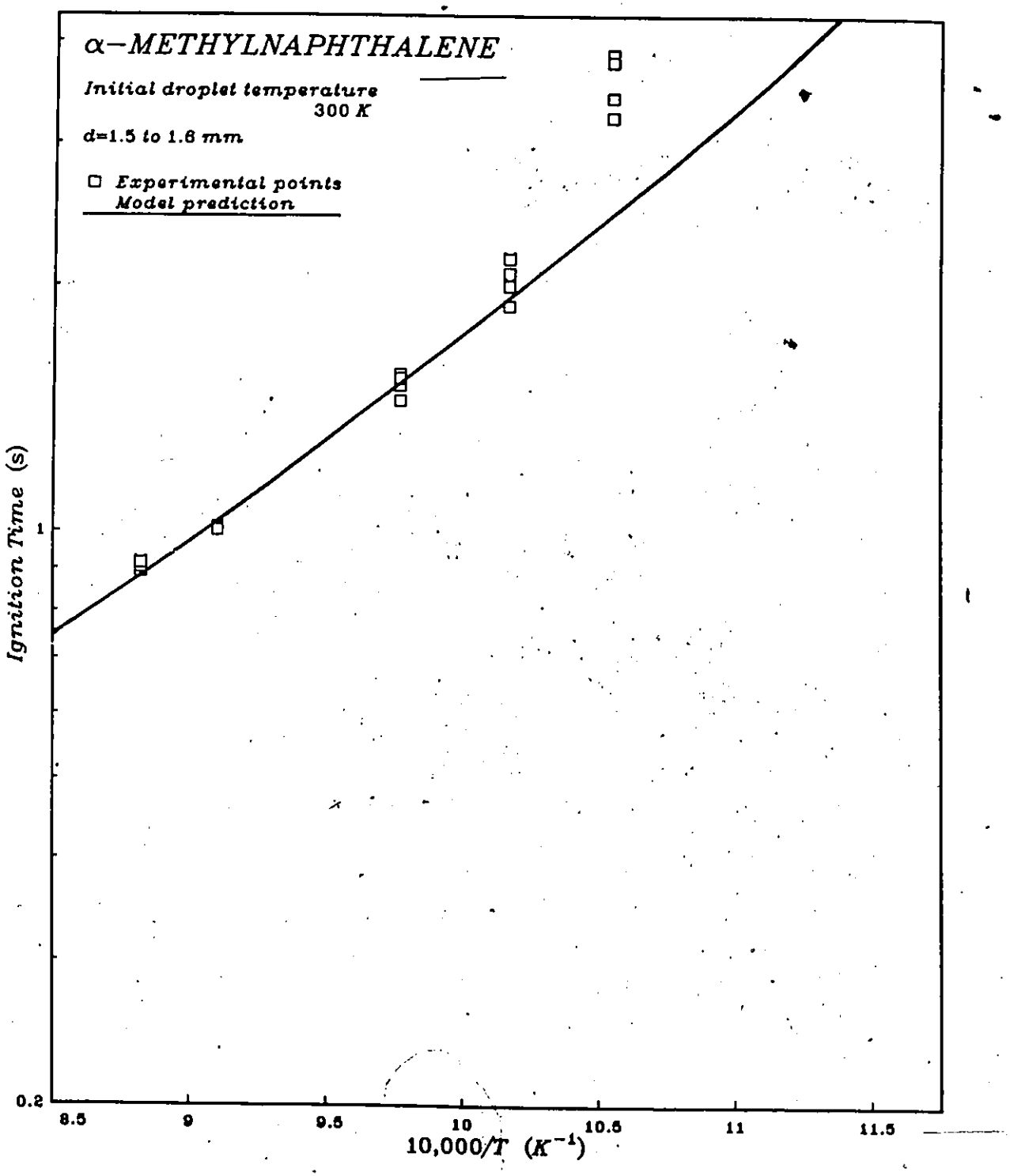

Figure 5.11: Ignition delay as a function of temperature for α-methylnaphthalene

5.3.2 The effect of physical properties

In order to study the effect of physical properties, two pairs of fuels were compared. Each of these pairs of fuels have different boiling points and similar spontaneous ignition temperatures and are as follows:

1. n-heptane versus n-hexadecane:
   Experimental results show that n-heptane ignites faster than n-hexadecane does and that n-hexadecane ignites at temperatures lower than the limiting temperature required for n-heptane. The reason for this is that n-heptane has a lower boiling point than n-hexadecane does ($98.4°C$ vs $287.5°C$), therefore its evaporation rate is faster and the ignitable mixture required for ignition is obtained more quickly. At lower temperatures, on the other hand, the residence time of the fuel vapour in the zone of ignitable concentration is too short, because of the rapid vaporization, for droplets of n-heptane to ignite. The less volatile n-hexadecane gives a longer vapour residence time for reaction to be initiated.

2. benzene versus α-methylnaphthalene:
   Experimental results show that benzene ignites much faster than α-methylnaphthalene does; this is as expected because the boiling point of benzene is much lower than that for α-methylnaphthalene ($80.1°C$ and $244.4°C$ respectively). Although the physical properties of these two fuels are different their limiting ignition temperatures are similar; this suggests that the chemical reaction is the controlling process near the ignition limit for these fuels, while for the paraffins physical processes were also significant.

The physical properties of the fuels therefore have a significant effect on their ignition characteristics.

5.4 General Results

5.4.1 The effect of chemical reaction

In order to show that it is the addition of chemical reaction to the model that gives ignition, the development of the temperature profile around the droplet has been plotted for a droplet vaporizing without reaction and with reaction in Figures 5.12 and 5.13 respectively. As shown in Figure 5.12 for n-heptane, initially the temperature profile rises rapidly; this is due to the fact that the vaporization rate of the droplet is still relatively low. As time increases the droplet surface temperature approaches the wet bulb temperature of the fuel and becomes constant, at which point the vaporization rate of the fuel droplet is maximum and the fuel diffusing outward reduces the temperature of the vapour immediately surrounding the droplet.

Figure 5.13 shows the effect that chemical reaction has on the temperature profile development. Again we note that the temperature at the droplet surface reaches the wet bulb temperature of the fuel after a certain amount of time. As the droplet vaporizes, chemical reaction occurs which is exothermic, and produces a localised temperature increase shown by the peak developed. As the temperature increases, chemical reaction attains a runaway state making the temperature increase exponentially, marking the onset of ignition. Figure 5.13 also shows the radial position at which ignition occurs, in this case being approximately 30 radii. This agrees well with experimental observation.

5.4.2 The effect of initial droplet temperature

In order to show the effect of the initial temperature of the droplet on ignition delay, the model was run for both a heavy fuel (n-hexadecane) and a light fuel (n-heptane) varying the initial droplet temperature from $300K$ to the fuel's boiling point. Results have been plotted and are shown in Figure 5.14. As shown the initial droplet temperature has very little effect on ignition delay for n-heptane. N-heptane, having a low boiling point, is very volatile and the time required for the droplet heating is very short compared to the chemical delay. Therefore, increasing the droplet temperature by $60°C$ may shorten the droplet heating period slightly, but

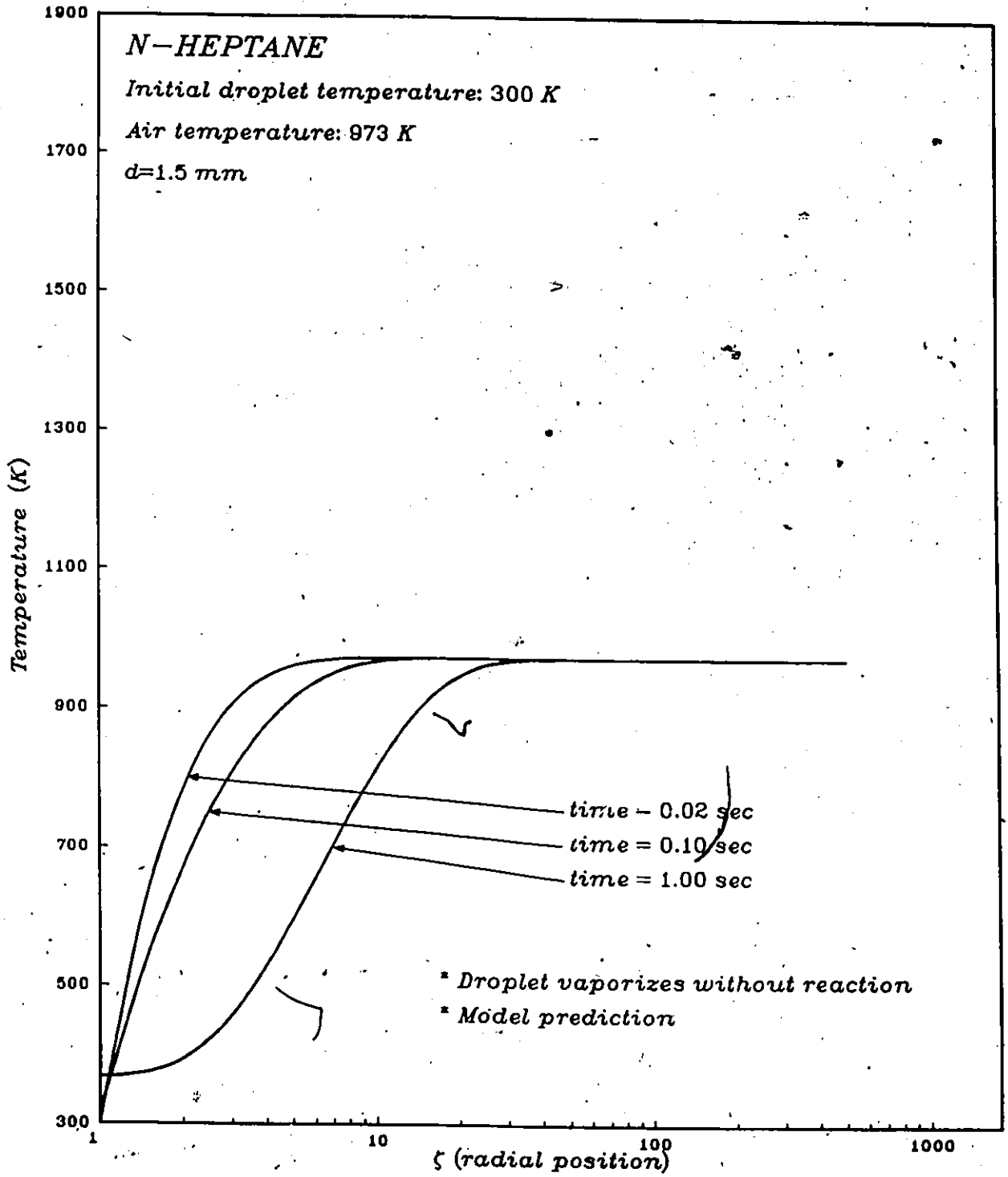

Figure 5.12: Temperature profile development around droplet (without reaction)

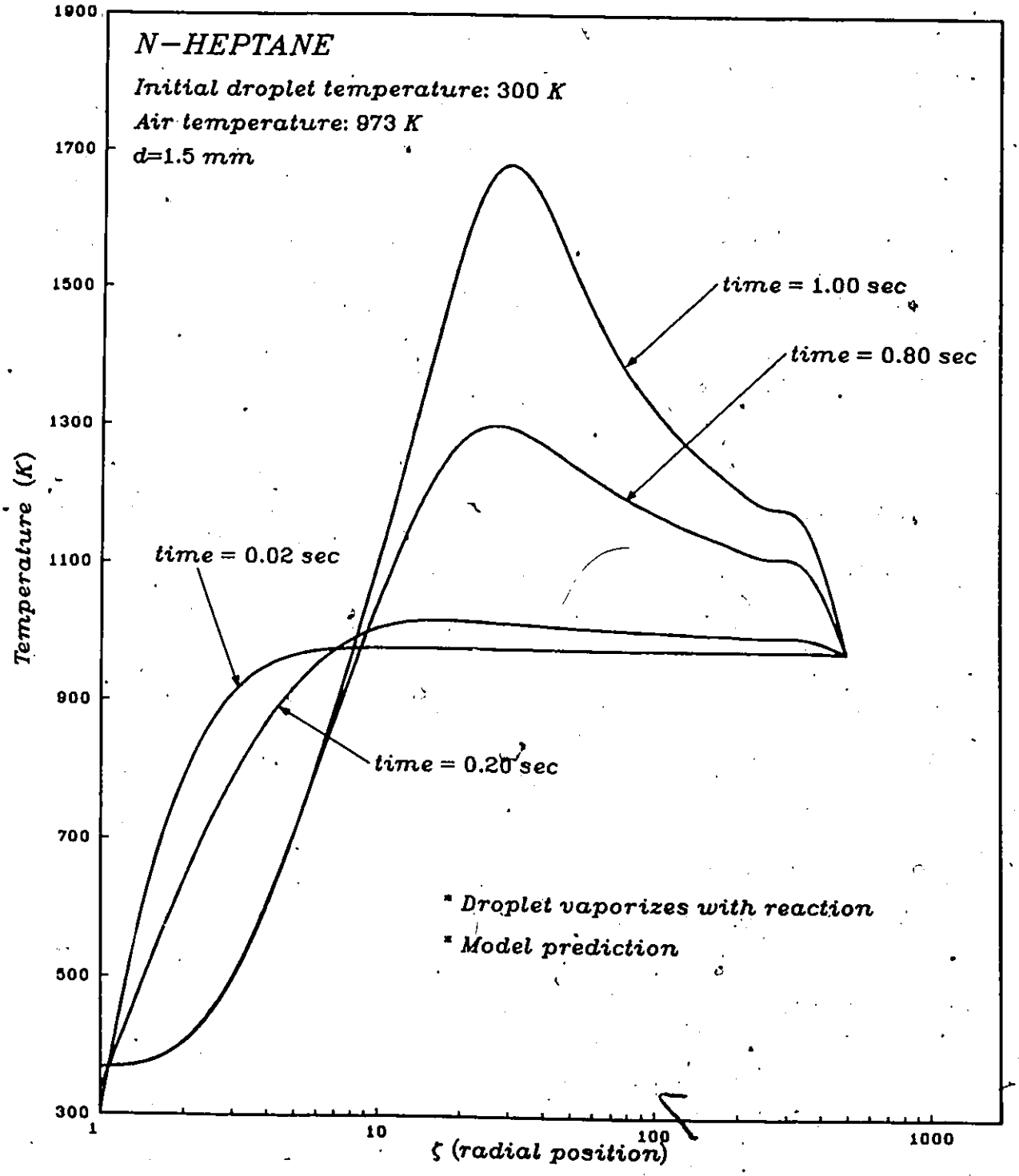

Figure 5.13: Temperature profile development around droplet (with reaction)

since this period is a small fraction of the total ignition delay, the effect will be minimal and will decrease the total ignition delay by only a small amount as shown.

Figure 5.14 shows that for n-hexadecane the initial droplet temperature has a strong effect on total ignition delay. Since n-hexadecane has a high boiling point it is not very volatile, therefore its droplet heating period or physical delay represents a major part of the total ignition delay time required for ignition. Initially, as the initial droplet temperature is increased to approximately $450K$, the droplet requires less heating and the droplet heating time decreases, resulting in a substantial decrease in total ignition delay. However, as the initial temperature of the droplet increases, its vaporization rate also increases, making the residence time of the vapour inside the ignitable region shorter. This results in an increase in the chemical delay; this increase becomes more significant than the decrease in physical delay at approximately $450K$; therefore making the total ignition delay increase for droplets initially at a temperature of $450K$ or more.

5.4.3 The effect of radiation

In order to show the effect of radiation on the total ignition delay of liquid fuel droplets, the model was run for both a light fuel (benzene) and a heavy fuel (α-methylnaphthalene) with and without radiation absorption. Figures 5.15 and 5.16 show results plotted for benzene and α-methylnaphthalene respectively; the ignition limit representing the minimum droplet diameter for which ignition was obtained is shown for both cases.

As shown in Figure 5.15 for benzene, radiation has very little or no effect on the total ignition delay. The reason for this is that benzene is a fuel with a low boiling point, therefore very volatile, making the droplet heating period very short in respect with the total ignition delay. Since radiation is simply a means of heating the droplet, the physical delay being short, the effect cannot be very important.

However, as shown in Figure 5.16 for α-methylnaphthalene, the effect of radiation on total ignition delay is significant. This is due to the fact that α-methylnaphthalene has a high boiling point and therefore is not very volatile, meaning that droplet heating represents a significant part of the total ignition delay. As shown in Figure 5.16 radiation has a larger

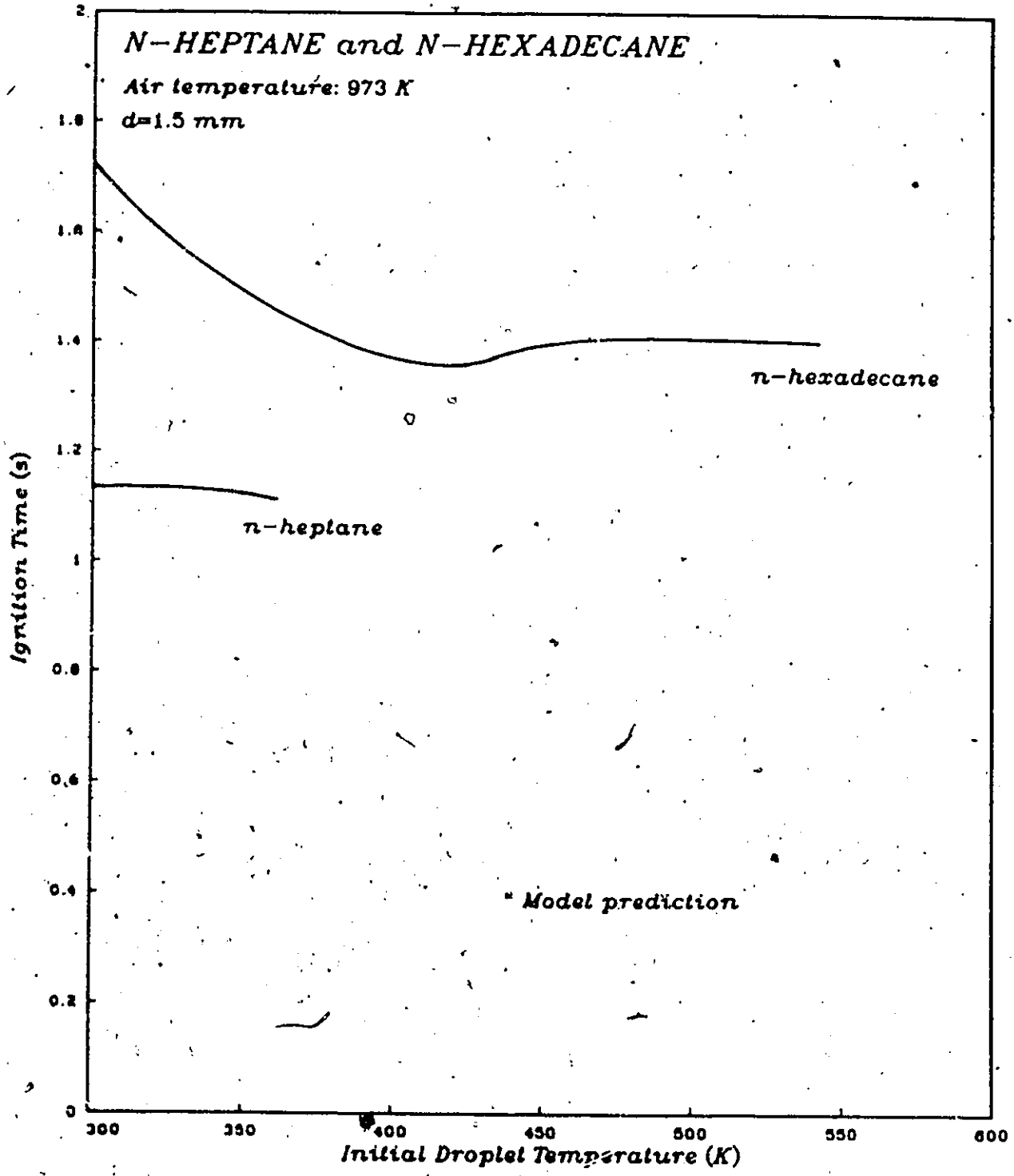

Figure 5.14: Ignition delay as a function of initial droplet temperature

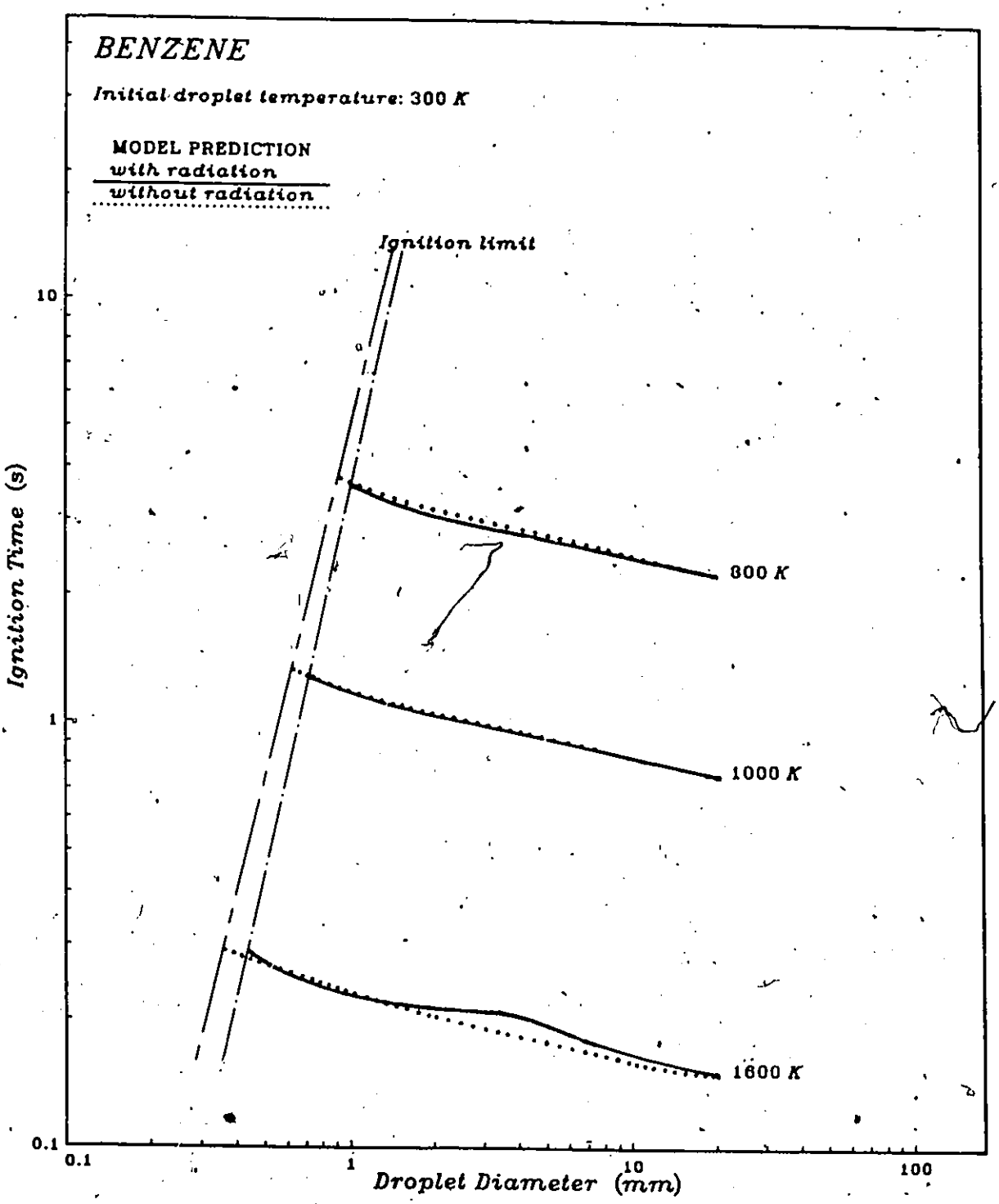

Figure 5.15: Ignition delay as a function of droplet diameter with and without radiation for benzene

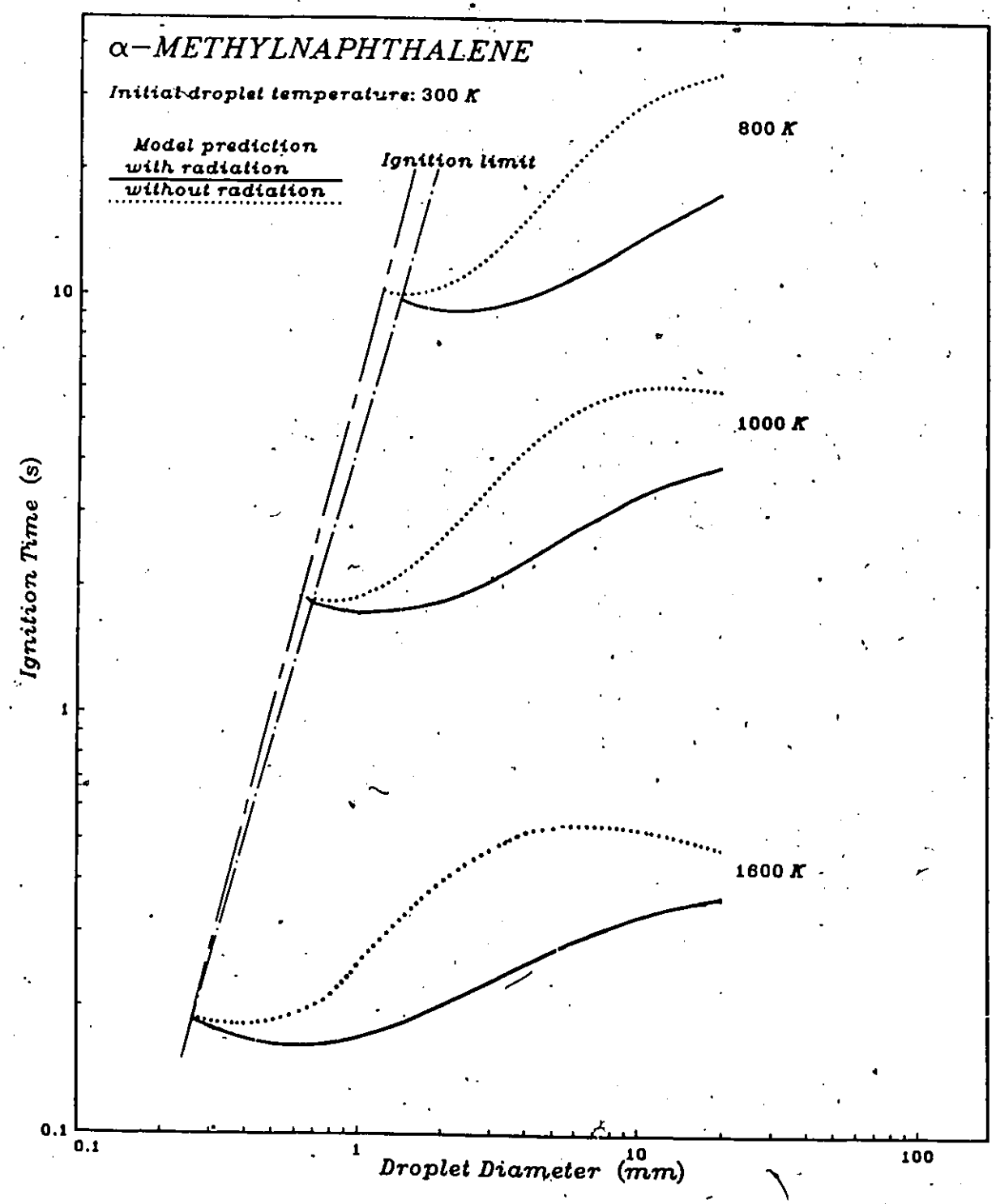

Figure 5.16: Ignition delay as a function of droplet diameter with and without radiation for α-methylnaphthalene

effect for large droplets, since the droplet heating period is longer. As the droplet diameter decreases, droplet heating becomes less important and total ignition delays become similar with and without radiation absorption. For small droplets, two processes are occurring opposite one another: 1) radiation absorption heats up the droplet faster, decreasing the physical delay; 2) the droplet being smaller, the vaporization rate is faster, reducing the residence time and increasing the chemical delay time.

5.4.4 The effect of reaction constants

In order to determine the effect of chemical properties using the model, runs were made for n-heptane using the reaction constants (pre-exponential constant, energy of activation) for fuels of different chemical reactivity, iso-octane and benzene. Figure 5.17 shows that changing the reaction constants does not have a significant effect on ignition delay. Figure 5.18 shows results obtained for n-hexadecane when the reaction constants are substituted by those for α-methylnaphthalene. As above, results show little effect by changing the reaction constants. Therefore the chemical properties of a fuel have a limited effect on total ignition delay.

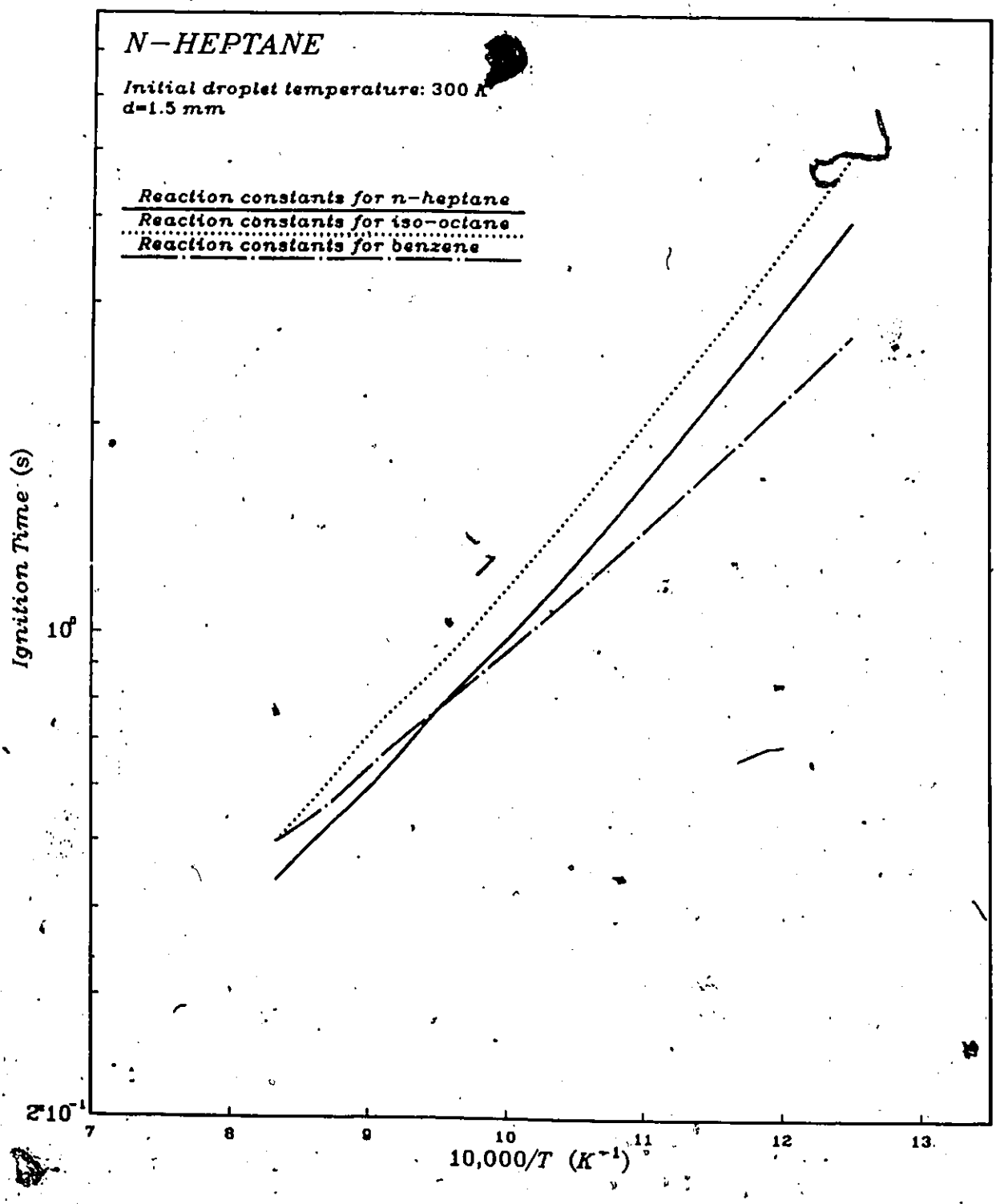

Figure 5.17: Ignition delay as a function of temperature for n-heptane using different reaction constants

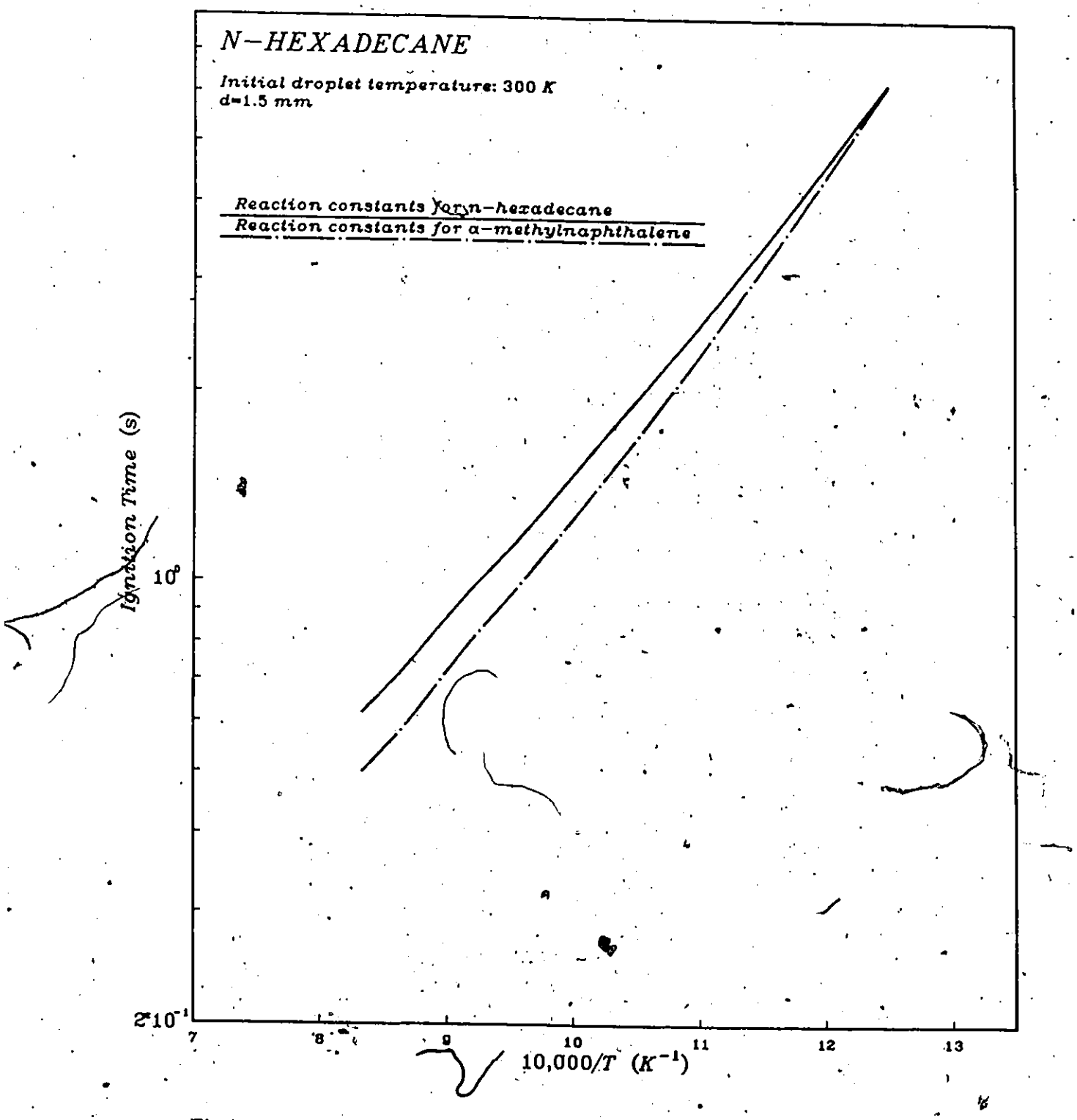

Figure 5.18: Ignition delay as a function of temperature for n-hexadecane using different reaction constants

Chapter 6

Conclusions and Recommendations

6.1 Conclusions

In this research, an experimental apparatus was built and an experimental technique developed for performing single droplet ignition experiments. After extensive testing the experimental technique was found to give satisfactory and consistent results. Experiments have shown that droplet diameter has very little effect on ignition delay for droplets measuring 0.90 to 1.80 mm in diameter, whereas the furnace temperature has a large effect.

A mathematical ignition model was developed in parallel with the experiments. The model having been fitted predicts experimental results satisfactorily within ignition limits for all fuels tested.

The effect of physical and chemical properties on droplet ignition delay was determined. It was concluded that the physical properties of the fuels have a significant effect on ignition delay, whereas the chemical properties have little effect and this effect diminishes as the ambient temperature increases.

After extensive testing with the model and comparing experimental results with those of other researchers, it was determined that radiation affects droplet heating. The strange behaviour observed for the paraffins n-heptane and iso-octane (radical drop in ignition delay at high temperatures) leads to the conclusion that at high temperatures paraffins undergo a change in chemical kinetics which may result from two-stage ignition.

6.2 Recommendations

In order to better understand the behaviour of fuel sprays in diesel engines and gas turbines, the following studies on single liquid fuel droplets are recommended:

1. Due to the differences obtained with the model for droplet ignition with and without radiation, it is necessary to study in more detail the absorption of radiation by fuel droplets.

2. Having observed a radical change in ignition behaviour for n-heptane and iso-octane at high temperatures, it is believed that the reason for this change is two-stage ignition; therefore a study of the process of two-stage ignition in paraffins is recommended.

3. Since the model did not predict the ignition limits very well because of natural convection effects, a detailed study of the effect of natural convection on the ignition limits should be performed.

Additional studies could be performed in order to reproduce the conditions encountered in diesel engines and gas turbines:

1. Perform studies on single two-component fuel droplets, multi-component fuel droplets and eventually actual fuel blends being used today.

2. Perform droplet ignition experiments at pressures typical of that required in diesel engines.

Bibliography

[1] ASTM Standards on Petroleum Products and Lubricants. pp.199-200, Philadelphia, American Society for Testing Materials (1948).

[2] G. A. Agoston / H. Wise / W. A. Rosser. *Dynamic factors affecting the combustion of liquid spheres.* 6^{th} Symp. (Int.) on Combustion pp.708-717 (1957).

[3] S. Black / W. L. H. Hallett. *Combustion test methods for the evaluation of future liquid fuels.* Report (Department of National Defence) (1982).

[4] ECG Semiconductors Master Replacement Guide p.119.

[5] M. M. El-Wakil / M. I. Abdou. *The self-ignition of fuel droplets in heated air streams.* Fuel 45 pp.177-205 (1966).

[6] G. M. Faeth / D. R. Olson. *The ignition of hydrocarbon fuel droplets in air.* SAE Paper 680465 (1968).

[7] W. L. H. Hallett. *Vapour pressure relations for droplet combustion models.* Combustion and Flame 65 pp.117-119 (1986).

[8] M. P. Halstead / L. J. Kirsch / C. P. Quinn. *The autoignition of hydrocarbon fuels at high temperatures and pressures - Fitting of a mathematical model.* Combustion and Flame 30 pp.45-60 (1977).

[9] G. M. Hieftje / H. V. Malmstadt. *A unique system for studying flame spectrometric processes.* Analytical Chemistry 40 p.1860 (1968).

[10] J. P. Holman. Heat Transfer. McGraw-Hill Inc. pp.394,243-244 (1981).

[11] H. C. Hottel / G. C. Williams / H. C. Simpson. *Combustion of fuel droplets.* 5^{th} Symp. (Int.) on Combustion pp.101-129 (1955).

[12] G. L. Hubbard / V. E. Denny / A. F. Mills. *Droplet evaporation: effects of transients and variable properties.* Int. J. Ht. and Mass Transfer 18 pp.1003-1008 (1975).

[13] A. M. Kanury. Introduction to Combustion Phenomena, Gordon and Breach, NY, pp.81-141 (1975).

[14] K. Kobayasi. *An experimental study on the combustion of a fuel droplet.* 5^{th} Symp. (Int.) on Combustion pp.141-148 (1954).

[15] S. Kumagai. *Combustion of fuel sprays.* 6^{th} Symp. (Int.) on Combustion pp.668-674 (1956).

[16] C. K. Law. *Quasi-steady droplet vaporization theory with property variations.* The Physics of Fluids 18 pp.1426-1432 (1975).

[17] C. K. Law *Asymptotic theory for ignition and extinction in fuel droplet burning.* Combustion and Flame 24 pp.89-98 (1975).

[18] C. K. Law. *Multicomponent droplet combustion with rapid internal mixing.* Combustion and Flame 26 pp.219-233 (1976).

[19] C. K. Law / W. A. Sirignano. *Unsteady droplet combustion with droplet heating - II: Conduction limit.* Combustion and Flame 28 pp.175-186 (1977).

[20] C. K. Law. *Theory of thermal ignition in fuel droplet burning.* Combustion and Flame 31 pp.285-296 (1978).

[21] C. K. Law *Recent advances in droplet vaporization and combustion.* Prog. Energy and Combustion Sci. 8 pp.171-201 (1982).

[22] M. Matalon / C. K. Law. *Gas-phase transient diffusion in droplet vaporization and combustion.* Combustion and Flame 50 pp.219-229 (1983).

[23] M. T. Monaghan / R. G. Siddall / M. W. Thring. *The influence of initial diameter on the combustion of single drops of liquid fuel.* Combustion and Flame 12 pp.45-53 (1968).

[24] National Advisory Comm. on Aeronautics Report 1300. *Basic Considerations in the Combustion of Hydrocarbon Fuels.* Table 32 (1959).

[25] T. Niioka / S. Ishiguro / T. Saitoh. *A numerical approach to fuel droplet ignition.* Technical Report of National Aerospace Lab (Japan) TR-628T pp.1-8 (1980).

[26] N. Nishiwaki. *Evaporation and ignition lag of fuel droplets.* 5^{th} Symp. (Int.) on Combustion pp.148-158 (1954).

[27] S. Okajima / S. Kumagai. *Experimental studies on combustion of fuel droplets in flowing air under zero- and high-gravity conditions.* 19^{th} Symp. (Int.) on Combustion pp.1021-1027 (1982).

[28] S. V. Patankar. Numerical Heat Transfer and Fluid Flow. McGraw-Hill Inc. pp.41-59 (1980).

[29] C. E. Polymeropoulos / R. L. Peskin. *Ignition and extinction of liquid fuel drops - numerical computations.* Combustion and Flame 13 pp.166-172 (1969).

[30] R. C. Reid / J. M. Prausnitz / T. K. Sherwood. The Properties of Gases and Liquids, Third edition. McGraw-Hill Book Company (1977).

[31] T. Saitoh / O. Nagano. *Transient combustion of a fuel droplet with finite rate of chemical reaction.* Combustion Science and Technology 22 pp.227-234 (1980).

[32] T. Saitoh. *An analysis of the burning of a single fuel droplet via quasi-steady model.* Technology Reports (Tohoku Univ.) 43 pp.47-56 (1978).

[33] T. Saitoh / S. Ishiguro / T. Niioka. *An experimental study of droplet ignition characteristics near the ignitable limit.* Combustion and Flame 48 pp.27-32 (1982).

[34] J. J. Sangiovanni / A. S. Kesten. *A theoretical and experimental investigation of the ignition of fuel droplets.* Combustion Science and Technology 16 pp.59-70 (1977).

[35] J. J. Sangiovanni. *A model for the nonsteady ignition and combustion of a droplet.* in J. T. Zung (ed.) *Evaporation-Combustion of Fuels.* Advances in Chemistry 166 pp.27-53 (1978).

[36] C. K. Westbrook / F. L. Dryer. *Simplified reaction mechanisms for the oxidation of hydrocarbon fuels in flames.* Combustion Sci. & Tech. 27 pp.31-43 (1981).

Appendix A

Simplification of the Energy Equation

In order to simplify the energy equation, the convection and diffusion terms which are

$$\rho v C_P \frac{\partial T}{\partial r} \qquad and \qquad \sum C_{Pi} j_i \frac{\partial T}{\partial r}$$

in Equation 3.19 are combined.

Using the following assumptions:

1. Fuel diffuses in still air, therefore

$$Y_F + Y_{air} = 1 \qquad or \qquad Y_{air} = 1 - Y_F$$

$$\sum j_i = 0 \qquad therefore \qquad j_F = -j_{air}$$

2. The total mass flux is equal to the fuel mass flux

$$\rho v = \rho_F v_F$$

This follows from the quasi-steady assumption for the vapour phase concentration and velocity fields.

and the fact that $j_i = \rho_i v_i - \rho_i v$, the sum of the two terms may be reduced as follows:

$$\rho v C_P \frac{\partial T}{\partial r} + \sum C_{Pi} j_i \frac{\partial T}{\partial r}$$

$$= \rho v(Y_F C_{PF} + Y_{air} C_{Pair}) \frac{\partial T}{\partial r} + (C_{PF} j_F + C_{Pair} j_{air}) \frac{\partial T}{\partial r}$$

$$= \{\rho v Y_F C_{PF} + \rho v(1 - Y_F) C_{Pair} + C_{PF} j_F - C_{Pair} j_F\} \frac{\partial T}{\partial r}$$

Since $\rho Y_F = \rho_F$, this becomes

$$\{\rho_F v C_{PF} + \rho v C_{Pair} - \rho_F v C_{Pair} + \rho v C_{PF} - \rho_F v C_{PF} - \rho v C_{Pair} + \rho_F v C_{Pair}\} \frac{\partial T}{\partial r}$$

$$= \rho v C_{PF} \frac{\partial T}{\partial r}$$

The energy equation then reduces to

$$\rho C_P \frac{\partial T}{\partial t} + \rho v C_{PF} \frac{\partial T}{\partial r} = \frac{1}{r^2} \frac{\partial}{\partial r} \left(r^2 k \frac{\partial T}{\partial r} \right) - W_F \Delta H_F$$

Appendix B

Integration of the Energy Equation

The final form of the energy equation is

$$\varsigma^2\rho\frac{\partial T}{\partial t}+\frac{G}{R}\left(\frac{C_{PF}}{C_P}+\frac{\rho}{\rho_t}\varsigma^3\right)\frac{\partial T}{\partial \varsigma}=\frac{1}{R^2}\frac{k}{C_P}\frac{\partial}{\partial \varsigma}\left(\varsigma^2\frac{\partial T}{\partial \varsigma}\right)-\frac{W_F\varsigma^2}{C_P}\Delta H_F \quad \text{(B.1)}$$

The discretization equation is obtained by integrating each term over the control volume shown in Figure 3.1 and over the time interval from t to $t+\Delta t$.

The control volume boundaries are located midway between the grid points. An implicit scheme is used for the time step, so that all T's are evaluated at time $t+\Delta t$, except those with a "0" superscript, which are evaluated at t.

First term:

$$\int_w^e\int_t^{t+\Delta t}\varsigma^2\rho\frac{\partial T}{\partial t}dtd\varsigma$$
$$=\rho\int_w^e\varsigma^2(T_P-T_P^0)d\varsigma$$
$$=\frac{\rho}{3}(\varsigma_e^3-\varsigma_w^3)(T_P-T_P^0)$$

Second term:

$$\int_t^{t+\Delta t}\int_w^e \frac{G}{R}\frac{C_{PF}}{C_P}\frac{\partial T}{\partial \varsigma}d\varsigma dt$$

$$= \int_t^{t+\Delta t}\frac{G}{R}\frac{C_{PF}}{C_P}(T_e - T_w)dt$$

Values T_e and T_w refer to the cell boundaries, and are found by linear interpolation between grid points:

$$T_e = \frac{T_E + T_P}{2} \qquad T_w = \frac{T_P + T_W}{2}$$

This gives the second term as

$$= \frac{G}{R}\frac{C_{PF}}{C_P}\frac{(T_E + T_P - T_W - T_P)}{2}\Delta t$$

$$= \frac{G}{R}\frac{C_{PF}}{C_P}\left(\frac{T_E - T_W}{2}\right)\Delta t$$

Third term:

$$\int_t^{t+\Delta t}\int_w^e \frac{G}{R}\frac{\rho}{\rho_\ell}\varsigma^3\frac{\partial T}{\partial \varsigma}d\varsigma dt$$

note:

$$\frac{\partial(\varsigma^3 T)}{\partial \varsigma} = 3\varsigma^2 T + \varsigma^3\frac{\partial T}{\partial \varsigma}$$

$$\int_t^{t+\Delta t}\int_w^e \frac{G}{R}\frac{\rho}{\rho_\ell}\left\{\frac{\partial(\varsigma^3 T)}{\partial \varsigma} - 3\varsigma^2 T\right\}d\varsigma dt$$

$$= \int_t^{t+\Delta t}\frac{G}{R\rho_\ell}\left\{(\rho_e\varsigma_e^3 T_e - \rho_w\varsigma_w^3 T_w) - (\rho_e\varsigma_e^3 - \rho_w\varsigma_w^3)T_P\right\}dt$$

$$= \frac{G}{R\rho_\ell}\left\{\frac{\rho_e\varsigma_e^3(T_E - T_P) - \rho_w\varsigma_w^3(T_W - T_P)}{2}\right\}\Delta t$$

Fourth term:

$$\int_t^{t+\Delta t}\int_w^e \frac{1}{R^2}\frac{k}{C_P}\frac{\partial}{\partial \varsigma}\left(\varsigma^2\frac{\partial T}{\partial \varsigma}\right)d\varsigma dt$$

$$= \int_t^{t+\Delta t}\frac{1}{R^2}\frac{k}{C_P}\left\{\frac{\varsigma_e^2(T_E-T_P)}{\varsigma_E-\varsigma_P} - \frac{\varsigma_w^2(T_P-T_W)}{\varsigma_P-\varsigma_W}\right\}dt$$

$$= \frac{1}{R^2}\frac{k}{C_P}\left\{\frac{\varsigma_e^2(T_E-T_P)}{\varsigma_E-\varsigma_P} - \frac{\varsigma_w^2(T_P-T_W)}{\varsigma_P-\varsigma_W}\right\}\Delta t$$

Fifth term:

$$\int_t^{t+\Delta t}\int_w^e -\frac{W_F\varsigma^2}{3C_P}\Delta H_F d\varsigma dt$$

$$\int_t^{t+\Delta t} -\frac{W_F\Delta H_F}{3C_P}\left(\varsigma_e^3-\varsigma_w^3\right)dt$$

$$= -\frac{W_F\Delta H_F}{3C_P}\left(\varsigma_e^3-\varsigma_w^3\right)\Delta t$$

These expressions for the second and third term are based on central differencing; the value of T carried into the cell by the flow is considered to be that on the cell boundary, T_w or T_e. At high flows (see Section 3.6) it is more realistic to use upwind differencing, in which the T from the upstream node is assumed to be convected into the cell. For flow from W to E (radially outwards), upwind differencing results when T_W is substituted for T_w and T_P for T_e [28], yielding

Second term:

$$\frac{G}{R}\frac{C_{PF}}{C_P}(T_P-T_W)\Delta t$$

Third term:

$$\frac{G\rho_w}{R\rho_l}\varsigma_w^3(T_P-T_W)\Delta t$$

The upwind and central differencing schemes are combined in the hybrid scheme in Section 3.6. Rearranging and simplying the integrated equation, the discretization equation is obtained with the coefficients having the forms shown in Section 3.6.1.

Appendix C

TriDiagonal-Matrix Algorithm

Grid points are numbered $1, 2, 3, \ldots, N$ with points 1 and N denoting the boundary points.

$$a_i T_i = b_i T_{i+1} + c_i T_{i-1} + d_i \tag{C.1}$$

Set $c_1 = 0$ and $b_N = 0$ so that the temperatures T_0 and T_{N+1} will not have any meaningful role to play. In the forward-substitution process we seek a relation

$$T_i = P_i T_{i+1} + Q_i \tag{C.2}$$

after having obtained

$$T_{i-1} = P_{i-1} T_i + Q_{i-1} \tag{C.3}$$

Substitute Equation C.3 into Equation C.1,

$$a_i T_i = b_i T_{i+1} + c_i \left(P_{i-1} T_i + Q_{i-1}\right) + d_i \tag{C.4}$$

Rearranging,

$$P_i = \frac{b_i}{a_i - c_i P_{i-1}} \tag{C.5}$$

and

$$Q_i = \frac{d_i + c_i Q_{i-1}}{a_i - c_i P_{i-1}} \tag{C.6}$$

For $i = 1$ ($c_1 = 0$):

$$P_1 = \frac{b_1}{a_1} \tag{C.7}$$

$$Q_1 = \frac{d_1}{a_1} \tag{C.8}$$

For $i = N$ ($b_N = 0$):

$$P_N = 0$$

and from Equation C.2,

$$Q_N = T_N = \textit{known from boundary conditions.}$$

Using Equation C.2 back substitution may now start, giving all temperatures T_i.

Algorithm:

1. Calculate P_1 and Q_1 from Equations C.7 and C.8.
2. Use the recurrence relations (Equations C.5 and C.6) to obtain P_i and Q_i for $i = 2, 3, \ldots, N$.
3. Set $T_N = Q_N$.
4. Use Equation C.2 for $i = N-1, N-2, \ldots, 3, 2, 1$ to obtain $T_{N-1}, T_{N-2}, \ldots, T_3, T_2, T_1$.

Appendix D

Estimating the Temperature Gradient at the Droplet Surface

The temperature gradient at the surface is required for calculating the heat flux to the droplet surface (Equation 3.26). A linear variation of T between grid points was not adequate. The estimation method used was to fit an exponential function to the temperature profile near the surface. Let

$$\Theta = \frac{T - T_R}{T_\infty - T_R}$$

be represented by

$$\Theta = 1 - Ae^{\{-B(\varsigma-1)\}} \tag{D.1}$$

Note that as $\varsigma \to \infty \quad \Theta \to 1$.

At $\varsigma = 1 \quad \Theta = 0$, therefore $A = 1$.

Now

$$\Theta = 1 - exp\{-B(\varsigma - 1)\} \tag{D.2}$$

and the slope is

$$\frac{d\Theta}{dr} = \frac{1}{R}\frac{d\Theta}{d\varsigma} = \frac{B}{R}exp\{-B(\varsigma - 1)\}$$

Note that,

$$T = \Theta\,(T_\infty - T_R) + T_R$$

and

$$\frac{dT}{dr} = \frac{d\Theta}{dr}\,(T_\infty - T_R)$$

At $r = R$ (or $\varsigma = 1$):

$$\left.\frac{d\Theta}{dr}\right|_R = \frac{B}{R}$$

and

$$\left.\frac{dT}{dr}\right|_R = \frac{B}{R}\,(T_\infty - T_R) \tag{D.3}$$

Rearranging Equation D.2,

$$B = \frac{\ell n(1-\Theta)}{1-\varsigma}$$

B is evaluated by inserting values for Θ and ς at the first grid point from the surface, point 2. Substituting B in Equation D.3 the following form is obtained:

$$\left.\frac{dT}{dr}\right|_R = \frac{\ell n(1-\Theta_2)}{R(1-\varsigma_2)}\,(T_\infty - T_R) \tag{D.4}$$

Appendix E

Temperature Correction Due To Radiation

Thermocouple heat balance,

$$h(T_G - T_T) = h_R(T_T - T_R) \tag{E.1}$$

where:

- T_G = true gas temperature
- T_T = measured temperature
- T_R = effective radiating temperature of the environment.

taking the temperature probe as a cylinder in cross flow produced by natural convection from the heater plates the heat transfer coefficeint is calculated using equation 6-17 in Holman [10],

$$\frac{hd}{k_f} = C\left(\frac{u_\infty d}{\nu_f}\right)^n Pr^{1/3}$$

where the constants C and n are tabulated in Holman. The heat transfer coefficient for radiation is calculated using,

$$h_R = \frac{\sigma\left(T_d^2 + T_\infty^2\right)\left(T_d + T_\infty\right)}{1/\epsilon_d + (A_d/A_w)(1/\epsilon_w - 1)}$$

since $A_w >> A_d$,

$$h_R = \epsilon\sigma(T_d^2 + T_\infty^2)(T_d + T_\infty)$$

Solving Equation E.1,

$$T_G = T_T + \underbrace{\frac{h_R}{h}(T_T - T_R)}_{\text{radiation correction}} \tag{E.2}$$

For low Re, $Nu \propto Re^{1/3} \propto d^{1/3}$ or $h \propto d^{-2/3}$.
h_R is independent of d (small variations of T_T with d can be neglected). Then Equation E.2 can be written as

$$T_G = T_T + Cd^{2/3}(T_T - T_R) \tag{E.3}$$

where C = a constant. We now have three unknowns: C, T_G and T_R. If temperatures are measured with three different probe diameters, the following system of equations results:

$$T_1 = T_G - CD_1(T_1 - T_R) \tag{E.4}$$

$$T_2 = T_G - CD_2(T_2 - T_R) \tag{E.5}$$

$$T_3 = T_G - CD_3(T_3 - T_R) \tag{E.6}$$

where $D = d^{2/3}$.
Subtract Equation E.5 from Equation E.4,

$$T_1 - T_2 = C\{D_2T_2 - D_1T_1 + T_R(D_1 - D_2)\} \tag{E.7}$$

Substract Equation E.6 from Equation E.4,

$$T_1 - T_3 = C\{D_3T_3 - D_1T_1 + T_R(D_1 - D_3)\} \tag{E.8}$$

Divide Equation E.7 by Equation E.8; the constant C cancels.

$$\Theta = \frac{T_1 - T_2}{T_1 - T_3} = \frac{D_2T_2 - D_1T_1 + T_R(D_1 - D_2)}{D_3T_3 - D_1T_1 + T_R(D_1 - D_3)} \tag{E.9}$$

Solve for T_R:

$$T_R = \frac{D_2T_2 - D_1T_1 + \Theta(D_1T_1 - D_3T_3)}{\Theta(D_1 - D_3) + D_2 - D_1} \tag{E.10}$$

Back-substitute T_R in Equation E.8,

$$C = \frac{T_1 - T_3}{D_3T_3 - D_1T_1 + T_R(D_1 - D_3)} \tag{E.11}$$

then substitute C in Equation E.3 to obtain T_G.

Appendix F

Listing of Computer Program for Ignition Model

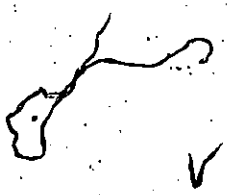

```
      FILE: MODELC   FORTRAN  A   UNIV D'/OF OTTAWA CMS RE-LEASE 4

C     DROPLET IGNITION MODEL
C     **********************
C
      INTEGER CNT,TOTIGN,TLOOP
      REAL MF,K,MA,MO,MN,KCOND,M(80),KLR,KTRAA,KTRAF,KTRFA,KTRFF
      REAL KCONDA,KCONDF,MOLEA,MOLEF
      DIMENSION T(40),ZETA(40),YF(40),YO(40),YN(40),RHO(40),
     *ZETAE(40),RHOE(40),A(40),B(40),C(40),D(40),WF(40),P(40),
     *Q(40),TOLD(40),AO(40),DIFE(40),DNEW(40),CNVW(40),CNVE(40),
     *WFO(40),DO(40),DOO(40),DOOO(40)
      CHARACTER*23 FUEL
C
CC    10=N-HEXADECANE
CC    20=N-HEPTANE
C     30=ISO-OCTANE
C     40=BENZENE
C     50=ALPHA-METHYLNAPHTHALENE
C
CC    INPUT PROPERTIES AND CONSTANTS FOR FUEL:
C
      READ(30,500)AANT,BANT,CANT,MF,K,EA,RCA,RCB,CPVAPA
      READ(30,501)CPVAPB,CPVAPC,CPVAPD,RHOL,CPL,DHF,HFG
      READ(30,502)N,ZETAN,TC,PC,W,SNICI,FUEL
  500 FORMAT(1X,F7.4,1X,2(F7.2,1X),F7.3,1X,E8.2,1X,F5.2,1X,F5.2,
     *1X,F4.2,1X,F7.3)
  501 FORMAT(1X,E9.3,1X,E10.3,1X,E9.3,1X,F5.0,1X,F5.0,1X,E10.0,1X,
     *E8.0)
  502 FORMAT(1X,I3,1X,F4.0,1X,F5.1,1X,F4.1,1X,F5.3,1X,F6.2,1X,A23)
C
C   PRINT PROPERTIES AND CONSTANTS FOR CHECK:
      WRITE(80,530)AANT,BANT,CANT,MF,K,EA,RCA,RCB,CPVAPA
  530 FORMAT(1X,F7.4,1X,2(F7.2,1X),F7.3,1X,E8.2,1X,F4.1,1X,F5.2,1X,
     *F4.2,1X,F7.3)
      WRITE(80,531)CPVAPB,CPVAPC,CPVAPD,RHOL,CPL,DHF,HFG
  531 FORMAT(1X,E10.4,1X,E11.4,1X,E10.4,1X,F5.0,1X,F5.0,1X,E11.5,1X,
     *E9.3)
      WRITE(80,502)N,ZETAN,TC,PC,W,SNICI,FUEL
C
C     INPUT INITIAL CONDITIONS:
C
      READ(70,503)TDROP,TFURN1,RDROP
  503 FORMAT(1X,F4.0,1X,F5.0,1X,F8.6)
      WRITE(6,504)FUEL
  504 FORMAT(1X,'FUEL: ',A23)
      WRITE(6,505)TDROP
  505 FORMAT(/,' INITIAL DROPLET TEMPERATURE: ',F4.0,' K')
      WRITE(6,506)TFURN1
  506 FORMAT(1X,'FURNACE TEMPERATURE: ',F5.0,' K')
      WRITE(6,507)TFURN1-20.0
  507 FORMAT(1X,'EFFECTIVE RADIATING TEMPERATURE: ',F5.0,' K')
      WRITE(6,508)RDROP
  508 FORMAT(1X,'INITIAL RADIUS: ',F8.6,' M')
      WRITE(6,509)EA
  509 FORMAT(1X,'ACTIVATION ENERGY: ',F4.1,' KCAL/MOL')
C
```

```
FILE: MODELC   FORTRAN  A   UNIV D'/OF OTTAWA CMS RELEASE 4

C   DATA REQUIRED (CONSTANTS & PROPERTIES):
      MA=28.97
      MO=32.
      MN=28.
      PAMB=760.
      PRES=101.3
      PATM=1.0
      RUGC=8.314
      YOAMB=0.232
      YNAMB=0.768
      SIGMA=5.669E-8
      DTIME=0.02
C
C   BOILING POINT TEMPERATURE (K):
      TBOIL=BANT/(AANT-LOG(PAMB))-CANT
      WRITE(80,705)TBOIL
  705 FORMAT(/,'TBOIL=',F9.2)
C
C   DATA REQUIRED FOR ESTIMATING THE DIFFUSION COEFFICIENT:
C
C   CONSTANTS:
      AD=1.06036
      BD=0.15610
      CD=0.19300
      DD=0.47635
      ED=1.03587
      FD=1.52996
      GD=1.76474
      HD=3.89411
C
C   SIGMA FOR AIR AND FUEL:
      SA=3.711
      SF=(TC/PC)**(1./3.)*(2.3551-0.087*W)
C
C   E/K FOR AIR AND FUEL:
      EKA=78.6
      EKF=TC*(0.7915+0.1693*W)
C
C   SIGMA AND E/K FOR AIR-FUEL MIXTURE:
      SAF=(SA+SF)/2.
      EKAF=(EKA*EKF)**(1./2.)
C
C   CONSTANTS REQUIRED FOR ESTIMATING THE VISCOSITY:
      AV=1.16145
      BV=0.14874
      CV=0.52487
      DV=0.77320
      EV=2.16178
      FV=2.43787
C
C   GEOMETRY OF GRID:
C     N=NUMBER OF GRID POINTS
C     ZETA(N)=THE LAST GRID POINT
      ZETA(N)=ZETAN
      DZ=LOG(ZETA(N))/(N-1)
```

```
FILE: MODELC   FORTRAN  A   UNIV O*/OF OTTAWA CMS RELEASE 4

      DO 11 I=1,N
         ZETA(I)=EXP(DZ*(I-1))
         IF (I.EQ.1) GOTO 11
         ZETAE(I-1)=(ZETA(I-1)+ZETA(I))/2.
 11   CONTINUE
C
C     LOOP FOR PRE-EXPONENTIAL CONSTANT K:
C     ------------------------------------
C
 5000 WRITE(6,630)
 630  FORMAT(/,78('-'))
      WRITE(6,510)K
 510  FORMAT(/,' PRE-EXPONENTIAL CONSTANT: ',E9.3,' M^3/KMOL.S')
      TFURN=TFURN1
      TRAD=TFURN-20.0
C
C     LOOP FOR FURNACE TEMPERATURE:
C     -----------------------------
C
 3000 TIME=0.0
      CNT=0
      IGNITE=0
      TR=TDROP
      R=RDROP
C
C     INITIAL TEMPERATURE FIELD:
      T(1)=TR
      DO 22 I=2,N
         T(I)=TFURN
 22   CONTINUE
C
C     CALCULATE SURFACE VAPOUR PRESSURE (MMHG):
      PV=EXP(AANT-BANT/(TR+CANT))
C
C     CALCULATE FUEL MASS FRACTION AT THE SURFACE:
      YFR=1./(1.+MA/MF*(PAMB/PV-1.))
      YOR=0.23*(1.-YFR)
C
C     CALCULATE THE FUEL AND OXYGEN CONCENTRATION FIELDS:
      DO 33 I=1,N
         YF(I)=1.-(1.-YFR)**(1./ZETA(I))
         YO(I)=YOAMB*(YOR/YOAMB)**(1./ZETA(I))
         YN(I)=YO(I)*(YNAMB/YOAMB)
 33   CONTINUE
C
C     LOOP FOR START OF EACH TIME STEP:
C     ---------------------------------
C
C     AVERAGE TEMPERATURE CALCULATED ACCORDING TO HUBBARD ET AL.:
 1000 TAVG=2./3.*T(1)+1./3.*T(N)
C
      EMISS=0.0
      IF((5.4*R*1000.).GT.170.)THEN
         EMISS=0.89
      ELSE
         EMISS=0.89*(1.-EXP(-5.4*R*1000.))
```

```
      ENDIF
C     WRITE(6,702)R*1000.,EMISS
C.702 FORMAT(1X,'RADIUS =',F5.3,'MM',5X,'EMISSIVITY =',F5.3)
C
C     CALCULATE SPECIFIC HEAT FOR FUEL AND AIR (J/KG.K):
      CPF=(CPVAPA+CPVAP3*TAVG+CPVAPC*TAVG**2+CPVAPD*TAVG**3)*4186./MF
      CPO=(6.713-0.879E-6*TAVG+4.170E-6*TAVG**2-2.544E-9*TAVG**3)
     **4186./MO
      CPN=(7.440-0.324E-2*TAVG+6.400E-6*TAVG**2-2.790E-9*TAVG**3)
     **4186./MN
      CPAIR=0.23*CPO+0.77*CPN
C
C     CALCULATE THE MIXTURE MOLECULAR WEIGHT AND DENSITY:
      DO 133 I=1,N
         M(I)=1./(YF(I)/MF+YO(I)/MO+YN(I)/MN)
         RHO(I)=PRES*M(I)/(RUGC*T(I))
  133 CONTINUE
C
C     CALCULATE SPECIFIC HEAT OF MIXTURE:
      YFAVG=2./3.*YF(I)+1./3.*YF(N)
      YOAVG=2./3.*YO(I)+1./3.*YO(N)
      CP=YFAVG*CPF+(1.-YFAVG)*CPAIR
      RAVG=(YFAVG/MF+(1.-YFAVG)/MA)*RUGC
      RHOAVG=PRES/(RAVG*TAVG)
      DO 44 I=1,N-1
         RHOE(I)=(RHO(I)+RHO(I+1))/2.
   44 CONTINUE
C
C     ***************************************************************
C
C     *** ESTIMATION METHOD FOR THE DIFFUSION COEFFICIENT ***
C     *** LENNARD-JONES 12-6 POTENTIAL ***
C
C     DIMENSIONLESS TEMPERATURE (T*):
      TAST=TAVG/EKAF
C
C     OMEGA FOR THE DIFFUSION COEFFICIENT:
      OMEGAD=AD/TAST**BD+CD/EXP(DD*TAST)+ED/EXP(FD*TAST)
     *+GD/EXP(HD*TAST)
C
C     DIFFUSION COEFFICIENT (M^2/S):
C
      DIFFUS=1.858E-3*TAVG**(3./2.)*((MA+MF)/(MA*MF))**(1./2.)
     */(PATM*SAF**2.*OMEGAD)*1.0E-4
C
C     ***************************************************************
C
C     CALCULATE THE INITIAL MASS FLUX:
      BMF=YFR/(1.-YFR)
      GAMMA=RHOAVG*DIFFUS
      GO=GAMMA/R*LOG(1.+BMF)
C
C     ***************************************************************
C
C     *** ESTIMATION OF LOW PRESSURE THERMAL CONDUCTIVITY FOR MIXTURE ***
```

```
FILE: MODELC   FORTRAN  A   UNIV O*/OF OTTAWA CMS RELEASE 4

C
C     ESTIMATE VISCOSITY USING THE LENNARD-JONES 12-6 POTENTIAL:
C
C     SIGMA AND E/K FOR AIR AND FUEL ARE THE SAME AS THOSE USED FOR
C     ESTIMATING THE DIFFUSION COEFFICIENT.
C
C     DIMENSIONLESS TEMPERATURES:
        TASTA=TAVG/EKA
        TASTF=TAVG/EKF
C
C     OMEGA FOR THE VISCOSITY FOR AIR AND FUEL:
        OMGVA=AV/TASTA**BV+CV/EXP(DV*TASTA)+EV/EXP(FV*TASTA)
        OMGVF=AV/TASTF**BV+CV/EXP(DV*TASTF)+EV/EXP(FV*TASTF)
C
C     VISCOSITY OF AIR AND FUEL:
        VISCA=26.69*(MA*TAVG)**(1./2.)/(SA**2.*OMGVA)
        VISCF=26.69*(MF*TAVG)**(1./2.)/(SF**2.*OMGVF)
C
C     MONATOMIC VALUES OF THERMAL CONDUCTIVITY (KTR(I)/KTR(J)):
        KTRAA=1.0
        KTRFF=1.0
        KTRAF=VISCA/VISCF*MF/MA
        KTRFA=1./KTRAF
C
C     FUNCTION (A(I,J)):
        AAA=1.0
        AFF=1.0
        AAF=(1.+KTRAF**(1./2.)*(MA/MF)**(1./4.))**2./(8.*(1.+MA/MF))
       ***(1./2.)
        AFA=(1.+KTRFA**(1./2.)*(MF/MA)**(1./4.))**2./(8.*(1.+MF/MA))
       ***(1./2.)
C
C     ESTIMATE INDIVIDUAL THERMAL CONDUCTIVITIES USING THE EUCKEN EQUATION
C
C     ESTIMATE CV AS CV=CP-R (CAL/GMOL.K):
        CVA=CPAIR*0.239*MA/1000.-1.99
        CVF=CPF*MF/4186.-1.99
C
        KCONDA=(CVA+4.47)*VISCA*1.E-6/MA
        KCONDF=(CVF+4.47)*VISCF*1.E-6/MF
C
C     CONVERT MASS FRACTIONS TO MOLE FRACTIONS:
        MOLEA=YOAVG/0.23/MA
        MOLEF=YFAVG/MF
        YAMOLE=MOLEA/(MOLEA+MOLEF)
        YFMOLE=MOLEF/(MOLEA+MOLEF)
C
C     THERMAL CONDUCTIVITY OF AIR-FUEL MIXTURE:
        KCOND=(YAMOLE*KCONDA/(YAMOLE*AAA+YFMOLE*AAF)
       *+YFMOLE*KCONDF/(YAMOLE*AFA+YFMOLE*AFF))*418.6
C
C     ***************************************************************
C
C     PREVIOUS TEMPERATURE PROFILE:
        DO 122 I=1,N
```

```
          TOLD(I)=T(I)
  122   CONTINUE
C
C     TEMPERATURE EQUATION COEFFICIENTS THAT ARE CONSTANT:
        DO 55 I=2,N-1
           AO(I)=RHO(I)/3.*(ZETAE(I)**3-ZETAE(I-1)**3)
           DIFE(I)=KCOND/R**2/CP*ZETAE(I)**2/(ZETA(I+1)-ZETA(I))
           DIFW(I)=KCOND/R**2/CP*ZETAE(I-1)**2/(ZETA(I)-ZETA(I-1))
           WFO(I)=-MF*K*RHO(I)**(RCA+RCB)/(MF**RCA*MO**RCB)
           DO(I)=RHO(I)/3.*(ZETAE(I)**3-ZETAE(I-1)**3)
           DOO(I)=(ZETAE(I)**3-ZETAE(I-1)**3)*DHF*DTIME/3./CP
           DOOO(I)=0.0
           CNVW(I)=1./2./R*(RHOE(I-1)/RHOL*ZETAE(I-1)**3+CPF/CP)
           CNVE(I)=1./2./R*(RHOE(I)/RHOL*ZETAE(I)**3+CPF/CP)
   55    CONTINUE
C
C     CALCULATE AN INITIAL THEORETICAL HEAT FLUX (QO) FOR THE FIRST TIME
C     STEP. FOR ALL OTHER TIME STEPS USE THE CALCULATED VALUE OF HEAT FL
C     FROM THE PREVIOUS TIME STEP.
C
        IF(TIME.EQ.0.0)THEN
          QO=GO*CPF*(TFURN-TR)/(EXP(GO*CPF*R/KCOND)-1.)
        ELSE
          QO=QTOT
        ENDIF
        IF(QO.LT.GO*HFG)GO=QO/HFG
        DTLDT=3./(RHOL*CPL*R)*(QO-GO*HFG)
C
C     SET DTLDT=0 FOR QUASI-STEADY TEST:
C       DTLDT=0.
C
C     PREDICT VALUE OF TR AT END OF TIME STEP:
        TRP=TR+DTLDT*DTIME
        IF(TRP.GE.TBOIL)TRP=TBOIL-0.25
C
C     LOOP FOR TEMPERATURE CONVERGENCE ITERATIONS:
C     -------------------------------------------
C
 7000 T(1)=TRP
C
C     CALCULATE A NEW SURFACE VAPOUR PRESSURE (MMHG):
        PV=EXP(AANT-BANT/(TRP+CANT))
C
C     CALCULATE A NEW FUEL MASS FRACTION AT THE SURFACE:
        YFR=1./(1.+MA/MF*(PAMB/PV-1.))
        YOR=0.23*(1.-YFR)
C
C     CALCULATE THE FUEL AND OXYGEN CONCENTRATION FIELDS:
        DO 66 I=1,N
           YF(I)=1.-(1.-YFR)**(1./ZETA(I))
           YO(I)=YOAMB*(YOR/YOAMB)**(1./ZETA(I))
           YN(I)=YO(I)*(YNAMB/YOAMB)
   66   CONTINUE
C
C     CALCULATE THE NEW MASS FLUX (AT THE END OF TIME STEP):
        BMF=YFR/(1.-YFR)
```

```
FILE: MODELC   FORTRAN  A   UNIV D*/OF OTTAWA CMS RELEASE 4

      GO=GAMMA/R*LOG(1.+BMF)
      BB=EXP(GO*CPF*R/KCOND)
C
C   CALCULATE THE COEFFICIENTS FOR THE ENERGY EQUATION:
      DO 77 I=2,N-1
         CNV=CNVE(I)*GO
         B(I)=(AMAX1(CNV,DIFE(I))-CNV)*DTIME
         CNV=CNVW(I)*GO
         C(I)=(AMAX1(CNV,DIFW(I))+CNV)*DTIME
         A(I)=AO(I)+B(I)+C(I)
C
C        CALCULATE THE REACTION RATE TERM:
C
C        FOR TESTING SET WF EQUAL TO ZERO:
C        WF(I)=0.
C
         WEXP=-EA*4186./RUGC/TOLD(I)
         WFACT=WFO(I)*YF(I)**RCA*YO(I)**RCB
         WEXP=EXP(WEXP)
         WF(I)=WFACT*WEXP
         D(I)=DO(I)*TOLD(I)-DOO(I)*WF(I)+DOOO(I)*GO
 77   CONTINUE
C
C   TRIDIAGONAL-MATRIX ALGORITHM:
      A(1)=1.0
      B(1)=0.0
      C(1)=0.0
      D(1)=T(1)
      P(1)=B(1)/A(1)
      Q(1)=D(1)/A(1)
      DO 88 I=2,N-1
         P(I)=B(I)/(A(I)-C(I)*P(I-1))
         Q(I)=(D(I)+C(I)*Q(I-1))/(A(I)-C(I)*P(I-1))
 88   CONTINUE
      DO 99 I=N-1,2,-1
         T(I)=P(I)*T(I+1)+Q(I)
         IF(T(I).GT.2500.)THEN
            IGNITE=1
            GOTO 113
         ENDIF
 99   CONTINUE
C
C   CALCULATE THE TEMPERATURE GRADIENT AT THE SURFACE:
      THETA2=(T(2)-T(1))/(TFURN-T(1))
      IF(THETA2.GE.1.0)THEN
         IGNITE=1
         GOTO 113
      ENDIF
      DTDR=LOG(1.-THETA2)/(R*(1.-ZETA(2)))*(TFURN-T(1))
C
C   THERMAL RADIATION TRANSFER TO THE DROPLET:
      QRAD=SIGMA*EMISS*(T(1)**4-TRAD**4)
C
C   TOTAL HEAT FLUX DURING TIME STEP:
      QTOT=KCOND*DTDR-QRAD
```

```
      IF(QTOT.LT.GO*HFG)GO=QTOT/HFG
C
C     RISE IN DROPLET TEMPERATURE DURING TIME STEP:
      DTLDT=3./(RHOL*CPL)*(QTOT-GO*HFG)/R
C
C     SET DTLDT=0 FOR QUASI-STEADY TEST:
C     DTLDT=0.0
C
C     CALCULATED DROPLET TEMPERATURE AT END OF TIME STEP:
      TRC=TR+DTLDT*DTIME
      IF(TRC.GE.TBOIL)TRC=TBOIL-0.25
C
C     CHECK IF CONVERGENCE HAS BEEN ACHIEVED:
      IF(ABS(TRC-TRP)/TRP.GT.0.002)THEN
C        RELAXATION FACTOR:
         TRP=0.30*TRC+0.70*TRP
         GOTO 7000
      ENDIF
C
  113 TIME=TIME+DTIME
      TR=TRP
C
C     CNT=CNT+1
      IF(IGNITE.EQ.0)GOTO 112
C     IF(CNT.GE.2)THEN
C     PRINT TEMPERATURE PROFILE AT END OF TIME STEP:
C        WRITE(6,603)
C603     FORMAT(/,' TEMPERATURE PROFILE AT END OF TIME STEP')
C        WRITE(6,613)
C613     FORMAT(1X,39('-'))
C        WRITE(6,604)TIME
C604     FORMAT(/,' TIME = ',F5.2,' S')
C        WRITE(6,612)RDROP*1000.0,R*1000.0
C612     FORMAT(/,' INITIAL RADIUS:',F6.3,'  DROPLET RADIUS:',F6.3,' MM')
C        WRITE(6,611)QTOT,GO*HFG,GO,CPF
C611     FORMAT(/,' QTOT=',E10.4,10X,'GO*HFG=',E10.4,/,' GO=',E10.4,12X,
C    *   'CPF=',E10.4)
C        WRITE(6,605)
C605     FORMAT(/,'  I',5X,'ZETA(I)',8X,'T(I)',7X,'YF(I)',7X,'YO(I)')
C        WRITE(6,621)
C621     FORMAT(1X,'---',5X,'-------',8X,'----',7X,'-----',7X,'-----')
C        DO 111 I=1,N
C           WRITE(6,606)I,ZETA(I),T(I),YF(I),YO(I)
C606        FORMAT(1X,I2,5X,F7.3,4X,F10.3,5X,F6.4,6X,F6.4)
C111     CONTINUE
C        CNT=0
C     ENDIF
C
C    NEW DROPLET RADIUS
  112 R=R-GO/RHOL*DTIME
C
      IF(IGNITE.EQ.1)THEN
         WRITE(6,623)RDROP*2000.
  623    FORMAT(/,' DROPLET DIAMETER =',F7.3,' MM')
         WRITE(6,622)TIME,TFURN
```

```
FILE: MODELC   FORTRAN  A   UNIV O'/OF OTTAWA CMS RELEASE 4

 622      FORMAT(1X,'IGNITION OCCURRED AFTER ',F7.3,' SECONDS IN A FURNA
     *E AT ',F5.0,' KELVIN.')
C         WRITE(6,622)TIME,TDROP
C622      FORMAT(1X,'IGNITION OCCURRED AFTER ',F5.3,' SECONDS WITH AN IN
C    *TIAL TDROP AT ',F5.0,' KELVIN.')
          GOTO 2000
        ENDIF
        IF(R.GT.0.)GOTO 1000
C       WRITE(6,612)RDROP*1000.0,R*1000.0
        WRITE(6,610)TFURN
 610    FORMAT(1X,'DROPLET VAPORIZED WITHOUT IGNITION IN A FURNACE AT ',
     *F5.0,' KELVIN.')
C2000   IF(IGNITE.EQ.0.OR.RDROP.LT.0.000050)GOTO 6000
 2000   IF(IGNITE.EQ.0)GOTO 6000
C2000   IF(IGNITE.EQ.0.OR.TDROP.GT.(TBOIL-25.0))GOTO 6000
C2000   IF(IGNITE.EQ.0.OR.TFURN.LE.823.0)GOTO 6000
C2000   IF(TFURN.EQ.986.0)GOTO 6000
C       TFURN=TFURN-50.0
C       TRAD=TFURN-20.0
C       IF(RDROP.GE.0.00010)DRDROP=0.00005
C       IF(RDROP.GE.0.00020)DRDROP=0.00010
C       IF(RDROP.GE.0.00100)DRDROP=0.00050
C       IF(RDROP.GE.0.00200)DRDROP=0.00100
C       IF(RDROP.GE.0.01000)DRDROP=0.00500
C       IF(RDROP.GE.0.02000)DRDROP=0.01000
C       DRDROP=0.000010
C       RDROP=RDROP-DRDROP
C       TDROP=TDROP+20.0
C       GOTO 3000
C4000   IF(K.GE.0.20E+09)GOTO 6000
C4000   IF(K.LT.0.80E+06)GOTO 6000
C       K=K*10.0
C       K=K-0.10E+06
C       GOTO 5000
 6000   END
```